Scaling laws for turbulent relative dispersion in two-dimensional energy inverse-cascade turbulence

Tatsuro Kishi

Abstract

Transport phenomena are ubiquitous in nature. Turbulence efficiently transports and promptly disperses substances such as pollutants, chemical and biological agents because of its nonlinearity of the dynamics. Turbulent relative dispersion, which is statistics of Lagrangian particle pairs, is probably the simplest statistics to characterize the nature of turbulent diffusion such as superdiffusivity and multiscaling. Here, Lagrangian particles are passively advected by turbulent flow and give no back-reaction on the flow. According to the classical phenomenology initiated by L. F. Richardson, particle pairs in turbulence completely forget information on their initial conditions such as initial separations, and the mean square of the relative separation exhibits superdiffusive scaling law, that is, so-called Richardson–Obukhov law, $\langle r^2(t) \rangle \propto t^3$. Here, $r(t)$ is the relative separation between two particles at time t elapsed since the particle pair started to be advected in the turbulent flow. The bracket $\langle \cdot \rangle$ is an ensemble average.

The Richardson–Obukhov law, however, has never been clearly observed in both laboratory experiments and numerical simulations. Furthermore, the mean square of the relative separation strongly depends on the initial separation for a long time. As a result, the mean square of the relative separation exhibits the t^3 power law at a special initial separation because of the initial separation dependence. Here, we cannot immediately conclude that this apparent t^3 law is consistent with the Richardson–Obukhov law because the mean squares of the relative separations at the other initial separations do not exhibit the t^3 power law.

In this thesis, we study the turbulent relative dispersion in two-dimensional energy inverse-cascade turbulence in terms of the initial separation dependence in two ways: conditional sampling method and two-time Lagrangian velocity correlation function. First we develop a conditional sampling method by which the conditional mean square becomes independent of the initial separation and exhibits the t^3 scaling law for all initial separations. On the other hand, the unconditional mean square of relative velocity of the particle pairs exhibits anomalous scaling law deviated from the prediction of Kolmogorov phenomenology which is the standard phenomenology of Eulerian turbulence. According to these results, we conjecture that the t^3 power law exhibiting at the special initial separation is not consistent with the Richardson–Obukhov law, or Kolmogorov phenomenology cannot be always applied to the statistics on the turbulent relative dispersion. It is noted that the Richardson–Obukhov law is also derived

in terms of Kolmogorov phenomenology.

Second, we investigate the two-time Lagrangian velocity correlation function which is defined as $\langle \delta \boldsymbol{v}(t_1) \cdot \delta \boldsymbol{v}(t_2) \rangle$, where $\delta \boldsymbol{v}(t)$ is relative velocity of a particle pair. We propose a scaling law for the two-time Lagrangian velocity correlation function adapting incomplete similarity. Then, we confirm that the proposed scaling law is consistent with the experimental data in two-dimensional energy inverse-cascade turbulence. From the scaling law for the two-time Lagrangian velocity correlation function, we demonstrate that the t^3 power law exhibiting at the special initial separation is an artifact induced by finite-size effects of turbulence. Finally, we improve the Richardson–Obukhov law to be consistent with experimental data and discuss the validity of the Richardson–Obukhov law at infinite Reynolds number.

Acknowledgements

I would like to express my sincerest gratitude to Professor Dr. Sadayoshi Toh for serving as my advisor of PhD course of science in Kyoto University, for his insightful suggestions and great tolerance, and for always encouraging me to pursue my own path in my research.

I wish to express deepest gratitude to Professor Dr. Takeshi Matsumoto for his generosity in sharing his ideas and insight. Without his guidance and persistent help this thesis would not have been possible.

I would like to thank my colleagues of Fluid Physics Group of Kyoto University, Dr. Toshiki Teramura, Dr. Yoshiki Hiruta, Ryo Murakami, Tin Unkai, Michinori Sato, Yo Yamada, Takafumi Maruishi, Ryo Sakai, Yusuke Ohnishi, Ryo Hirano, Takumi Nakata, and Kohei Okuyama for their discussion, comments and suggestions. I am also grateful for stimulating discussion with Professor Dr. Yukio Kaneda.

Most of numerical computations in the work were performed at the Yukawa Institute Computer Facility.

Finally I would like to thank my mother and father, Naoko and Itsuro and my sisters, Mikako and Mayuko, for their constant encouragement and support.

Contents

Chapter 1

General Introduction

1.1 Lagrangian turbulence

Motions of substances in turbulence, such as smoke spreading and fallen leaves fluttering about, are very complicated and unpredictable. Most of us have experienced an airplane shaking. We recognize from such motions that there is turbulence.

We know a priori that milk in a cup of coffee becomes uniform faster by stirring with a spoon. We usually utilize the ability of turbulence to enhance the diffusion and the mixing. However, we poorly understand why turbulence can rapidly diffuse and mix substances. The mechanics of turbulent diffusion and mixing is still unknown. In this thesis, we focus on the mechanics of turbulent diffusion. Here we define turbulent diffusion as spreading of substances which are only advected by turbulent flow and give no back-reaction on the flow. Hence, we suppose that the molecular diffusivity and the inertia of the substances are small enough to be negligible [1].

In turbulent flows, there are a lot of eddies of various sizes. These eddies interact with each other and randomly move because of the nonlinear dynamics of turbulence. Such randomness induced by the nonlinearity of turbulence probably gives rise to the efficient diffusivity (superdiffusivity).

In more mathematical view points, turbulent diffusion is described by statistics of Lagrangian fluid elements, which are passively advected by turbulent flow and give no back-reaction on the flow. In this thesis, we call the Lagrangian fluid element Lagrangian particle for simplicity though such a particle does not exist in real world. The velocity of the Lagrangian particle is same as the fluid velocity at the particle position. Thus, the motions of Lagrangian particles initially seeded at various positions can fully describe turbulence itself. Therefore, there are two kinds of descriptions for velocity field of a fluid: Eulerian description and Lagrangian description.

[1] This definition may be more limited than usual. In this thesis, we consider such an ideal case and pursue the universal properties of turbulent diffusion.

1.1.1 Eulerian description and Lagrangian description

There are two ways of descriptions of field, i.e., Eulerian and Lagrangian descriptions, see [12] for detail. First, we consider two observers; one is always located at a position $\boldsymbol{x}$, the other is moving with a tracer particle, which is passively advected by the fluid. The former is called Eulerian observer and the latter is called Lagrangian observer. The position of the Lagrangian observer at time t who passes a position $\boldsymbol{x}$ at time s is denoted as $\boldsymbol{X}(\boldsymbol{x}, s|t)$. Here, there are two times, s and t, which are called the labeling time and the measuring time, respectively.

An Eulerian observer at a position x can measure fluid velocity at time t only at its position $\boldsymbol{x}$, which is denoted as $\boldsymbol{u}(\boldsymbol{x}, t)$. This is called Eulerian velocity. On the other hand, a Lagrangian observer can measure fluid velocity at time t only at the position of the particle riding on, which is denoted as $\boldsymbol{v}(\boldsymbol{x}, s|t)$. This is called Lagrangian velocity [73]. It is defined through its position $\boldsymbol{X}(\boldsymbol{x}, s|t)$ as,

$$\boldsymbol{v}(\boldsymbol{x}, s|t) \equiv \frac{d}{dt}\boldsymbol{X}(\boldsymbol{x}, s|t), \tag{1.1}$$

and is equivalent to

$$\boldsymbol{v}(\boldsymbol{x}, s|t) = \boldsymbol{u}(\boldsymbol{X}(\boldsymbol{x}, s|t), t). \tag{1.2}$$

In this thesis, we call the set of variables, $(\boldsymbol{x}, s, t)$, the Lagrangian data.

In general, Eulerian description simplifies mathematical treatments of the phenomenon on which one focuses. The Navier-Stokes equations are described by the Eulerian description. On the other hand, it seems to be incompatible with human imagination because we have to imagine infinite number of observer. Lagrangian description is rather more useful to analyze a phenomenon at first. Of course, once the equations by the Eulerian description are obtained, these numerical calculations and analytical considerations are more feasible than those by the Lagrangian description. Therefore, due to the simplicity, the study of Eulerian turbulence, which means analysis on Eulerian velocity in turbulence, has developed prior to that of Lagrangian turbulence, which means analysis on Lagrangian velocity in turbulence.

Lagrangian description is, however, frequently required for analysis of phenomena in nature [12]. All of the phenomena below require Lagrangian description: particle motions in turbulence, diffusion of substances such as smoke in atmosphere and ink in water, mixing of two kinds of immiscible materials such as oil and water, and thermal transport in ocean. These phenomena are often called Lagrangian turbulence. In this thesis, we consider statistical properties of Lagrangian turbulence, especially, in terms of turbulent diffusion. Hence, let us consider a diffusion similar to Brownian motion, namely, statistical properties of Lagrangian particles in turbulence where particles initially occupy a very small region and are loosed at same time. It is noted that we do not deal with particles loosed in succession. First of all, we consider which quantity characterizes well Lagrangian turbulence.

1.1.2 Characteristics of Lagrangian turbulence

In this thesis, we only deal with homogeneous turbulence. Thus, we suppose that particles move in a fluid which occupies an unbounded domain without boundaries. For the approximation, we also suppose that particles move in a fluid within a finite domain, and all of the particles are far from the boundaries at any time

We study time evolutions of n particles described as,

$$\frac{d}{dt}\boldsymbol{X}(\boldsymbol{x}_i, s|t) = \boldsymbol{v}(\boldsymbol{x}_i, s|t), \quad (i = 1, \cdots, n) \tag{1.3}$$

for large n. The domain which particles initially occupy is supposed to be much smaller than turbulent domain. All particles are loosed at same time s. In general, we consider statistics on a quantity, A, in terms of n particles with Lagrangian data set, $\{(\boldsymbol{x}_1, s, t_1), \cdots, (\boldsymbol{x}_n, s, t_n)\}$. For example, one-particle displacement is the quantity for $n = 1$ in terms of one particle , and relative separation of particle pairs is the quantity for $n = 2$, in terms of two particles, etc. Here, this quantity is denoted as $A(\boldsymbol{x}_1, s, t_1; \cdots; \boldsymbol{x}_m, s, t_m)$.

There are several versions of ensemble averages for particle statistics. The first one takes the average over realizations obtained by repeating N-times experiments under exactly the same conditions for large N. We can define the ensemble average of a quantity A in terms of n particles as,

$$\langle\langle A(\boldsymbol{x}_1, s, t_1; \cdots; \boldsymbol{x}_n, s, t_n)\rangle\rangle = \frac{1}{N}\sum_{i=1}^{N} A_i(\boldsymbol{x}_1, s, t_1; \cdots; \boldsymbol{x}_n, s, t_n), \tag{1.4}$$

Here $A_i(\boldsymbol{x}_1, s, t_1; \cdots; \boldsymbol{x}_n; s, t_n)$ is a realization of A at the i-th experiment [86]. Under this average, we can estimate n-point joint probability distribution function (PDF) for the positions of particles:

$$p(\boldsymbol{X}_1, t_1; \cdots; \boldsymbol{X}_n, t_n|\boldsymbol{x}_1, s; \cdots; \boldsymbol{x}_n; s) = \langle\langle\delta[\boldsymbol{X}_1 - \boldsymbol{X}(\boldsymbol{x}_1, s|t_1)] \cdots \delta[\boldsymbol{X}_n - \boldsymbol{X}(\boldsymbol{x}_n, s|t_n)]\rangle\rangle, \tag{1.5}$$

where $\delta[\boldsymbol{y}]$ is the Dirac delta function. This definition of the ensemble average is the most general, but is not practical.

The second is provided for more practical reasons. It is often difficult to take the ensemble average (1.4) with the large number N enough to obtain the accurate statistics at laboratory experiments and numerical simulations. Then, we alternatively use the following ensemble average in this thesis. For this ensemble average, the only one experiment is required. In this experiment, N particles are loosed at an initial time s. Next, we find M set of particles which have the same values of $\boldsymbol{x}_1 - \boldsymbol{x}_2, \boldsymbol{x}_1 - \boldsymbol{x}_3, \ldots, \boldsymbol{x}_{n-1} - \boldsymbol{x}_n$ in each set. It should be noted that M can be large if N is sufficiently large. Then, the ensemble average is defined as,

$$\langle A(\boldsymbol{x}_1, s, t_1; \cdots; \boldsymbol{x}_n, s, t_n)\rangle = \frac{1}{M}\sum_{j=1}^{M} A(\boldsymbol{x}_1^{(j)}, s, t_1; \cdots; \boldsymbol{x}_n^{(j)}, s, t_n), \tag{1.6}$$

where $\{\boldsymbol{x}_1^{(j)}, \ldots, \boldsymbol{x}_n^{(j)}\}$ is j-th set of such particles. Thus, $A(\boldsymbol{x}_1^{(j)}, s, t_1; \cdots; \boldsymbol{x}_n^{(j)}, s, t_n)$ is a realization of A for the j-th set of particles. This definition is efficient for small n. We expect that this ensemble average (1.6) provides the same results as the ensemble average (1.4), and therefore we use it in this thesis.

Now we consider which statistical quantity characterizes Lagrangian turbulence, especially, turbulent diffusion. Strictly speaking, the n-point joint probability distribution function (1.5) contains the full information about turbulent diffusion, and therefore we should consider properties of it. However, we believe that there are simpler quantities to characterize turbulent diffusion.

In this regard, at a first sight, statistics on one-particle displacement, such as the root mean squared displacement (RMSD) [12],

$$l(t) \equiv \sqrt{\langle |\boldsymbol{X}(\boldsymbol{x}_0, s|t) - \boldsymbol{x}_0|^2 \rangle}, \tag{1.7}$$

seems good as in the case of the Brownian motion. Here, $\boldsymbol{x}_0$ is an initial position of the particle. However, this is insufficient to turbulent diffusion because the RMSD, $l(t)$, exhibits asymptotically power-law behavior similar to Brownian motion as follows [110]:

$$l(t) \simeq \begin{cases} v_{rms} t & \text{at } t \ll T_L, \\ v_{rms}\sqrt{T_L t} & \text{at } t \gg T_L, \end{cases} \tag{1.8}$$

where v_{rms} is the root mean square of Eulerian turbulence energy for unit mass and T_L is an integral time scale of turbulence, which is the largest characteristic time scale of turbulence. The scaling laws (1.8) mean that diffusion with respect to one-particle displacement is only influenced by the largest eddy of turbulence with velocity v_{rms}. Therefore, we cannot understand the scale-by-scale effects of turbulent diffusion induced by the nonlinearity of turbulence.

As initiated by Richardson [98], it is good to deal with relative separation of particle pairs, that is,

$$\boldsymbol{r}(t) \equiv \boldsymbol{X}(\boldsymbol{x}_1, s|t) - \boldsymbol{X}(\boldsymbol{x}_2, s|t). \tag{1.9}$$

This quantity may be influenced only by the eddies of the same size as $|\boldsymbol{r}(t)|$ of turbulence, or by eddies of various sizes of turbulence at least. In any case, statistics on the relative separation of particle pairs have information on multiscailng of turbulent diffusion. This diffusion is called the turbulent relative dispersion. The scaling laws for the relative dispersion is the main themes in this thesis.

Before considering the scaling properties of turbulent relative dispersion, we will take a look at them from a more general point of view: anomalous diffusion and scaling laws.

1.2 Anomalous diffusion

Anomalous diffusion [67, 107] is a diffusion process with the mean-square displacement which does not grow linearly in time, i.e.,

$$\langle |\boldsymbol{x}(t)|^2 \rangle \propto t^{2\nu} \quad (\nu \neq 1/2). \tag{1.10}$$

In particular, the case of $\nu < 1/2$ is called subdiffusion, and the case of $\nu > 1/2$ is called superdiffusion.

Anomalous diffusion is ubiquitous in various systems [84, 127]. One of the characteristics is non-universarity of the scaling exponent. Various values of ν are observed in various phenomena. Its value of ν is determined by specific mechanisms of the individual phenomenon. Such non-universality results from deviations from the central limit theorem. To our best knowledge, however, it is unclear whether there is universal mechanism of the anomalous diffusion.

Here, we review superdiffusion and its models in the following subsection. It is well known that the turbulence enhances diffusion and mixing of substances. Thus, turbulent diffusion probably exhibits superdiffusive nature, which was indeed found so by Richardson [98].

1.2.1 Models for superdiffusion

Superdiffusion has been widely studied with various models such as fractional Brownian motion [83], generalized Langevin equations [95], continuous time random walk (CTRW) models [68], and Lévy walk models [127]. Several of these models can lead to an equation with a fractional operator [84], for the PDF, $p(x,t)$, which has a self-similar asymptotic form such as,

$$p(x,t) \sim t^{-\nu} f\left(\frac{x}{t^\nu}\right), \tag{1.11}$$

where f is a function with a single argument. Here, we suppose one dimensional space. This self-similar distribution implies the mono scaling of the moments:

$$\langle |x(t)|^q \rangle \propto t^{q\nu}. \tag{1.12}$$

On the other hand, several studies report deviations from the mono-scaling law in experiments for various systems. In such systems, the moments exhibit so-called strong anomalous diffusion [35], i.e.,

$$\langle |x(t)|^q \rangle \propto t^{q\nu(q)}, \tag{1.13}$$

where $\nu(q)$ is a nonlinear function of q. It indicates breaking of self-similar distribution, (1.11). In the framework of Lévy walk models, one can explain that this strong anomalous distribution is originated from rare events, which are due to fat-tails of the PDFs. Furthermore, this dynamical basis is investigated by non-normalizable densities and big-jump principle [96, 97, 117, 118].

1.2.2 Turbulent diffusion as superdiffusion

Turbulent diffusion also exhibits superdiffusion. Especially, Richardson [98] proposed, as we will describe later in detail, the superdiffusive behavior of relative separations of particle pairs,

$$\langle r^2(t) \rangle \propto t^3,$$

where $r(t)$ is the relative separation of a particle pair. Moreover, he stated that the PDF is self-similar and thus leads to a mono scaling such as Eq.(1.12). Recently, CTRW models are proposed for the dynamical origin of the Richardson model [29, 113].

On the other hand, recent numerical investigations show the deviation from the above Richardson picture [16, 105]. Furthermore, they state that the deviations are resulted from the rare events[2] which include pairs separating very fast or very slowly. Thus, the PDF is not self-similar [16, 105]. However, the origins of such rare events are not clear.

It seems that the Lévy walk models are compatible with the turbulent relative dispersion. The motion of Lévy walker is similar to that of particle pairs in the Batchelor–Obkuhov regime, which will be described in section 1.5. Moreover, the Lévy walk models can explain the rare events as mentioned above. However, the convincing evidence has never been shown that the particle pairs in turbulence behave as Lévy walker. We will discuss again the relation between the turbulent relative dispersion and the Lévy walk models in chapter 4.

1.3 Scaling law

Scaling laws are observed in turbulence. We describe scaling properties of turbulence in the following sections. In this section, we review general properties of phenomena exhibiting scaling laws and also theoretical techniques such as dimensional analysis which enable to find scaling laws and determine the values of the scaling exponents For more information about dimensional analysis and self-similarity, see, for example, Ref. [5, 6, 7]. Here, this section is described based on [6]

Scaling laws appear in various phenomena in nature. The scaling laws reveal self-similarities behind the processes in the phenomena. Here, the scaling law for a quantity, A, is a power-law monomial relation among the others, $a_1, \ldots, a_k$,

$$A = C a_1^{\alpha_1} \cdots a_k^{\alpha_k}, \tag{1.14}$$

where C is a constant factor and $\alpha_1, \ldots, \alpha_k$ are scaling exponents.

In general, physical quantities have dimensions. Hence, the value of the quantity is measured by adopting one unit of the dimension. Using this property, we can estimate how the quantity depends on the other quantities, which is dimensional analysis.

[2] They are termed extreme events in their papers.

1.3.1 Dimensional analysis

Dimensional analysis of a quantity, A, is a theoretical technique to determine a power-law monomial relationship with the other quantities. The scaling law for the quantity, A, is obtained by dimensional analysis as follows. First, we list quantities called governing parameters on which the quantity A depends as,

$$A = f(a_1, \ldots, a_k, b_1, \ldots, b_m), \tag{1.15}$$

Here, we group the governing parameters separately into two categories, i.e., the k parameters $\{a_1, \ldots, a_k\}$ and the m parameters $\{b_1, \ldots, b_m\}$. The parameters $\{a_1, \ldots, a_k\}$ have independent dimensions while the dimensions of the parameters $\{b_1, \ldots, b_m\}$ can be expressed as products of the dimensions of $\{a_1, \ldots, a_k\}$:

$$\begin{cases} [b_1] = & [a_1]^{\beta 11} \cdots [a_k]^{\beta 1k}, \\ \quad \vdots & \\ [b_i] = & [a_1]^{\beta i1} \cdots [a_k]^{\beta ik}, \\ \quad \vdots & \\ [b_m] = & [a_1]^{\beta_{m1}} \cdots [a_k]^{\beta mk}. \end{cases} \tag{1.16}$$

Here, f is an unknown function. Dimensional analysis cannot determine the functional form of f except in special cases. Similarly, the dimension of A can be expressed by the dimensions of $\{a_1, \ldots, a_k\}$:

$$[A] = [a_1]^{\alpha_1} \cdots [a_k]^{\alpha_k}. \tag{1.17}$$

Here, we assume that the governing parameters, $\{a_1, \ldots, a_k\}$ and $\{b_1, \ldots, b_m\}$, are given. For systems with many degrees of freedom such as turbulence, the number of the quantities related to the phenomenon is too large, maybe infinity, to efficiently perform the dimensional analysis. We should reduce some of the parameters in advance. Furthermore, we have to classify the governing parameters into two $\{a_1, \ldots, a_k\}$ and $\{b_1, \ldots, b_m\}$ for dimensional analysis. The parameters $\{a_1, \ldots, a_k\}$ are of significant for the scaling laws while the parameters $\{b_1, \ldots, b_m\}$ are not always crucial, as described later. However, we cannot know how to classify them a priori. We should perform the classification with carefully considering which quantity is important for the phenomenon.

Next, we define some dimensionless parameters, $\{\Pi, \Pi_1, \ldots, \Pi_m\}$. The parameter A is non-dimensionalized by using the parameter $a_1, \ldots a_k$:

$$\Pi \equiv \frac{A}{a_1^{\alpha_1} \cdots a_k^{\alpha_k}} \tag{1.18}$$

Similarly, the governing parameters $\{b_1, \ldots, b_m\}$ are also non-dimensionalized:

$$\begin{cases} \Pi_1 \equiv & \dfrac{b_1}{a_1^{\beta 11} \cdots a_k^{\beta 1k}}, \\ \quad \vdots & \\ \Pi_m \equiv & \dfrac{b_m}{a_1^{\beta m1} \cdots a_k^{\beta mk}} \end{cases} \tag{1.19}$$

The number of arguments of the relationship (1.15) can be reduced from $k+m$ to m by using the following theorem:

Buckingham Π-theorem The relationship (1.15) is equivalent to

$$\Pi = \Phi(\Pi_1, \ldots, \Pi_m), \tag{1.20}$$

where Φ is a dimensionless function with m arguments. The proof of the Buckingham Π-theorem is provided by, for example, Ref. [17]. The unknown arguments of the relationship among the quantity A and the governing parameters are reduced from $k+m$ to m:

$$A = a_1^{\alpha_1} \cdots a_k^{\alpha_k} \Phi\left(\frac{b_1}{a_1^{\beta 11} \cdots a_k^{\beta 1k}}, \ldots, \frac{b_m}{a_1^{\beta m1} \cdots a_k^{\beta mk}} \right) \tag{1.21}$$

This is a consequence of dimensional analysis. In particular, when $m = 0$, the dimensionless function Φ is just a constant. Thus, the relationship (1.21) is simply described as,

$$A = C a_1^{\alpha_1} \cdots a_k^{\alpha_k}, \tag{1.22}$$

where C is a constant factor. Therefore, we can completely determine the relation between the quantity A and the governing parameters except for the constant factor.

On the other hand, when $m \neq 0$, we can not determine the functional form of Φ by dimensional analysis. Nevertheless, we feel like we kind of understand if Φ is a one-variable function, i.e., $m = 1$. Especially, if the parameter Π_1, which is the argument of Φ, is independent of both time and spatial coordinates, the function Φ can be regarded a constant again. This is called the physical similarity. An example for this case is the relation for the hydrodynamic drag in a long cylindrical pipeline. In this case, the parameter Π_1 is the Reynolds number.

Furthermore, when Π_1 is dependent on time or spatial coordinates, the relationship between the quantity A and the parameter Π_1 is called self-similar. For instance, let the quantity A a time dependent scalar field, i.e., $A = A(x,t)$. The quantity A is self-similar in time if the following relation holds:

$$A = \tilde{C} t^{-\alpha} \Phi\left(\frac{x}{X(t)} \right), \tag{1.23}$$

where $\tilde{C}$ is a parameter independent of both t and x, and $X(t)$ is a time-dependent variable whose dimension is the same for x. Examples for this case include thermal diffusion in the infinite space and the PDF of Brownian motion. We can determine the functional form of Φ when we know the governing equation such as the diffusion equation. At this point, the assumption that the quantity has the self-similar form (1.23) simplifies to find a solution to the governing equation. There are many other examples for the physical similarity and the self-similarity in Ref.[5, 6, 7].

As we can see from the above examples, it is important to reduce a priori the number of the parameters $\{b_1, \dots b_m\}$, whose dimensions are given by the products of those of $\{a_1, \dots a_k\}$, in order to obtain the relationship that allows physical interpretation. However, the number of governing parameters becomes larger if the phenomenon is more complicated. In this sense, the self-similarity emerges only as an approximation. Therefore, we focus on asymptotic behaviors of the quantity A. Let us consider time when and scale where the system is independent of fine details of initial conditions and boundary conditions, and also still far from its final equilibrium state. This situation is often found at problems of physics. This is intermediate asymptotics.

1.3.2 Intermediate Asymptotics

Let us consider three independent variables, b_1, b_2, and b which are governing parameters for a quantity A under consideration. Assume that b_2 is quite a bit larger than b_1:

$$b_1 \ll b_2. \tag{1.24}$$

Then, we consider an asymptotic behavior of the quantity A in an intermediate range,

$$b_1 \ll b \ll b_2. \tag{1.25}$$

This asymptotics is called intermediate asymptotics. Namely, b is large enough in comparison with b_1 but small enough in comparison with b_2. An example for b is a spatial coordinate x or time t. Intermediate asymptotics appears frequently at problems of physics. It is the case for turbulence as we will mention in the following sections. In the intermediate asymptotics, we can expect that the number of the independent variables for the quantity A is reduced. At a first sight, it seems that the quantity A becomes independent of the dimensionless parameters b_1/b and b_2/b at intermediate asymptotics because the parameter b_1/b is infinitesimally small and the parameter b_2/b is infinitely large. In such a case, the parameters are no longer significant. As a result, a self-similarity arises. For the simplest case, we may find the scaling law for the quantity A only by using dimensional analysis. However, it does not always the case for all phenomena. The parameters b_1/b and b_2/b remain essential at intermediate asymptotics for some phenomena. In this case, we can still expect that a self-similarity arises for the quantity A. The former self-similarity of the simplest case is called complete similarity and the latter incomplete similarity. Of course, the self-similarity does not arise in either case for some phenomena. In this case, we have to attack the

phenomenon in other ways. In the next subsection, we describe more quantitatively the two kinds of self-similarity.

1.3.3 Complete and Incomplete Similarities

According to the Π-theorem, a quantity A can be represented as Eq.(1.21). For clear discussion, let m be 2, and we assume that the dimension of b_1 is the same as one of b_2, that is, $[b_1] = [b_2]$. See Ref. [6] for more general case.

In such a case, Eq.(1.21) is simplified as

$$A = a_1^{\alpha_1} \cdots a_k^{\alpha_k} \Phi \left(\frac{b_1}{a_1^{\beta_1} \cdots a_k^{\beta_k}}, \frac{b_2}{a_1^{\beta_1} \cdots a_k^{\beta_k}}, \right). \tag{1.26}$$

Here, we denote $a_1^{\beta_1} \cdots a_k^{\beta_k}$ as b for simplicity, that is

$$A = a_1^{\alpha_1} \cdots a_k^{\alpha_k} \Phi \left(\frac{b_1}{b}, \frac{b_2}{b} \right) \tag{1.27}$$

Then we consider the intermediate asymptotics for $b_1 \ll b \ll b_2$. In this intermediate asymptotics, i.e., at $b_1/b \to 0$ and $b_2/b \to \infty$, we can expect that the dimensionless function Φ approaches a non-zero and finite constant C. In this case, the scaling law for A is revealed as

$$A \sim C a_1^{\alpha_1} \cdots a_k^{\alpha_k} \quad \text{for} \quad b_1 \ll b \ll b_2 \tag{1.28}$$

Here, C is no longer dependent on b_1 and b_2. Therefore, the scaling law for A is determined only by dimensional analysis. This kind of the self-similarity is called complete similarity or similarity of the first kind.

On the other hand, for some phenomena, the parameters b_1 and b_2 remain essential no matter how large or small the corresponding dimensionless parameters b_1/b and b_2/b are. In such a case, at a limit $b_1/b \to 0$ and $b_2/b \to \infty$, the dimensionless function Φ behaves singular, namely, approaches neither non-zero nor finite value. Nevertheless, we can expect that there is another type of self-similarity. One possibility is that the dimensionless function Φ has the properties of generalized homogeneity in its own arguments:

$$\Phi \left(\frac{b_1}{b}, \frac{b_2}{b} \right) \sim \left(\frac{b_2}{b} \right)^p \Phi_* \left(\frac{b_1/b}{(b_2/b)^q} \right), \tag{1.29}$$

at small value of b_1/b and large value of b_2/b, where p and q are constants. This relation (1.29) is similar to the result of the Buckingham Π-theorem, but the role is quite different. The values of the scaling exponents, p and q, are not determined by dimensional analysis. As a result, the scaling law for A is as follows:

$$A \sim a_1^{\alpha_1 - p\beta_1} \cdots a_k^{\alpha_k - p\beta_k} \; b_2^p \; \Phi_* \left(\frac{b_1}{a_1^{\beta_1(1-q)} \cdots a_k^{\beta_k(1-q)} b_2^q} \right). \tag{1.30}$$

The result is quite different from complete similarity. The quantity A is essentially dependent on b_1 and b_2 for $b_1 \ll b \ll b_2$. The additional exponents p and q are determined not by dimensional analysis but by experimental data or by solving the governing equations for A under the assumption of the self-similarity (1.30). This self-similarity is called incomplete similarity or the similarity of second kind. When $p = q = 0$, *complete similarity* recovers. Therefore, incomplete similarity contains complete similarity.

1.3.4 Experimental asymptotics

Then, how can we know which type of self-similarities the phenomenon is classified into, or the phenomenon is not classified into both types? Strictly speaking, this is attained only when we obtain the solution of the governing equations for the phenomenon without self-similarity assumptions. We cannot know it a prior. Therefore we only assume, in succession, complete similarity, incomplete similarity, and no similarity, and then compare it with the experimental data from laboratory experiments and numerical experiments etc. This analysis is experimental asymptotics, which is termed by N. Zabusky [6].

The Richardson–Obukhov law is the standard and widely accepted scaling law for the turbulent relative dispersion as we will describe in section 1.5 in detail. However, in terms of the experimental asymptotics, the Richardson–Obukhov law does not converge enough because it is not observed by any laboratory and numerical experiments.

1.4 Eulerian turbulence

In this section, we review theories and some experimental results of Eulerian turbulence before we consider Lagrangian turbulence. This is because the phenomenology applied to Lagrangian turbulence is based on that of Eulerian turbulence.

A starting point is the Navier-Stokes equations:

$$\begin{cases} \dfrac{\partial}{\partial t}u_i(\boldsymbol{x},t) + \boldsymbol{u}\cdot\nabla u_i(\boldsymbol{x},t) = -\dfrac{\partial}{\partial x_i}p(\boldsymbol{x},t) + \nu\Delta u_i(\boldsymbol{x},t) + f_i(\boldsymbol{x},t), \\ \dfrac{\partial}{\partial x_j}u_j(\boldsymbol{x},t) = 0. \end{cases} \tag{1.31}$$

Here, $\boldsymbol{u}(\boldsymbol{x},t)$, $p(\boldsymbol{x},t)$, and $\boldsymbol{f}(\boldsymbol{x},t)$ denote fluid velocity, pressure per unit mass, and an external force per unit mass at a d-dimensional spatial point $\boldsymbol{x} = (x_1,\ldots,x_d)$ and a time t, respectively. ν is a coefficient of kinematic viscosity.

We consider fully developed turbulence, i.e., $\nu \to 0$. At this condition, it is believed that one can regard turbulence as locally homogeneous in regions far from boundaries such as solid walls or free surface. Nevertheless, in this thesis, we restrict the boundary conditions to the periodic boundary conditions in a squared plane for $d = 2$ or in a

cubic box for $d = 3$:

$$\boldsymbol{u}(x_1, \cdots, x_d, t) = \boldsymbol{u}(x_1 + m_1\mathcal{L}_1, \cdots, x_d + m_d\mathcal{L}_d, t), \tag{1.32}$$

for all integers, $m_1, \ldots m_d$. Here $\mathcal{L}_i$ is a positive real number, say, the period. For simplicity, we set $\mathcal{L}_i = \mathcal{L}$ hereafter. There are some reasons why we assume the periodic boundary conditions as below. First, effects of boundaries such as solid walls occur only in the vicinity of the boundaries, say boundary layers [77]. Thus, we expect universal properties of turbulence irrespective of the boundary conditions in domains far from the boundaries. Given that $\mathcal{L}$ is infinitely large, i.e., $\mathcal{L} \to \infty$, the domain filled by the fluid is regarded as infinitely large. Therefore we expect homogeneous turbulence at $\mathcal{L} \to \infty$. Second, for the periodic boundary conditions, we can use the Fourier analysis. It simplifies analytical treatments for the Navier-Stokes equations and facilitates understanding of physics of nonlinearity of turbulence. Third, numerical simulations are more feasible.

In this thesis, we denote the Fourier coefficient of a periodic function $g(\boldsymbol{x})$ with period $\mathcal{L}$ as $\hat{g}(\boldsymbol{k})$, which is defined through the Fourier series in d-dimensional space,

$$g(\boldsymbol{x}) = \left(\frac{2\pi}{\mathcal{L}}\right)^d \sum_{\boldsymbol{k}} \hat{g}(\boldsymbol{k}, t) e^{i\boldsymbol{k}\cdot\boldsymbol{x}}, \tag{1.33}$$

and the inverse transform is

$$\hat{g}(\boldsymbol{k}) = \frac{1}{(2\pi)^d} \int g(\boldsymbol{x}) e^{-i\boldsymbol{k}\cdot\boldsymbol{x}} d\boldsymbol{x}. \tag{1.34}$$

1.4.1 Statistically homogeneous and isotropic turbulence

From now on, we consider more idealized settings. Namely, we assume that the turbulent velocity is statistically homogeneous, i.e., homogeneous turbulence. Strictly speaking, to realize homogeneous turbulence, the fluid fills all of the space with no boundaries. In order to rule out problems at infinity, we assume periodic boundary conditions with the period $\mathcal{L}$, that is, Eq.(1.32) and we can recover the unbounded conditions by letting $\mathcal{L} \to \infty$. In laboratory experiments, it is known that grid turbulence [66] can realize homogeneous turbulence approximately.

In homogeneous turbulence, one-point statistics of velocity is independent of spatial coordinates, $\boldsymbol{x}$. In this thesis, we assume that a mean flow is zero, that is,

$$\langle \boldsymbol{u} \rangle = 0, \tag{1.35}$$

where the bracket $\langle \cdot \rangle$ denotes an ensemble average.

Kinetic energy is input by the external forcing and dissipated by the viscosity of the fluid:

$$\frac{\partial}{\partial t}\left(\frac{1}{2}\langle \boldsymbol{u}^2 \rangle\right) = -\nu \langle \boldsymbol{\omega}^2 \rangle + \langle \boldsymbol{f} \cdot \boldsymbol{u} \rangle. \tag{1.36}$$

Here, $\boldsymbol{\omega} = \nabla \times \boldsymbol{u}$ is vorticity, and $\frac{1}{2}\langle \boldsymbol{\omega}^2 \rangle$ is called enstrophy. Thus, turbulence cannot be maintained unless energy is injected by the external force when the dissipation term, $\nu\langle \boldsymbol{\omega}^2 \rangle$, is finite.

Enstrophy is dissipated by the viscosity of the fluid via palinstrophy $\langle |\nabla \times \boldsymbol{\omega}|^2 \rangle$. On the other hand, enstrophy is input not only by the external force but also by a vorticity stretching:

$$\frac{\partial}{\partial t}\left(\frac{1}{2}\langle \boldsymbol{\omega}^2 \rangle\right) = \langle \boldsymbol{\omega} \cdot \boldsymbol{S} \cdot \boldsymbol{\omega} \rangle - \nu\langle |\nabla \times \boldsymbol{\omega}|^2 \rangle + \langle \boldsymbol{\omega} \cdot (\nabla \times \boldsymbol{f}) \rangle, \tag{1.37}$$

where $\boldsymbol{S} = \{S_{ij}\} = \{\frac{1}{2}(\partial u_i/\partial x_j + \partial u_j/\partial x_i)\}$ is the velocity gradient tensor [128]. The first term in the right-hand side of Eq. (1.37) arises from the nonlinear term and increases with vorticity stretching. It should be noted that for two-dimensional turbulence, the vorticity stretching term is vanished so that the mechanism of maintaining the enstrophy, as well as kinetic energy, is different between two-dimensional (2D) and three-dimensional (3D) turbulence.

In homogeneous turbulence, one-point statistics such as the kinetic energy is constant, and therefore, statistics that characterize the spatial structure of turbulence are multi-point ones. The fundamental one is (second-order) Eulerian velocity correlation tensor:

$$U_{ij}(\boldsymbol{r}) \equiv \langle u_i(\boldsymbol{x} + \boldsymbol{r}, t) u_j(\boldsymbol{x}, t) \rangle, \tag{1.38}$$

which are independent of each spatial points $\boldsymbol{x}$ and $\boldsymbol{x} + \boldsymbol{r}$ and only dependent on the relative distance, $\boldsymbol{r}$, between the two points because of the statistical homogeneity. According to the Navier-Stokes equations (1.31), the Eulerian velocity correlation tensor satisfies the following equation,

$$\left(\frac{\partial}{\partial t} - 2\nu\nabla_k^2\right) U_{ij}(\boldsymbol{r}) = -\nabla_k \left[U_{ik,j}(\boldsymbol{r}) - U_{jk,i}(-\boldsymbol{r})\right] + \langle u_i(\boldsymbol{x}) f_j(\boldsymbol{x}+\boldsymbol{r}) \rangle + \langle u_j(\boldsymbol{x}) f_i(\boldsymbol{x}-\boldsymbol{r}) \rangle, \tag{1.39}$$

where ∇ denotes the gradient vector of $\boldsymbol{r}$, and $U_{ij,k}(\boldsymbol{r})$ is third-order Eulerian velocity correlation tensor:

$$U_{ij,k}(\boldsymbol{r}) = \langle u_i(\boldsymbol{x} + \boldsymbol{r}) u_j(\boldsymbol{x} + \boldsymbol{r}) u_k(\boldsymbol{x}) \rangle. \tag{1.40}$$

It is noted that this equation for the second-order correlation tensor contains the third-order one. Similarly, the equation for the third-order correlation tensor contains the forth-order one, and so forth, ad infinitum. Hence, we cannot calculate any correlation functions unless we give rules or assumptions for closing this infinite chain of coupled equations. The rules for closing the equations have not yet been given deductively from the Navier-Stokes equations.

To simplify calculations, we assume statistical isotropy in strict sense, which requires symmetries with respect to rotation and parity inversion of the coordinate system.

For isotropic turbulence, the degree of freedom of the Eulerian velocity correlation tensor reduces to one dimension and all components are represented by longitudinal

one defined as,

$$U_{LL}(r) = U_{ij}(\boldsymbol{r})\frac{r_i r_j}{r^2}, \tag{1.41}$$

$$U_{LL,L}(r) = U_{ij,k}(\boldsymbol{r})\frac{r_i r_j r_k}{r^2}, \tag{1.42}$$

such as

$$U_{ij}(\boldsymbol{r}) = -\frac{r}{d-1}\frac{\partial}{\partial r}U_{LL}(r)\frac{r_i r_j}{r^2} + \left(1 + \frac{r}{d-1}\frac{\partial}{\partial r}\right)U_{LL}(r)\delta_{ij} \tag{1.43}$$

$$\begin{aligned} U_{ij,k}(\boldsymbol{r}) = {} & \frac{1}{d-1}\left(1 - r\frac{\partial}{\partial r}\right)U_{LL,L}(r)\frac{r_i r_j r_k}{r^3} - \frac{1}{d-1}U_{LL,L}(r)\delta_{ij}\frac{r_k}{r} \\ & + \frac{1}{2}\left(1 + \frac{r}{d-1}\frac{\partial}{\partial r}\right)U_{LL,L}(r)\left(\delta_{ik}\frac{r_j}{r} + \delta_{jk}\frac{r_i}{r}\right). \end{aligned} \tag{1.44}$$

We obtain the so-called Kármán-Howarth equation [62] by substituting these relations to Eq.(1.39) and by calculating straightforwardly,

$$\begin{aligned} U_{LL,L}(r) = {} & 2\nu\frac{\partial}{\partial r}U_{LL}(r) - \frac{1}{r^{d+1}}\int_0^r r_1^{d+1}\frac{\partial}{\partial t}U_{LL}(r_1)\, dr_1 \\ & - \frac{1}{r^{d+1}}\int_0^r 2r_1\int_0^{r_1} r_2^{d-1}\langle u_i(\boldsymbol{x}+\boldsymbol{r}_2)f_i(\boldsymbol{x})\rangle\, dr_2 dr_1. \end{aligned} \tag{1.45}$$

The Kármán-Howarth equation is fundamental to Kolmogorov phenomenology reviewed in next subsection, which gives the assumptions for closing equations by the experimental result which the energy dissipation rate remains finite at $\nu \to 0$.

In the Fourier space, the Navier-Stokes equations (1.31) are represented as,

$$\begin{aligned} \left(\frac{\partial}{\partial t} + \nu k^2\right)\tilde{u}_i(\boldsymbol{k},t) = -\frac{i}{2}P_{ilm}(\boldsymbol{k}) \sum_{\substack{\boldsymbol{p},\boldsymbol{q} \\ (\boldsymbol{k}+\boldsymbol{p}+\boldsymbol{q}=\boldsymbol{o})}} \tilde{u}_l(-\boldsymbol{p},t)\tilde{u}_m(-\boldsymbol{q},t) + P_{il}(\boldsymbol{k})\tilde{f}_l(\boldsymbol{k},t), \\ k_i\tilde{u}_i(\boldsymbol{k},t) = 0, \end{aligned} \tag{1.46}$$

where $P_{ij}(\boldsymbol{k})$ and $P_{ijk}(\boldsymbol{k})$ are tensor operators defined respectively as,

$$P_{ij}(\boldsymbol{k}) = \delta_{ij} - \frac{k_i k_j}{k^2}, \tag{1.47}$$

$$P_{ijk}(\boldsymbol{k}) = k_k P_{ij}(\boldsymbol{k}) + k_j P_{ik}(\boldsymbol{k}). \tag{1.48}$$

In homogeneous turbulence, the Fourier coefficient of the Eulerian velocity correlation tensor is as follows:

$$\tilde{U}_{ij}(\boldsymbol{k},t) = \langle\tilde{u}_i(\boldsymbol{k},t)\tilde{u}_j(-\boldsymbol{k},t)\rangle. \tag{1.49}$$

Furthermore, in isotropic turbulence, the degrees of freedom of this correlation tensor is reduced to one dimension and represented by $\tilde{U}_{ii}(\boldsymbol{k},t)$ or the energy spectrum,

$$E(k) = \int_{|\boldsymbol{k}'|=k}\frac{1}{2}\tilde{U}_{ii}(\boldsymbol{k}')\, dS(\boldsymbol{k}'), \tag{1.50}$$

where the integral on the right hand side is performed on a sphere of radius k. Here, the discrete wavenumber has been changed to a continuous one for the sake of convenience.

The governing equation of the energy spectrum $E(k)$ is as follows:

$$\left(\frac{\partial}{\partial t} + 2\nu k^2\right) E(k) = -\frac{\partial}{\partial k}\Pi(k) + F(k), \tag{1.51}$$

where

$$\Pi(k) = -\frac{1}{2}\left(\frac{2\pi}{\mathcal{L}}\right)^{2d} \sum_{|\boldsymbol{k}'|>k} \sum_{\substack{\boldsymbol{p},\boldsymbol{q} \\ (\boldsymbol{k}'+\boldsymbol{p}+\boldsymbol{q}=\boldsymbol{o})}} \mathrm{Im}\left(P_{ilm}(\boldsymbol{k}')\langle \tilde{u}_i(\boldsymbol{k}')\tilde{u}_l(-\boldsymbol{p})\tilde{u}_m(-\boldsymbol{q})\rangle\right), \tag{1.52}$$

$$F(k) = \int_{|\boldsymbol{k}'|=k} \langle \tilde{f}_i(\boldsymbol{k}')\tilde{u}_i(-\boldsymbol{k}')\rangle dS(\boldsymbol{k}'). \tag{1.53}$$

Here, $\Pi(k)$ is the energy flux function, which represents flux of the energy going to larger wavenumbers than k due to the nonlinear interactions. By integrating Eq.(1.51) in terms of k, we obtain,

$$\Pi(k) = \frac{\partial}{\partial t}\mathscr{E}(k) + 2\nu\Omega(k) - \mathscr{F}(k), \tag{1.54}$$

where

$$\mathscr{E}(k) \equiv \sum_{k'\le k} E(k'), \quad \Omega(k) \equiv \sum_{k'\le k} k'^2 E(k'), \quad \mathscr{F}(k) \equiv \sum_{k'\le k} F(k') \tag{1.55}$$

In this subsection, we have derived the exact relations of statistics of a velocity under the assumptions of statistical homogeneity and isotropy. However, as already mentioned, the equations obtained above are not closed. The assumptions for closing equations have been given by Kolmogorov [69] for 3D turbulence based on the experimental result which the energy dissipation rate remain finite as $\nu \to 0$. Moreover, Kolmogorov [70] have assumed additional conditions, which are called Kolmogorov self-similarity hypothesis, and have performed dimensional analysis of statistics of turbulence.

On the other hand, for 2D turbulence, the situation is quite different. This is because the material derivative of vorticity is zero at the inviscid limit. As a result, n-th moment in terms of vorticity for any n is invariant at the inviscid limit. In particular, the conservation of the second moment, which is called enstrophy, makes it crucially different from 3D turbulence. Therefore, we consider 3D and 2D turbulence separately.

1.4.2 Kolmogorov phenomenology for 3D turbulence

First, we assume that the energy dissipation rate, $\nu\langle\boldsymbol{\omega}^2\rangle$, is finite as $\nu \to 0$, and we denote it by ε. This assumption, at first sight, is doubtful because enstrophy is diverged if ε is finite as $\nu \to 0$. This assumption is based on experiments, where the energy dissipation rate ε is kept constant with decreasing the viscosity ν or increasing

the corresponding Reynolds number. Of course, the energy dissipation rate might be suddenly zero at larger Reynolds number which has not yet been attained at present, but such behavior is not conceivable. Hence, we can still accept this assumption.

This assumption enables us to close the infinite chain of equations. Under this assumption, we can assume that the turbulent velocity is statistically stationary:

$$\frac{\partial}{\partial t}\left(\frac{1}{2}\langle \boldsymbol{u}^2 \rangle\right) = 0, \tag{1.56}$$

which is equivalent to,

$$\varepsilon = \langle \boldsymbol{f} \cdot \boldsymbol{u} \rangle, \tag{1.57}$$

from Eq.(1.36). The right hand side is the energy input rate by the external force. It is finite. Thus, the energy dissipation rate ε should be finite as $\nu \to 0$ in order to realize the statistically stationary state (1.56) at $\nu \to 0$.

Furthermore, we assume that the external force is acting only at large scales, that is the Fourier coefficients of it are non-zero only at small wavenumbers, $k \lesssim k_f \sim 1/L$ [45]:

$$\boldsymbol{f}(\boldsymbol{x}, t) \simeq \sum_{|\boldsymbol{k}|<k_f} \hat{\boldsymbol{f}}(\boldsymbol{k}, t), \tag{1.58}$$

where L is the integral length as defined by [112, 128],

$$L \equiv \frac{1}{U_{LL}(0)} \int_0^\infty U_{LL}(r)\, dr. \tag{1.59}$$

This assumption connects the external forcing terms in Eq.(1.45) and Eq.(1.54) at $r \ll 1/k_f$ and $k \gg k_f$ with the energy dissipation rate such as,

$$\langle \boldsymbol{u}(\boldsymbol{x}+\boldsymbol{r}) \cdot \boldsymbol{f}(\boldsymbol{x}) \rangle \simeq \langle \boldsymbol{u}(\boldsymbol{x}) \cdot \boldsymbol{f}(\boldsymbol{x}) \rangle = \varepsilon, \tag{1.60}$$

$$\mathscr{F}(k) \simeq \sum_{k=0}^{\infty} F(k) = \langle \boldsymbol{u}(\boldsymbol{x}) \cdot \boldsymbol{f}(\boldsymbol{x}) \rangle = \varepsilon. \tag{1.61}$$

As $\nu \to 0$, the viscous terms in Eq.(1.45) and Eq.(1.54) vanish if the following relations hold:

$$\left| 2\nu \frac{\partial U_{LL}}{\partial r} \right| \ll \varepsilon r, \tag{1.62}$$

$$|2\nu\Omega(k)| \ll \varepsilon, \tag{1.63}$$

that is [3] [4],

$$r \gg \lambda, \tag{1.64}$$

$$k \ll \frac{1}{\lambda}, \tag{1.65}$$

where η is the Kolmogorov length as we will define later and λ is the Taylor micro-scale defined as [10, 112],

$$\lambda^2 \equiv -\frac{U_{LL}(0)}{U''_{LL}(0)} = \frac{5\langle \boldsymbol{u}^2 \rangle}{\langle \boldsymbol{\omega}^2 \rangle} = \frac{5\nu\langle \boldsymbol{u}^2 \rangle}{\varepsilon}. \tag{1.66}$$

It is noted that we can define a Reynolds number by using the Taylor micro-scale:

$$\mathrm{Re}_\lambda = \frac{\lambda\sqrt{U_{LL}(0)}}{\nu}, \tag{1.67}$$

which is called Taylor micro-scale Reynolds number.

These equations (1.45) and (1.54) are, therefore, closed by third order quantities, which are $U_{LL,L}(r)$ and $\Pi(k)$ in the intermediate subrange $\lambda \ll r \ll L$ or $k_f \ll k \ll 1/\lambda$. This intermediate range is called the inertial subrange. Here, we introduce the n-th order structure function [5],

$$S_n(r) = \langle [\delta u_L(r)]^n \rangle, \tag{1.68}$$

where $\delta u_L(r) = [\boldsymbol{u}(\boldsymbol{x}+\boldsymbol{r}, t) - \boldsymbol{u}(\boldsymbol{x}, t)] \cdot \boldsymbol{r}/|\boldsymbol{r}|$. Using the structure function, the Kármán-Howarth equation (1.45) leads to[6],

$$S_3(r) \simeq -\frac{4}{5}\varepsilon r \quad \text{at} \quad \lambda \ll r \ll L, \tag{1.69}$$

which is Kolmogorov four-fifth law [69]. Similarly, Eq.(1.54) leads to

$$\Pi(k) \simeq \varepsilon \quad \text{at} \quad k_f \ll k \ll \frac{1}{\lambda}. \tag{1.70}$$

[3] It is not obvious whether relation (1.64) is derived from relation (1.62). If we assume that the ratio, $\varepsilon r/|2\nu\partial U_{LL}/\partial r|$, monotonically increases with r, we can verify that relation (1.64) is a necessary condition for relation (1.62) because $\varepsilon r \sim |2\nu\partial U_{LL}/\partial r|$ at $r \sim \lambda$. Of course, if we adopt the Kolmogorov self-similarity hypothesis as we will describe later, relation (1.62) leads to $r \gg \eta$, where η is the Kolmogorov length as we will defined later.

[4] Relation (1.65) is derived from relation (1.63) via the following inequality:

$$|2\nu\Omega(k)| = \left|2\nu \sum_{k'<k} k'^2 E(k')\right| < \left|2\nu k^2 \sum_{k'} E(k')\right| = \nu k^2 \langle \boldsymbol{u}^2 \rangle,$$

where $\Omega(k)$ is defined in Eq. (1.55).

[5] This is because it is often used instead of the Eulerian velocity correlation function $U_{LL}(r), U_{LL,L}(r)$ as a convention.

[6] Here, $S_2(r) = 2[U_{LL}(r) - U_{LL}(0)]$ and $S_3(r) = -6\, U_{LL,L}(r)$.

This is the intermediate asymptotics for $S_3(r)$ and $\Pi(k)$. Therefore we further expect the self-similarity, especially complete self-similarity for the other quantities in the inertial subrange.

The scaling laws for $S_3(r)$ and $\Pi(k)$ lead to those for the other quantities. In the inertial subrange, we can assume that quantities related to the Eulerian velocity are affected only by the energy dissipation rate ε and the scale r in real space or k in Fourier space. Moreover, if the scale r is smaller than λ or k is larger than $1/\lambda$, the quantities are affected by the viscosity ν in addition to ε and r or k. These assumptions are called the Kolmogorov self-similarity hypothesis [70]. Under the hypothesis, we perform the dimensional analysis for *any* statistics in principle.

For example, the scaling law for the n-th order structure function, $S_n(r)$ is,

$$S_n(r) \simeq \varepsilon^{n/3} r^{n/3} \Phi_n\left(\frac{r}{\eta}\right). \tag{1.71}$$

in the small scale $r \ll L$, where Φ_n is a dimensionless function and η is the Kolmogorov length,

$$\eta \equiv \left(\frac{\nu^3}{\varepsilon}\right)^{1/4}. \tag{1.72}$$

Here, the Kolmogorov length η is estimated as, $\eta \sim \mathrm{Re}_\lambda^{-1/2}\lambda$, from the definitions (1.66) and (1.72). Similarly, the scaling law for the energy spectrum $E(k)$ is

$$E(k) \equiv \varepsilon^{2/3} k^{-5/3} \tilde{\Phi}(\eta k) \tag{1.73}$$

at $k \gg k_f$, where $\tilde{\Phi}$ is a dimensionless function.

Furthermore, the dimensionless function Φ_n and $\tilde{\Phi}$ are finite at a limit $r/\eta \to \infty$ and $\eta k \to 0$, respectively. Then Φ_n and $\tilde{\Phi}$ approach constants C_n and C_K,respectively. Here, C_K is called the Kolmogorov constant. Namely,

$$S_n(r) \simeq C_n \varepsilon^{n/3} r^{n/3} \quad \text{at} \quad \eta \ll r \ll L, \tag{1.74}$$

$$E(k) \simeq C_K \varepsilon^{2/3} k^{-5/3} \quad \text{at} \quad k_f \ll k \ll 1/\eta. \tag{1.75}$$

Therefore, the n-th order structure function, the energy spectrum, and also the other statistics, exhibit the complete self-similarity.

The intermediate scales, $\eta \ll r \ll L$ or $k_f \ll k \ll 1/\eta$, are estimated by a single quantity such as L/η. The ratio, L/η, is also estimated from the dimensional analysis by using the Kolmogorov phenomenology as follows [45]:

$$\frac{L}{\eta} \sim \mathrm{Re}_\lambda^{3/2}. \tag{1.76}$$

For this reason, the Taylor micro-scale Reynolds number Re_λ is frequently used for estimating the width of the inertial range of 3D turbulence.

1.4.3 Kraichnan–Leith–Batchelor phenomenology for 2D turbulence

Next, we review Kraichnan–Leith–Batchelor (KLB) phenomenology for 2D turbulence [11, 75, 78]. The main difference with respect to 3D turbulence is that enstrophy cannot blow up, and thus energy is not dissipated by viscosity at the limit, $\nu \to 0$. This means that the energy transfer to large wavenumber must be accompanied by comparable or greater transfer to small wavenumber [43, 75], see [79] for the detail. On the other hand, enstrophy can be dissipated by the viscosity at the limit, $\nu \to 0$, because of unbounded properties of palinstrophy and the finite enstrophy dissipation rate defined as,

$$\chi \equiv \nu \langle |\nabla \times \boldsymbol{\omega}|^2 \rangle. \tag{1.77}$$

As a result, one-way transfer of enstrophy to large wavenumber is admissible.

Nevertheless, we assume that the energy spectrum exhibits the same scaling law with Kolmogorov phenomenology, that is,

$$E(k) = C\varepsilon^{2/3} k^{-5/3}, \tag{1.78}$$

at a range. In this case, according to the formal calculations [75], the enstrophy flux $Z(k)$ is zero at this range of k. Here, the enstrophy flux, $Z(k)$, is defined as

$$Z(k) = -\frac{1}{2}\left(\frac{2\pi}{\mathcal{L}}\right)^{2d} \sum_{|\boldsymbol{k}'|>k} |\boldsymbol{k}'|^2 \sum_{\substack{\boldsymbol{p},\boldsymbol{q} \\ (\boldsymbol{k}'+\boldsymbol{p}+\boldsymbol{q}=\boldsymbol{o})}} \mathrm{Im}\left(P_{ilm}(\boldsymbol{k}')\langle \tilde{u}_i(\boldsymbol{k}')\tilde{u}_l(-\boldsymbol{p})\tilde{u}_m(-\boldsymbol{q})\rangle\right). \tag{1.79}$$

Furthermore, the energy flux $\Pi(k)$ becomes constant independent of k, that is,

$$\Pi(k) \propto \varepsilon. \tag{1.80}$$

On the other hand, if we assume that the energy spectrum exhibits the following scaling law,

$$E(k) = C'\chi^{2/3} k^{-3}, \tag{1.81}$$

in a range, which is resulted from the dimensional analysis by only using χ and k, the energy flux $\Pi(k)$ is zero in this range of k and the enstrophy flux $Z(k)$ becomes constant independent of k, that is,

$$Z(k) \propto \chi. \tag{1.82}$$

,

If such constant cascades of energy and enstrophy are realized in real physical flows, we expect $\Pi(k)$ is negative and $Z(k)$ is positive for such constant cascades range because of inviscid conservation properties of vorticity as mentioned above. Therefore, when we input energy at narrow high wavenumbers, $k \sim k_f$, by an external forcing, following double cascades are expected,

$$\Pi(k) = -\varepsilon, \quad Z(k) = 0 \quad \text{at} \quad k \ll k_f, \tag{1.83}$$

$$\Pi(k) = 0, \quad Z(k) = \chi \quad \text{at} \quad k \gg k_f. \tag{1.84}$$

The former is the energy inverse-cascade range, and the latter is the enstrophy direct-cascade range. Some experiments and numerical simulations corroborate the presence of the double cascade regimes of 2D turbulence.

As predicted by Kraichnan [75], when the fluid is confined to a finite domain, energy piles up at small wavenumbers because energy cannot dissipate at large scales. To avoid this, one often adds a linear or hypodrag term to the Navier-Stokes equations, which dissipates energy at large scales and enables a statistically steady state. Namely, we consider the following Navier-Stokes equations which are written for the vorticity field ω,

$$\frac{\partial \omega}{\partial t} + (\boldsymbol{u} \cdot \nabla)\omega = \nu \Delta \omega + (-1)^{m+1} \alpha \Delta^{-m} \omega + f_\omega, \tag{1.85}$$

where α is the (hypo)drag coefficient. Here, the linear drag corresponds to $m = 0$ and the hypodrag corresponds to $m > 0$. In this condition, the scaling law for 2D turbulence in the energy inverse-cascade range is consistent with Kolmogorov phenomenology for 3D turbulence except for the cascade direction of energy.

Similarly, we can expect the scaling laws in real space for 2D energy inverse-cascade turbulence. In particular, the constant energy flux leads the exact relation for the third-order structure function [14, 80, 124], that is,

$$S_3(r) = \frac{3}{2} \varepsilon_I r, \tag{1.86}$$

where ε_I is the energy input rate by the external force. Moreover, according to some experimental results of both laboratories [92] and numerical simulations [22, 24], the deviation from the self-similarity such as,

$$S_n(r) \propto \varepsilon_I^{n/3} r^{n/3}, \tag{1.87}$$

is not found in contrast to the 3D turbulence. In this sense, 2D energy inverse-cascade turbulence is an ideal framework for Kolmogorov phenomenology [26].

Here, it should be noted that the Taylor micro-scale Reynolds number Re_λ as defined in Eq. (1.67) is insufficient to characterize the width of the inertial range in 2D turbulence. In 2D turbulence, there are two kinds of inertial range: energy inverse-cascade range and enstrophy direct-cascade range. Accordingly, the number of characteristic length scales of 2D turbulence is larger than that of 3D turbulence due to the double cascades. Thus, another Reynolds number is required in order to characterize the double cascades. A candidate for the additional Reynolds number Re_Λ and an associated micro scale Λ is, in analogy with the Taylor micro-scale Reynolds number, as follows [53, 115]:

$$\mathrm{Re}_\Lambda \equiv \frac{(\Lambda \langle \omega^2 \rangle^{1/2}) \Lambda}{\nu}, \tag{1.88}$$

$$\Lambda^2 \equiv \frac{\langle \omega^2 \rangle}{\langle |\nabla \omega|^2 \rangle}. \tag{1.89}$$

This Reynolds number Re_Λ is estimated by the dimensional analysis using the KLB phenomenology as,

$$\mathrm{Re}_\Lambda \simeq \left(\frac{k_\eta}{k_\chi}\right)^6, \tag{1.90}$$

where $k_\eta \sim 1/\eta$ is a characteristic wavenumber of the energy dissipation called the Kolmogorov wavenumber and $k_\chi \equiv (\chi/\nu^3)^{1/6}$ is a characteristic wavenumber of the enstrophy dissipation. Moreover, as well as Eq.(1.76) for 3D turbulence, the Taylor micro-scale Reynolds number Re_λ is also estimated as $\mathrm{Re}_\lambda \sim (L/\eta)^{2/3}$ in 2D turbulence. Therefore, Taylor micro-scale Reynolds number Re_λ represents the intermediate range between the integral scale and energy dissipative scale while the additional Reynolds number Re_Λ represents that between the energy dissipative scale and the enstrophy dissipative scale. However, the energy inverse-cascade range and the enstrophy direct-cascade range do not correspond to these intermediate ranges. In particular, these Reynolds numbers have no information on the forcing scale, which is crucial for the double cascades in 2D turbulence. The forcing wavenumber k_f divides the double cascade ranges. Therefore, we require different Reynolds numbers in order to estimate the width of the two cascade ranges, which should include the forcing wavenumber k_f..

For this reason, the following Reynolds numbers are used for characterizing the double cascades in 2D turbulence:

$$\mathrm{Re}_\alpha \equiv \frac{k_f}{k_\alpha}, \tag{1.91}$$

$$\mathrm{Re}_\chi \equiv \frac{k_\chi}{k_f}, \tag{1.92}$$

where $k_\alpha \equiv (\alpha^3/\varepsilon)^{1/(6m+2)}$ is frictional wavenumber which is a characteristic wavenumber of the (hypo)drag term. The former is called the infrared Reynolds number [116] and characterizes the width of the energy inverse-cascade range. The latter may characterize the width of the enstrophy direct-cascade range. Especially, numerical simulations which we will perform in Chapter 2 and Chapter 3 resolve only the energy inverse-cascade range, i.e., $k_f \sim k_\chi$ so that we only use the infrared Reynolds number Re_α in this thesis.

1.4.4 Comparison with experimental results

We compare the phenomenology for both 2D and 3D turbulence with some experimental results of laboratories and numerical simulations. For 3D turbulence, many laboratory experiments and numerical simulations were performed and showed the consistent scaling laws for energy spectrum, energy flux, and velocity structure functions etc. with Kolmogorov phenomenology, and also the intermittency which is the deviation from Kolmogorov phenomenology, see [54, 108, 128] for review.

KLB phenomenology for 2D turbulence is less certain than Kolmogorov phenomenology for 3D turbulence as reviewed in 1.4.3. However, surprisingly, a lot of experimental

studies reported that the scaling laws for the energy spectrum, the energy flux, the velocity structure functions, etc., are consistent with those of KLB phenomenology: see [31, 44, 93, 94, 101, 102, 119] for the details of the results of laboratory experiments and [20, 22, 24, 31, 46, 114] for those of numerical simulations.

Some numerical simulations of 2D turbulence are performed by the modified Navier-Stokes equations with the hyperviscous term, $(-1)^{h+1}\nu\nabla^{2h}\boldsymbol{u}(\boldsymbol{x},t)\,(h>1)$, instead of the normal Laplacian term because the hyperviscosity can reduce the range of scales which the dissipative term influences. In these simulations, the same scaling laws are observed [38, 39, 85, 116, 122]. Therefore, it is considered that the hyperviscosity does not influence the scaling exponents in the energy inverse-cascade range at least. In Chapter 2, we verify that the hyperviscosity at $h=8$ does not also influence the scaling properties of turbulent relative dispersion in 2D energy inverse-cascade turbulence by comparing with a normal viscous simulation. See [23, 63, 109] for the other topics of 2D turbulence such as methods of experiments in laboratories, numerical simulation methods, non-local effects of the external forcing, vortex condensates, and free-intermittency nature of 2D turbulence.

1.5 Turbulent relative dispersion

We review phenomenology of turbulent relative dispersion and its comparison with experiments. Here, we consider statistics on relative motions of Lagrangian particle pairs, i.e., the particle pairs that are passively advected by turbulent velocity. We just call Lagrangian particle pairs particle pairs hereafter. The equation of motion is as follows:

$$\frac{d}{dt}\boldsymbol{r}(t)=\delta\boldsymbol{v}(t). \tag{1.93}$$

Here, $\boldsymbol{r}(t)\equiv\boldsymbol{X}(\boldsymbol{x}+\boldsymbol{r}_0,s|t)-\boldsymbol{X}(\boldsymbol{x},s|t)$ is a relative separation of a particle pair which is initially, i.e., at time s, separated by $\boldsymbol{r}_0$, and $\delta\boldsymbol{v}(t)\equiv\boldsymbol{v}(\boldsymbol{x}+\boldsymbol{r}_0,s|t)-\boldsymbol{v}(\boldsymbol{x},s|t)$ is its relative velocity, which corresponds to the Eulerian velocity increment at time t, $\delta\boldsymbol{v}(t)=\boldsymbol{u}(\boldsymbol{X}(\boldsymbol{x}+\boldsymbol{r}_0,s|t),t)-\boldsymbol{u}(\boldsymbol{X}(\boldsymbol{x},s|t),t)$. By integrating Eq.(1.93), we obtain

$$\boldsymbol{r}(t)=\boldsymbol{r}_0+\int_s^t\delta\boldsymbol{v}(t')\,dt'. \tag{1.94}$$

In this section, first, we consider the PDF and its moments of the relative separation of particle pairs. Throughout this section, except for the final subsection, we assume their self-similarity in time. We review the scaling laws of turbulent relative dispersion obtained from so-called Richardson phenomenology under this assumption. Although this assumption is historically standard, it seems to be inconsistent with experimental data. Recently, some numerical studies reported the deviation from the self-similarity due to extreme events of the motions of particle pairs [16, 105].

Second, we consider the exit-time statistics. The exit-time statistics have different features and advantages from the PDF and its moments of the relative separation of particle pairs.

Finally, we review some experimental results of both laboratory experiments and numerical simulations. Here we compare the phenomenology introduced in this section with the experimental results.

1.5.1 Richardson phenomenology

Richardson [98] proposed the following diffusion equation for the PDF of relative separation of particle pairs, $p(r,t)$,

$$\frac{\partial}{\partial t}p(r,t) = \frac{1}{r^{d-1}}\frac{\partial}{\partial r}\left(r^{d-1}D(r)\frac{\partial}{\partial r}p(r,t)\right), \tag{1.95}$$

where $D(r)$ is a scale-dependent diffusion coefficient. Furthermore, he suggested empirically,

$$D(r) = D_0 r^{4/3}, \tag{1.96}$$

where D_0 is a constant. It is noted that this four-thirds law for the diffusion coefficient $D(r)$ is also obtained by simple dimensinal analysis [87].

This diffusion equation with the initial condition, $p(r,0) = \delta(r - r_0)$, can be analytically solved and provides a self-similar solution at asymptotically large time [4, 105],

$$p(r,t) \propto \frac{r^2}{\langle r^2(t)\rangle^{3/2}} \exp\left[-A\left(\frac{r}{\langle r^2(t)\rangle^{1/2}}\right)^{2/3}\right], \tag{1.97}$$

with

$$\langle r^2(t)\rangle \propto t^3. \tag{1.98}$$

Here, A is a constant. Hence, in this model, particle pairs separate in a super-diffusive way and forget the initial separation r_0 at large time. Moreover, this model provides a self-similarity for the moments of relative separation $r(t)$,

$$\langle r^n(t)\rangle = \langle r^2(t)\rangle^{n/2} \propto t^{3n/2}. \tag{1.99}$$

Therefore, we can only consider $\langle r^2(t)\rangle$. In this thesis, we call the self-similar PDF (1.97) the Richardson self-similar PDF and the t^3 scaling (1.98) the Richardson–Obukhov law [103, 123][7].

As mentioned in the following subsection, the results of Richardson phenomenology are also derived via Kolmogorov phenomenology [70, 87]. Because of this, the Richardson phenomenology has been widely accepted in spite of inconsistency with recent experimental results.

[7] It should be noted that Yaglom [123] originally suggested that the four-thirds law for the diffusion coefficient $D(r)$, i.e., Eq. (1.96), should be called the Richardson–Obukhov law. On the other hand, the dimensional analysis by Kolmogorov phenomenology [70, 87] can derive both scaling laws (1.96) and (1.98). Therefore, in this thesis, we refer to the t^3 scaling law (1.98) as the Richardson–Obukhov law following convention [103].

1.5.2 Obukhov–Batchelor phenomenology via Kolmogorov phenomenology

Here, we apply Kolmogorov phenomenology to the turbulent relative dispersion [8, 87]. First, we assume the self-similarity for the moments of relative separation, namely, we assume the following relations:

$$\langle r^p(t)\rangle \simeq \langle r^2(t)\rangle^{p/2}. \tag{1.100}$$

Thus, we only deal with the mean square $\langle r^2(t)\rangle$.

Second, we also assume that all particle pairs are always in the inertial subrange, that is

$$\eta \ll r(t) \ll L, \tag{1.101}$$

or we assume the mean square $\langle r^2(t)\rangle$ is at least in the inertial subrange,

$$\eta \ll \langle r^2(t)\rangle^{1/2} \ll L, \tag{1.102}$$

Here, η is the Kolmogorov length (1.72) and L is the integral length (1.59), which is maximum characteristic length scale of turbulence. The intermediate range (1.102) may correspond to the intermediate range (1.101) if the self-similarity (1.100) holds. In particular, we assume that the initial separation r_0 is also in the inertial subrange:

$$\eta \ll r_0 \ll L. \tag{1.103}$$

On the other hand, statistics on the relative dispersion are dependent on time unlike the statistics on the Eulerian velocity. We would like to carry out intermediate asymptotics in terms of time scales. Thus, we introduce three time scales,

$$T_B = \left(\frac{r_0}{\varepsilon^{1/2}}\right)^{2/3}, \tag{1.104}$$

$$T_\eta = \left(\frac{\eta}{\varepsilon^{1/2}}\right)^{2/3}, \tag{1.105}$$

$$T_L = \left(\frac{L}{\varepsilon^{1/2}}\right)^{2/3}, \tag{1.106}$$

where T_B is the characteristic time scale of the initial separation r_0 called the Batchelor time, T_η is the characteristic time scale of the energy dissipation called the Kolmogorov time scale, and T_L is the integral time scale. Using these time scales, we carry out the intermediate asymptotics at

$$T_\eta \ll t \ll T_L, \quad \text{and,} \quad T_\eta \ll T_B \ll T_L. \tag{1.107}$$

Note that the former in (1.107) may correspond to relation (1.101) or (1.102) and the latter corresponds to relation (1.103). It is noted that the former cannot be directly derived from (1.101) or (1.102) unlike relation between the latter and (1.103).

Finally, we assume that we can apply Kolmogorov or KLB phenomenology to the time derivative of $\langle r^2(t)\rangle$. Thus, we apply Buckingham Π-theorem to the following equation,

$$\frac{d}{dt}\langle r^2(t)\rangle = G(t, \varepsilon, T_B, T_\eta, T_L), \tag{1.108}$$

where G is an unknown function with five arguments. Here we notice that there are two ways in the intermediate asymptotics, that is, we can carry out the intermediate asymptotics in both the intermediate ranges,

$$T_\eta \ll t \ll T_B \ll T_L, \tag{1.109}$$

$$T_\eta \ll T_B \ll t \ll T_L, \tag{1.110}$$

and the results obtained are different from each other.

Batchelor regime

In the intermediate range (1.109), the Π-theorem provides a dimensionless relation,

$$\left(\frac{1}{\varepsilon T_B^2}\right)\frac{d}{dt}\langle r^2(t)\rangle = \Phi_1\left(\frac{t}{T_B}, \frac{T_\eta}{T_B}, \frac{T_L}{T_B}\right), \tag{1.111}$$

Here we assume complete similarity at small value of T_η/T_B and large value of T_L/T_B but *incomplete similarity* at small value of t/T_B. Hence, Φ_1 has no finite limit at $t/T_B \to 0$. We, furthermore, assume the generalized homogeneity in terms of Φ_1, that is,

$$\Phi_1\left(\frac{t}{T_B}, \frac{T_\eta}{T_B}, \frac{T_L}{T_B}\right) \simeq \left(\frac{T_B}{t}\right)^p \Phi_1^*\left(\frac{T_\eta}{T_B}, \frac{T_L}{T_B}\right). \tag{1.112}$$

As described later, we can obtain the value of p from physical considerations, i.e., $p = -1$. We assume complete similarity for T_η and T_L so that Φ_1^* has a non-zero and finite limit, say $2C$. As a result, in the intermediate range (1.109), the scaling law for $\langle r^2(t)\rangle$ is,

$$\langle r^2(t)\rangle \simeq r_0^2 + C\varepsilon T_B t^2. \tag{1.113}$$

In this thesis, this ballistic scaling law for $\langle r^2(t)\rangle$ is called Batchelor scaling law.

Richardson-Obukhov regime

On the other hand, in the intermediate range (1.110), the Π-theorem provides a dimensionless relation,

$$\left(\frac{1}{\varepsilon t^2}\right)\frac{d}{dt}\langle r^2(t)\rangle = \Phi_2\left(\frac{T_B}{t}, \frac{T_\eta}{t}, \frac{T_L}{t}\right). \tag{1.114}$$

We assume complete similarity at large values of t/T_B and T_L/t, and small value of T_η/t, and therefore, Φ_2 has non-zero and finite limit, say $3g$. As a result, in the intermediate range (1.110), the scaling law for $\langle r^2(t)\rangle$ is,

$$\langle r^2(t)\rangle = g\varepsilon t^3, \tag{1.115}$$

which is Richardson–Obukhov law. Here, the universal constant g is called the Richardson constant. This is consistent with the results from Richardson phenomenology. At this regime, we use complete similarity for all of the arguments, T_B/t, T_η/t, and T_L/t. In terms of experimental asymptotics, we should verify that the resulted scaling law, i.e., Eq.(1.115), is consistent with the experimental data. However, the above complete similarity for $\langle r^2(t)\rangle$ is not verified by the experimental data, and therefore we should assume incomplete similarity, as we will discuss in Chapter 3.

Physical interpretations

We provide physical interpretations to the results of intermediate asymptotics (1.113) and (1.115). The mean square $\langle r^2(t)\rangle$ follows,

$$\frac{d}{dt}\langle r^2(t)\rangle = \boldsymbol{r}_0 \cdot \langle \delta\boldsymbol{v}(t)\rangle + 2\int_s^t \langle \delta\boldsymbol{v}(t)\cdot\delta\boldsymbol{v}(t')\rangle\, dt', \tag{1.116}$$

where s is the initial time, when particle pairs are loosed with an initial separation $r_0 = |\boldsymbol{r}_0|$. Hereafter, we set $s = 0$. Here we assume that the first term in the right hand side is so smaller than the second term that we can ignore the first term:

$$\frac{d}{dt}\langle r^2(t)\rangle \simeq 2\int_0^t \langle \delta\boldsymbol{v}(t)\cdot\delta\boldsymbol{v}(t')\rangle\, dt'. \tag{1.117}$$

In the intermediate range (1.109), in particular, at $t \ll T_B$, particle pairs almost persist their initial relative velocity, i.e.,

$$\langle \delta\boldsymbol{v}(t)\cdot\delta\boldsymbol{v}(t')\rangle \simeq \langle \delta\boldsymbol{v}^2(0)\rangle. \tag{1.118}$$

At the initial time, the relative velocity of particle pairs corresponds to the Eulerian velocity increment separated by r_0. Therefore we can apply Kolmogorov phenomenology,

$$\langle \delta\boldsymbol{v}^2(0)\rangle \simeq C\varepsilon^{2/3} r_0^{2/3}. \tag{1.119}$$

By substituting this and integrating Eq.(1.118), we obtain the same result as Eq.(1.113). Here, we set $t = 0$ in the right hand side of Eq.(1.118), and then the right hand side becomes zero. This is the reason why the complete similarity for small value of T_B/t fails.

On the other hand, the physical interpretation for Eq.(1.115) is more difficult. It seems that additional assumptions are required. Then, we rewrite Eq.(1.118) as,

$$\frac{d}{dt}\langle r^2(t)\rangle \simeq 2\langle \delta\boldsymbol{v}^2(t)\rangle \int_0^t g(t,t')dt', \tag{1.120}$$

$$g(t,t') \equiv \frac{\langle \delta\boldsymbol{v}(t)\cdot\delta\boldsymbol{v}(t')\rangle}{\langle \delta\boldsymbol{v}^2(t)\rangle}. \tag{1.121}$$

We assume that the correlation function $g(t, t')$ decays rapidly more than exponentially with increasing $t - t'$, and the time scale of its decay is represented as $\tau(t)$. Hence, we assume that the correlation function is as follows:

$$g(t, t') = \Psi\left(\frac{t - t'}{\tau(t)}\right). \tag{1.122}$$

Under these assumptions, the time-dependent variables can be taken out of the integral in Eq.(1.120):

$$\frac{d}{dt}\langle r^2(t)\rangle \simeq 2\left(\int_0^\infty \Psi(x)\ dx\right)\ \langle \delta \boldsymbol{v}^2(t)\rangle\ \tau(t). \tag{1.123}$$

Moreover, we assume that $\langle \delta \boldsymbol{v}^2\rangle$ and $\tau(t)$ have Kolmogorov like scalings:

$$\langle \delta \boldsymbol{v}^2(t)\rangle \simeq \varepsilon^{2/3}\langle r^2(t)\rangle^{1/3}, \quad \tau(t) \simeq \varepsilon^{-1/3}\langle r^2(t)\rangle^{1/3}, \tag{1.124}$$

which may correspond to the intermediate asymptotics at (1.102). By substituting them into and integrating Eq.(1.123), we can obtain Eq.(1.115). It is unclear whether these assumptions are allowed. The relative velocity $\delta \boldsymbol{v}(t)$ is essentially nonstationary. Nevertheless, the assumption (1.122) does not contain information about the time evolution in the direction of $t - t'$. We discuss the nonstationarity of the velocity correlation in Chapter 3.

1.5.3 Exit-time statistics

So far, we only consider the probability distribution function and its moments of the relative separation of particle pairs. Although, in stochastic dynamics, moments and probability distribution function are important characteristic quantities to feature the stochastic properties, it is useful to consider the other characteristic quantities. One of these quantities is mean exit time. Another is escape probability.

Exit time, $T_E(R, \rho)$, is defined as,

$$T_E(R, \rho) \equiv T_F(\rho R) - T_F(R), \tag{1.125}$$

where ρ is a constant slightly larger than 1, and $T_F(R)$ is the time when a relative separation of a particle pair reaches a threshold, R, for the first time, so-called first-passage time [3, 21, 25, 26]. The mean exit time is its ensemble average.

As well as the moments, we can apply Kolmogorov phenomenology to the mean exit time. From the dimensional analysis by means of Kolmogorov phenomenology,

$$\langle T_E(R, \rho)\rangle \simeq \varepsilon^{1/3} R^{2/3}. \tag{1.126}$$

It should be noted that the ensemble average in the left hand side is different from that for the moments of the relative separation of particle pairs at time t. It is rather similar to the ensemble average for the Eulerian velocity increments separated by r because both are given the scale in advance.

The scaling law (1.126) is observed at recent experiments and numerical simulations unlike the Richardson–Obukhov law. This is an advantage of mean exit time, but the reason is unclear why the scaling law (1.126) can be observed while the Richardson–Obukhov law cannot. Considering that, as mentioned above, the ensemble average for mean exit time is similar to that for the Eulerian velocity, we can infer that Kolmogorov scaling, which means scaling relations resulted from Kolmogorov phenomenology, can be observed when the corresponding quantity is related only to a single scale whether it is Eulerian or Lagrangian Anyway, it is difficult to consider a bridging relation between mean exit time and the moments of the relative separation.

Another quantity is escape probability, which is the probability of time when a particle pair starting from a separation R exits a threshold ρR first. In the current case, it is defined as the PDF of exit time. We denote it as $P_E(T_E|R,\rho)$.

The escape probability is calculated if the evolution equation for the PDF of the relative separation, $p(r,t)$ is given. The initial condition is $p(r,0) = \delta(r-R)$. The boundary conditions are the reflecting condition at $r = 0$ and the absorbing condition at $r = \rho R$. Then the relationship between $P_E(T_E|R,\rho)$ and $p(r,t)$ is as follow:

$$P_E(T_E|R,\rho) = -\frac{d}{dt}\int_{r<\rho R} p(r,t)\, dr\Big|_{t=T_E}. \tag{1.127}$$

Therefore we obtain the relationship between the exit-time statistics and the PDF of the relative separation though the time evolution of the PDF should be given in advance.

It is interesting to consider bridging relations between the PDF of the relative separation and the mean exit time or the escape probability. In Chapter 2, we introduce a conditional sampling method via exit-time statistics. It is used to recover the Richardson–Obukhov law at moderate Reynolds numbers which we can attain at present. Furthermore, it may be possible to obtain the relation between them numerically. The detail discussions are given in Chapter 4.

1.5.4 Experimental results

Square mean of relative separation

We survey comparison between the above phenomenology and experimental results. For 2D turbulence, in laboratory experiments, Jullien *et al.* [56] and Von Kameke *et al.* [119] observed the clear t^3 scaling for the mean square of relative separations of particle pairs and also estimated the Richardson constant. On the other hand, these results are puzzling because at these experiments, the initial separation of particle pairs is smaller than the inertial subrange, that is within the enstrophy cascade range or the dissipation range, as pointed out by Kellay & Goldburg [63]. Moreover, the initial separation dependence for the mean square $\langle r^2(t)\rangle$ is observed in the inertial subrange in other experiments [99, 100] and DNS for 2D energy inverse-cascade turbulence [26]. Boffetta & Sokolov [26] state that this initial separation dependence is resulted from the finite size effect of the inertial subrange because mean exit time exhibits the consistent

scaling with Kolmogorov phenomenology. Hence, the t^3 scaling observed in [56, 119] is probably due to the initial separation dependence. Here, it is noticed that the t^3 scaling for $\langle r^2(t)\rangle$ can be observed by carefully selecting a special value of the initial separation. However, it is unclear whether this t^3 scaling is consistent with the Richardson–Obukhov law.

For 3D turbulence, similar results are obtained. Ott & Mann [90] performed laboratory experiments at $\mathrm{Re}_\lambda = 78$ to 104. They performed a time shift $\tau = t - T_0$ for observing the t^3 scaling, where T_0 is estimated by the zero crossing of a linear fit of $\langle r^2(t)\rangle^{1/3}$ in the inertial subrange. The other experiments at $\mathrm{Re}_\lambda = 172$ by Berg *et al.* [13] also obtained similar results by introducing the shift. On the other hand, Bourgoin [28] and Ouellette *et al.* [91] performed laboratory experiments at $\mathrm{Re}_\lambda = 200$ to 815 but did not observe the Richardson–Obukhov t^3 law. They inferred that this is due to the finite size effect of the inertial subrange, that is decorrelation of relative velocity of particle pairs at the integral length.

Similarly, there are many DNS investigations of turbulent relative dispersion in 3D turbulence. Yeung [125] performed the DNS of 3D turbulence at $\mathrm{Re}_\lambda \sim 90$. Yeung [125] confirmed the Batchelor ballistic regime and normal diffusion beyond the integral scale, but did not observe the Richardson–Obukhov law. Yeung [125] also stated that the scaling exponent of $\langle r^2(t)\rangle$ is different depending on the initial separation. Such an initial separation dependence is also observed at the other DNS investigations [15, 19, 25, 30, 32, 33, 104, 126]. Ishihara & Kaneda [55] performed the DNS of 3D turbulence at $\mathrm{Re}_\lambda = 283$ and were convinced that the Richardson–Obukhov law is observed through the graph of $\langle r^2(t)\rangle^{1/3}$ similar to Ott & Mann [90] but this is not recommended because the time scale expected for the Richardson–Obukhov law is ambiguous as pointed out by Salazar & Collins [103]. Furthermore, there also exists the special value of the initial separation where the t^3 scaling is observed as well as 2D turbulence. Such an initial separation is around 3η to 4η from DNS data [15, 19, 30], where η is the Kolmogorov length. Recent DNS with high resolutions [30, 32, 33, 104] showed that the mean square asymptotically approaches the Richardson–Obukhov as increasing Reynolds number.

Therefore, for both laboratory experiments and numerical simulations, and for both 2D and 3D turbulence, the Richardson–Obukhov law for the mean square of relative separations of particle pairs, $\langle r^2(t)\rangle$ has never been clearly observed in the sense that the mean square $\langle r^2(t)\rangle$ becomes independent of the initial separation r_0 and exhibits t^3 scaling law in the inertial subrange. Almost all previous studies inferred that this is due to the finite size effects of the inertial subrange. However, there is no quantitative investigation of the finite size effects.

Exit-time statistics

On the other hand, the scaling law for the mean exit time is more clearly observed for both 2D [25, 89, 100] and 3D turbulence [15, 16, 26, 91]. This is perhaps because the exit-time statistics are more robust at finite Reynolds numbers. This clear scaling of mean exit time enables us to estimate the Richardson constant via the mean exit time.

It is noted that the Richardson constant is the universal constant, g, in Eq. (1.115). In fact, the Richardson constant is estimated as $g \sim 4$ in 2D turbulence and $g \sim 0.5$ in 3D turbulence. These studies also observe that the PDF of the exit time is self-similar in scale. However, recent DNS [16] showed the breaking of the self-similarity at large exit time.

Probability distribution function and higher moments of relative separation

In terms of the PDF of relative separations of particle pairs, the situation is more complicated. A central part of the PDF is approximately in agreement with the Richardson self-similar one for both 2D [25, 56, 99] and 3D turbulence [16, 19, 90, 91, 104, 105]. On the other hand, these studies confirmed that the central part is consistent with the Richardson self-similar PDF from the log-log plots of the PDF. Strictly speaking, the log-log plots of the experimental data are slightly different from the Richardson self-similar PDF. Although the difference is very small in the log-log plots, it appears to be larger in the log-lin plots. Therefore, it is probably necessary to investigate the central part by laboratory and numerical experiments at higher Reynolds numbers in order to confirm the consistency of the central part with the Richardson self-similar PDF.

According to the Richardson self-similar PDF the higher moments are dependent on the mean square and thus the scaling exponents are proportional to that of the mean square. However, these behaviors of the higher moments are not shown [15, 16, 19, 30, 32]. These higher moments are more influenced by large-separation pairs. Thus, these deviations from the self-similarity may be due to finite size effects of the inertial subrange. The deviation from the Richardson self-similar PDF is also confirmed directly by the tails of PDF of relative separations of particle pairs [15, 16, 19, 25, 32, 91, 99, 104, 105]. Furthermore, it is shown that the PDF deviates from the Richardson PDF at very small separations as well as very large separations in 2D turbulence [25, 99] and, in 3D turbulence [15, 16, 19, 32, 91, 104, 105]. These parts deviated from the self-similarity are strongly dependent on the initial separations.

1.5.5 Debates on Richardson phenomenology

Here we reconsider Richardson phenomenology, i.e., the Richardson–Obukhov law and Richardson self-similar PDF according to the experimental results.

Richardson–Obukhov law

Although the Richardson–Obukhov law for the mean square of relative separations of particle pairs has not been clearly observed, a few studies considered quantitatively the reasons of the deviation from the Richardson–Obukhov law. Boffetta & Sokolov [26] discussed the finite-size effects of the inertial subrange on the mean square, $\langle r^2(t) \rangle$ according to the results of the numerical simulations of a synthetic velocity field [3, 21].

In the synthetic velocity filed with sufficiently large shells, the expected scaling exponent for the mean square is observed though it is not observed for smaller shells, and instead, a different scaling exponent is estimated. They stated that this is due to a crossover of two or more different ranges: a range where the mean square grows exponentially, a range where it exhibits normal diffusion, and the inertial subrange. They concluded that the crossover is also the case for the turbulent velocity field because the inertial subrange is more limited in the laboratory experiments and numerical simulations.

It is obvious that some particle pairs are in the dissipation subrange and other particle pairs are in the large-scale range even when the mean square is within the inertial subrange. Thus, the finite-size effects due to the crossover seem to be plausible. However, we cannot estimate the value of the Reynolds number where the finite-size effects disappear, from the above consideration. This is because the Richardson–Obukhov law becomes valid only at infinite Reynolds number if Richardson phenomenology is valid. Moreover we cannot perform an asymptotic analysis for the mean square in the inertial subrange.

The crossover may be related to the mean-field approximation such as Eq.(1.124). This approximation is efficient to perform the dimensional analysis by means of Kolmogorov phenomenology because only one spatial length, $\langle r^2(t)\rangle^{1/2}$, appears explicitly. On the other hand, the approximation seems to contradict the crossover effects, which are intrinsically related to multi spatial scales. Recently more quantitative discussion are given by [41] in terms of the PDF of relative separations. However, it is not obvious how strongly the mean-filed approximation affects the mean square of the relative separation.

In such a situation, the problems to consider are as follows:

- to justify or invalidate the Richardson–Obukhov law at infinite Reynolds number.
- to estimate quantitatively the deviations from the Richardson–Obukhov law at finite Reynolds numbers.
- to estimate the crossover effects, which are probably the non-local effects between particle pairs whose separations are quite different.

In Chapter 2, we investigate numerically the Richardson–Obukhov law by means of conditional sampling methods and gain an insight not to rule out the possibility that the Richardson–Obukhov law is recovered at infinite Reynolds number according to non-Kolmogorov scaling of the relative velocity of particle pairs. Furthermore, in Chapter 3, we improve the Richardson–Obukhov law to be consistent with the experimental data even at finite Reynolds number based on the DNS data. According to the results in Chapters 2 and 3, we estimate qualitatively the crossover effects in terms of the final problem in Chapter 4.

Richardson self-similar PDF

In terms of the PDF of the relative separation of particle pairs, similar problems have been considered. Falkovich *et al.* [42] showed that the diffusion equation with scale-dependent diffusivity is exactly derived in the Kraichnan model [76], which is the Gaussian random velocity field with white noise in time. Nevertheless, this diffusion equation has a self-similar solution different from the Richardson one. As a result, the mean square is not proportional to t^3. The reason is that the temporal correlation of the velocity cannot be ignored as pointed out in [42]. It is noted that this fact does not require the validity of the Richardson diffusion equation to be delta-correlated velocity as carefully discussed by Eyink & Benveniste [41]. They concluded that the short-memory approximation is not necessary to obtain the Richardson diffusion equation.

The importance of the velocity temporal correlation was corroborated by Chaves *et al.* [36], who modified the Kraichnan model to be time correlated by using the Ornstein–Uhlenbeck type noise in time. On the other hand, this modified version of the Kraichnan model has still a different time correlation from that of Lagrangian turbulence. In Lagrangian turbulence, the time correlation develops in time. Namely, turbulent relative dispersion is an aging phenomenon. The aging effects on the turbulent relative dispersion have never been considered. In Chapter 3, we proposed a scaling relation of the velocity correlation function. There, we consider the aging effects explicitly.

Although the temporal correlation of the velocity is crucial to the scaling exponents, it does not probably lead the breaking of the self-similarity as observed in laboratory experiments and numerical simulations at finite Reynolds numbers. According to these experimental data, in particular, [16, 105], the breaking of the self-similarity, i.e, the deviations from the Richardson self-similar PDF, especially occurs at very large separations and very small separations, namely, right and left tails of the PDF. Furthermore, these tails are strongly dependent on the initial separations. This does not immediately mean that Richardson phenomenology is incorrect because such large or small separations are outside the inertial subrange, where Richardson phenomenology cannot be applied. Nevertheless, we do not conclude that these deviations are due to the finite-size effects of the inertial subrange because these particle pairs were in the inertial subrange at initial time and escaped from there by dynamics in the inertial subrange. Otherwise, these particle pairs are influenced by non-locality of turbulence. To our knowledge, nobody clearly understands the reasons why the tails of the PDF break the self-similarity. In Chapter 4, we consider these problems according to the results in Chapter 2 and 3.

1.6 Organization of the thesis

This thesis is composed of four chapters. Chapter 1 is **General Introduction** as already described above. Chapter 2 is entitled **Conditional sampling method via exit-time statistics**. There, we develop a conditional sampling method by which

the mean square of the relative separations of particle pairs exhibits the t^3 scaling for any initial separations. This method reveals the anomalous scaling of the conditional mean square of the relative velocity of particle pairs deviated from the prediction of Kolmogorov phenomenology. Chapter 3 is entitled **Two-time Lagrangian velocity correlation function**. There, we investigate the two-time Lagrangian velocity correlation function [55] and propose its scaling law by means of incomplete similarity. Then, we confirm that the proposed scaling law of the two-time Lagrangian velocity correlation function is consistent with the experimental data of numerical simulations in two-dimensional energy inverse-cascade turbulence. These two chapters are the main parts of this thesis. Chapter 4 is **General Conclusion**, where we discuss the results obtained the previous chapters and show some future prospects.

Chapter 2

Conditional sampling method via exit-time statistics

2.1 Introduction

Relative dispersion has been widely investigated following a pioneering study by Richardson [98], who observed the super-diffusive manner of separation between two particles in the atmosphere. The study introduced the diffusion-type differential equation for the probability distribution function (PDF) of separation, r. A significant part of this equation is that it includes the diffusion coefficient dependent on r itself. Furthermore, Richardson predicted the celebrated t^3 law of the second-order moment of the relative separation from the PDF, $\langle r^2(t)\rangle \propto t^3$, and this is referred to as the Richardson–Obukhov law. The scaling argument leading to this law (which was developed first for the three dimensional (3D) turbulence) can be applicable to two-dimensional (2D) turbulence, as reviewed in Ref. [103]. In this study, we restrict our attention to the relative dispersion in 2D turbulence.

The t^3 prediction was performed prior to Kolmogorov phenomenology for 3D turbulence proposed in 1941 (K41) [70], and later demonstrated as consistent with the K41 dimensional analysis [8, 87]. With respect to the 2D turbulence, specifically, in the inverse energy-cascade state, the Richardson–Obukhov law was similarly derived from a 2D analog of the K41, which was developed by Kraichnan [75], Leith [78], and Batchelor [11]; hereinafter, the analog is referred to as K41 for convenience. Specifically, based on the phenomenologies, the second-order moment of the relative separation in the inertial range can assume the following form:

$$\langle r^2(t)\rangle \simeq \begin{cases} \langle r_0^2\rangle + S_2(r_0)t^2 & (t \ll t_{\mathrm{B}}), \\ g\varepsilon t^3 & (t_{\mathrm{B}} \ll t \ll T_L), \end{cases} \tag{2.1}$$

where $r_0 \equiv |\boldsymbol{r}_0|$ denotes the initial separation of the pairs, ε denotes the energy dissipation rate or the energy flux in the inertial range, $S_2(r) = C_2\varepsilon^{2/3}r^{2/3}$ denotes the second-order longitudinal velocity structure function, C_2 is a constant, $t_{\mathrm{B}} = r_0^{2/3}\varepsilon^{-1/3}$

denotes the Batchelor time, T_L denotes the integral time scale, and g denotes the Richardson constant. Up to the Batchelor time t_B, each particle moves with the initial velocity. Subsequently, the relative separation becomes independent of r_0 and behaves according to the t^3 law, exhibiting super-diffusivity (Richardson–Obukhov regime).

With respect to 2D inverse energy-cascade turbulence, the t^3 law is observed in laboratory experiments [56, 119] for appropriately selected initial separations. Recently, Rivera & Ecke [99] and Rivera & Ecke [100] performed experiments by varying initial separations and observed that the power-law exponent of $\langle r^2(t)\rangle$ in the inertial range depends on the initial separation r_0. They also observed t^3-scaling behavior similar to the Richardson–Obukhov scaling law only for a certain range of initial separations. The initial separation dependence and existence of special initial separations leading to the t^3 law were observed in 2D direct numerical simulation (DNS) [25] as well. With respect to the 3D direct energy-cascade turbulence, the situation is similar: the slope of $\langle r^2(t)\rangle$ as a function of t varies due to the length of initial separations in laboratory experiments [90]. Recently, DNSs in 3D also indicated that the t^3 law only appears for a certain selected initial separation [19, 104, 126].

Based on 2D and 3D results, the conclusion at currently achievable Reynolds numbers is that the time evolution of $\langle r^2(t)\rangle$ strongly depends on the initial separation. Thus, the Richardson–Obukhov t^3 law emerges only for a selected initial separation, and this is termed as *the proper initial separation* in the current study (as detailed in Sec. 2.3.1). The problem to be solved is the dependence of the t^3 law on the initial separation; specifically, whether the t^3 law observed for the special initial separation is relevant with the K41 or just coincidental. It is known that the initial separation dependence is alleviated by considering $\langle|\boldsymbol{r}-\boldsymbol{r_0}|^2\rangle$ instead of $\langle r^2\rangle$. By analyzing $\langle|\boldsymbol{r}-\boldsymbol{r_0}|^2\rangle$ at sufficiently high Reynolds numbers, Bitane *et al.* [18] and Bitane *et al.* [19] introduced the modified scaling law including a subleading term, $\langle|\boldsymbol{r}(t)-\boldsymbol{r}_0|^2\rangle = g\varepsilon t^3(1+Ct_0/t)$ for $t \gg t_0$, where t_0 denotes a time scale of convergence to Richardson–Obukhov regime, $t_0 = S_2(r_0)/2\varepsilon$, and C denotes a parameter based on r_0. It is noted that $C = 0$ for $r_0 = 4\eta$, where η denotes the Kolmogorov length scale. The $r_0 = 4\eta$ is termed as "optimal choice" in their study and can correspond to the proper initial separation. Furthermore, Buaria *et al.* [32] suggested an asymptotic state, and this is independent of the initial separations. The same authors [33] investigated turbulent relative dispersion utilizing diffusing/Brownian particles, i.e., particles of various Schmidt numbers (Sc) with white/Brownian noise added to their trajectories. They found that the initial separation dependence is weaker and Richardson scaling is more robust for $Sc = O(1)$ than $Sc = \infty$ (fluid particles).

Several studies [25, 99] in the 2D inverse-energy cascade turbulence discussed the proper initial separation, and concluded that the t^3-scaling behavior observed only for the special initial separation is an artifact caused by the finite-size effect of the limited inertial range. Given the aforementioned reasons, they argued that proper initial separation exists even in the low Reynolds-number simulations and that the proper initial separation is significantly lower than the smallest lower bound of the inertial range. In particular, the observed scaling law $\langle r(t)^2\rangle \propto t^3$ started to hold

outside of the inertial range, as already noted in [63]. Subsequently, the t^3 law with the proper initial separation extends into the inertial range. However, details of the finite-size effects, e.g., the dependence of the t^3 law on the width of the inertial range, remains to be clarified.

There is another problem with respect to the proper initial separation. The K41 can be applied to the two-particle Lagrangian relative velocity, and predicts t^1 scaling for the second-order moment as

$$\langle v^2(t) \rangle \propto \varepsilon t^1, \tag{2.2}$$

in the inertial range, where $v(t)$ denotes the relative velocity. In recent 3D numerical studies [19, 126], the relative velocity is also observed to depend on the initial separation such as relative separation. Furthermore, it appears that the second-order moment of the relative velocity exhibits a different scaling exponent from the K41 prediction.

The long-standing problem of two-particle relative diffusion in turbulence can be the applicability of the K41 to the Lagrangian relative separation and velocity statistics and at least at presently available Reynolds numbers. It is well-known that the K41 scaling does not precisely hold, particularly for the 3D turbulence due to the intermittency effect. However, the deviation from the K41 is small with respect to the low-order statistics of the Eulerian velocity such as the energy spectrum or the second-order structure functions. Thus, the K41 is successful for the Eulerian velocity. In contrast, the K41 appears to fail in describing the second-order moments of the relative separation and velocity, which are Lagrangian quantities, to the same extent as the low-order Eulerian velocity. This large gap between Eulerian and Lagrangian statistics should be filled. It is possible that the gap is caused by a finite Reynolds-number effect.

In this study, we numerically examine two-particle relative diffusion in 2D energy inverse-cascade turbulence with either normal viscosity or hyperviscosity. The main reason for selecting the 2D system is that detailed numerical studies (e.g., a large number of particle-pair samples and long-time integration) are more feasible. Furthermore, the Eulerian velocity is intermittency free [22, 94], and consequently, corresponds to "an ideal framework to examine Richardson scaling in Kolmogorov turbulence", as noted by Boffetta & Sokolov [25]. Thus, we can factor out the intermittency effect on the deviation of the Lagrangian statistics from the K41 prediction when we analyze 2D results. Evidently, limitations exist while selecting the 2D system. As aforementioned, there are common problems in the Richardson–Obukhov law in 2D and 3D systems. However, their nature is not necessarily identical. Careful discussion and further investigations are required while applying our results in this study to the 3D case. Nevertheless, insights obtained here in 2D can be useful in addressing the 3D problem.

We conduct our numerical study as follows. First, we develop a conditional sampling to remove the initial-separation dependence. We demonstrate that the conditioned $\langle r^2(t) \rangle$ curves of various initial separations collapse on the unconditioned curve starting from the proper initial separation. From the robustness, we infer that the t^3 law of the proper initial separation is consistent with the K41. We then discuss the generality of the conditional sampling, namely, the dependence of the conditioned results on the

Table 2.1: Parameters of numerical simulations: N^2, $\delta x = 2\pi/N$, δt, ν, h, α, k_f, ε_{in}, ε, σ_ε, L, $u_{\rm rms}$, Re_α and N_p^2 denote the number of grid points, grid spacing, size of the time step, (hyper)viscosity coefficient, order of the Laplacian of the (hyper)viscosity, hypodrag coefficient, forcing wavenumber, energy input rate of the forcing, mean of the resultant energy flux in the inertial range, standard deviation of the resultant energy flux, integral scale, root-mean-square velocity, infrared Reynolds number and number of the Lagrangian particles, respectively.

N^2	δx	δt	ν	h	α	k_f	ε_{in}	ε	σ_ε	L	$u_{\rm rms}$	Re_α	N_p^2
1024^2	0.006	0.002	1.8×10^{-38}	8	35	249	0.1	0.019	2.9×10^{-4}	0.38	0.5	40	2048^2
2048^2	0.003	0.001	4.664×10^{-43}	8	35	496	0.1	0.019	2.9×10^{-4}	0.37	0.5	80	2048^2
4096^2	0.0015	0.001	1.13×10^{-47}	8	35	997	0.1	0.018	2.6×10^{-4}	0.36	0.5	160	2048^2
2048^2	0.003	0.004	7.666×10^{-6}	1	3.005	200	3.027×10^{-4}	5.28×10^{-5}	3.35×10^{-5}	0.47	0.076	39	2048^2

parameters of the conditional sampling. Finally, we examine the scaling behavior of the relative velocity with and without the conditional sampling in detail.

The two main results obtained in 2D energy inverse-cascade turbulence are: (i) relative velocity deviates from the K41 scaling ,i.e., scaling law (2.2), although the relative separation obeys the Richardson–Obukhov t^3 law; and (ii) relative velocity is self-similar (intermittency free).

Both suggest that the K41 does not hold for second-order statistics of relative velocity.

Sec. 2.2 presents the details of our 2D numerical study. Sec. 2.3.1 introduces a working hypothesis and describes the proper initial separation. In Sec. 2.3.2, we describe our conditional sampling and discuss what can be inferred from conditional statistics on the relative separation. Sec. 2.4 presents statistics on the relative velocity with and without conditional sampling.

2.2 Numerical simulation method

We mainly consider pair-dispersion statistics in a statistically steady, homogeneous, and isotropic 2D inverse-energy cascade turbulent velocity field $\boldsymbol{u}(\boldsymbol{x}, t)$. In the velocity field, we perform a set of DNSs of the 2D incompressible Navier-Stokes equation in a doubly periodic square of side length, 2π. We integrate the equation in the form of vorticity, $\omega(\boldsymbol{x}, t) = \partial_x u_y(\boldsymbol{x}, t) - \partial_y u_x(\boldsymbol{x}, t)$, which is

$$\frac{\partial \omega}{\partial t} + (\boldsymbol{u} \cdot \nabla)\, \omega = (-1)^{h+1} \nu \Delta^h \omega + \alpha \Delta^{-1} \omega + f. \tag{2.3}$$

The setting and our numerical method are identical to those used in [85, 122]. Here, ν denotes the (hyper)viscosity coefficient and α denotes the hypodrag coefficient. The order of the Laplacian of the (hyper)viscosity, h, is set to 8 or 1. The forcing term,

$f(\boldsymbol{x},t)$, is given in terms of the Fourier coefficients, $\hat{f}(\boldsymbol{k},t) = k^2\varepsilon_{in}/[n_f\hat{\omega}^*(\boldsymbol{k},t)]$, where $\hat{f}$ denotes the Fourier transform of the function $f(\boldsymbol{x},t)$. The energy input rate is denoted by ε_{in}, and n_f denotes the number of the Fourier modes in the following forcing wavenumber range. We select the coefficients, $\hat{f}(\boldsymbol{k},t)$, as non-zero only in high wave numbers, $\boldsymbol{k}$, satisfying $k_f - 1 < |\boldsymbol{k}| < k_f + 1$. Thus, the energy input rate is maintained as constant in time. Numerical integration of Eq. (2.3) is performed via the pseudospectral method with the 2/3 dealiasing rule in space and the 4-th order Runge–Kutta method in time. In this DNS, the maximum wavenumber is $k_{max} = \sqrt{2}N/3$, where N^2 is the number of grid points. Here, $k_{max}\eta \simeq 1.8$ and 1.6 for $h = 8$ and 1, respectively, where η is the Kolmogorov length. Moreover, $l_f/\eta \simeq 6.7$ and 1.8×10 for $h = 8$ and 1, respectively. Table 2.1 lists the parameters of simulations used in the study.

In the 2D energy inverse-cascade turbulence, the energy pumped in at the small scale is transported to larger scales with a constant flux on average in the inertial range. To measure this flux, we use the standard method to calculate the energy flux function in the Fourier space. As shown in Fig. 2.1(a) and (c), the flux becomes wavenumber independent in the intermediate wavenumbers. We consider the range of the wavenumbers as the inertial range. Strictly speaking, a flat region is absent in Fig. 2.1 (c) due to normal viscosity. The energy flux in the inertial range is equal to the energy dissipation rate taken out by the large-scale hypodrag, $\varepsilon = \int_0^\infty 2\alpha k^{-2}E(k)\mathrm{d}k$, where $E(k)$ denotes the time-averaged energy spectrum. This corresponds to a standard method to numerically realize a statistically steady state of 2D energy inverse-cascade turbulence in a periodic domain. A statistically steady state is judged from behavior of energy as a function of time. The typical wavenumber of the hypodrag is dimensionally estimated as $(\alpha^3/\varepsilon)^{1/8}$, which is termed as the frictional wave number, k_α. Here, we use the infrared Reynolds number, $Re_\alpha \equiv k_f/k_\alpha$, as proposed by Vallgren [116] in order to quantify the span of the inertial range. At the end of Sec. 2.4, we simulate a statistically quasi-steady state [75] by solving Eq. (2.3) without the hypodrag.

Subsequently, we demonstrate that the Eulerian statistics on the velocity field are consistent with the established picture of the 2D inverse energy-cascade turbulence. As shown in the inset of Fig. 2.1(a) and (c), the energy spectra in the inertial range is consistent with the K41 and more precisely with the Kraichnan-Leith-Batchelor phenomenology. Figures 2.1(b) and (d) show that the PDFs of the longitudinal velocity increments, $\delta u_l(r,t) = [\boldsymbol{u}(\boldsymbol{x}+\boldsymbol{r},t) - \boldsymbol{u}(\boldsymbol{x},t)]\cdot\boldsymbol{r}/r$, at various r's in the inertial range collapse well to the Gaussian distribution irrespective of r, and this is in agreement with [22]. Here, $l_f = 2\pi/k_f$ denotes the forcing length scale.

To obtain the Lagrangian statistics, we employ a standard particle tracking method. The flow is seeded with a large number of tracer particles, i.e., N_p^2, in the velocity field. The particles are tracked in time via integrating the advection equation,

$$\frac{\mathrm{d}}{\mathrm{d}t}\boldsymbol{x}_p(t) = \boldsymbol{u}(\boldsymbol{x}_p(t),t), \tag{2.4}$$

where $\boldsymbol{x}_p(t)$ denotes the particle position vector. The numerical integration of Eq. (2.4)

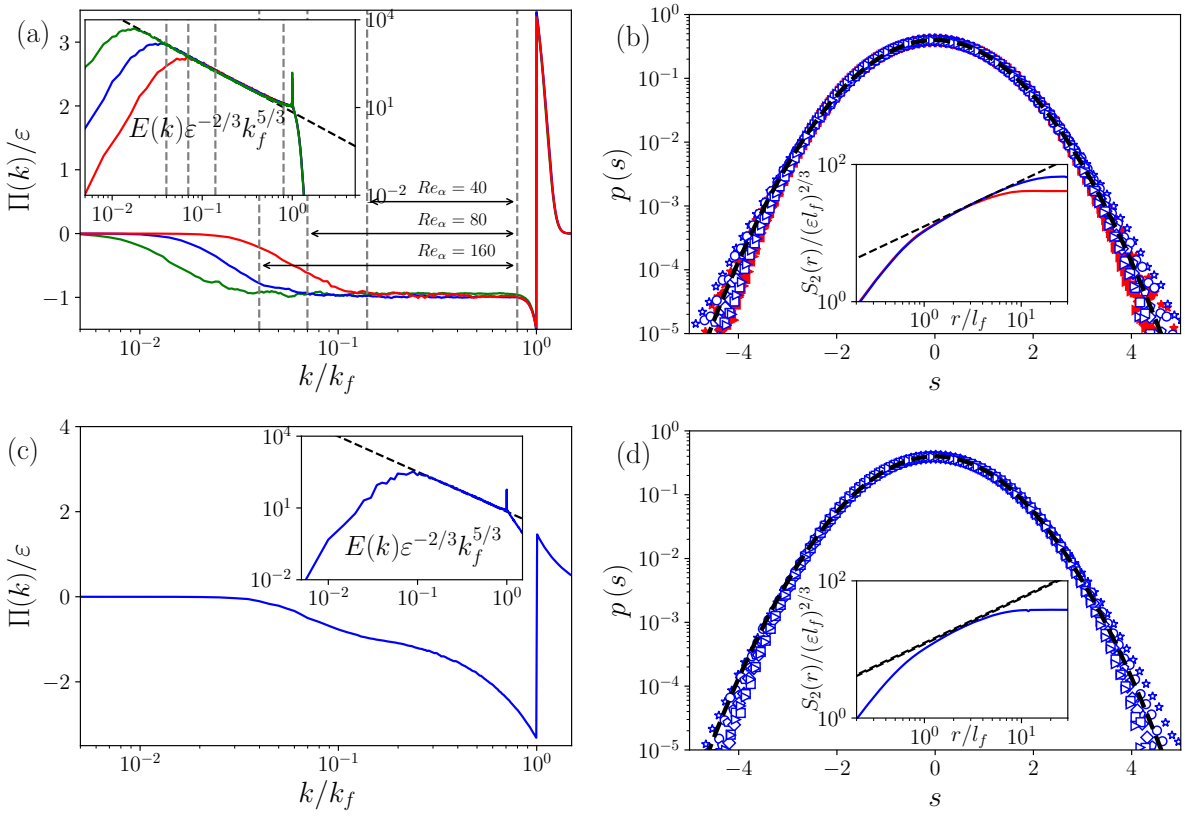

Figure 2.1: (a) Time-averaged energy flux $\Pi(k)$ for $Re_\alpha = 40$ (red line), $Re_\alpha = 80$ (blue line) and $Re_\alpha = 160$ (green line). Ranges between the two gray dotted lines correspond to the inertial ranges as determined by the plateau regions of the energy flux in the Fourier space. The inset shows the time-averaged energy spectrum $E(k)$ for $Re_\alpha = 40$ (red line), $Re_\alpha = 80$ (blue line) and $Re_\alpha = 160$ (green line). (b) Normalized PDFs of the longitudinal velocity increments for $Re_\alpha = 40$ (red) and $Re_\alpha = 80$ (blue) at various separations, $r/l_f = 1.1, 1.5, 2.2, 3.2, 4.8$ and 7.1. Here, $l_f = 2\pi/k_f$ is the forcing scale and longitudinal velocity increment, δu_l, normalized by the second-order moment and is denoted by s: $s = \delta u_l/\sqrt{\langle \delta u_l^2 \rangle}$. The dotted line denotes the Gaussian distribution with zero mean and unit variance. The inset shows the second-order longitudinal structure function, $S_2(r)$ for $Re_\alpha = 40$(red) and $Re_\alpha = 80$(blue). The dashed line represents the K41 scaling, $r^{2/3}$, for $S_2(r)$. (c) Same as (a) albeit for the normal viscous case ($h = 1$). (d) Same as (b) albeit for the normal viscous case ($h = 1$).

is performed using the Euler method. The velocity value at an off-grid particle position is estimated by the fourth-order Lagrangian interpolation of the velocity calculated on the grid points.

The relative separation, $\boldsymbol{r}(t)$, is defined by $\boldsymbol{r}(t) = \boldsymbol{x}_1(t) - \boldsymbol{x}_2(t)$, where $\boldsymbol{x}_1$ and $\boldsymbol{x}_2$ denote the positions of a particle pair. The particles are initially seeded on square grid points where the grid spacing corresponds to r_0. The statistics on the relative separation are calculated for the nearest neighbor particles at the initial time. In this study, we vary the initial separation r_0 while maintaining the same total number, N_p^2, of the particles for each r_0. For small values of r_0 (which are typically lower than the Eulerian grid size δx), the initial particles do not cover the whole periodic domain. We verify that the inhomogeneity of the initial positions of the particles does not affect Lagrangian statistics that are examined here by comparing results with different initial particle positions covering different parts of the periodic domain. In addition to the separation, $r(t)$, our focus is on the longitudinal relative velocity of particle pairs as defined by $v_l(t) \equiv [\boldsymbol{u}(\boldsymbol{x}_1(t), t) - \boldsymbol{u}(\boldsymbol{x}_2(t), t)] \cdot \boldsymbol{r}(t)/r(t)$.

We next discuss on how long we track the particles. We continue the tracking until all the particle pairs leave the inertial range. We observe that this time typically concerns 10 large-scale eddy turn-over times (L/u_{rms}) for the hyperviscous $Re_\alpha = 40$ case and approximately 20 turn-over times for the hyperviscous $Re_\alpha = 80$ case. With respect to each r_0, we perform the simulation of the duration twice.

The largest resolution simulation ($N^2 = 4098^2$) as listed in Table 2.1 is used only for confirming self-similarity of PDF of $v_l(t)$ in Sec. 2.4. We define the Lagrangian average $\langle\cdot\rangle$ as $\langle A\rangle = \frac{1}{N_{\mathrm{adj}}} \sum_{i=1}^{N_{\mathrm{adj}}} A_i$, where A denotes any Lagrangian quantity and A_i denotes a realization of A by the i-th particle pair. $N_{\mathrm{adj}} = 2N_p(N_p - 1)$ denotes the number of pairs of particles which adjoin each other at the initial time.

In the following sections, we mainly use hyperviscosity rather than normal viscosity for DNSs. This is because the hyperviscosity extends the inertial range for a given spatial resolution. However, it is known to affect the statistics at the transition between the inertial and dissipation ranges [23]. Thus, it is possible that the hyperviscosity affects particle-pair statistics. Therefore, we perform hyperviscous and normal-viscous simulations and confirm that the hyperviscosity does not affect the particle-pair statistics.

2.3 Initial separation dependence of relative diffusion statistics and conditional sampling

2.3.1 Proper initial separation

At the Reynolds numbers currently available in experiments and numerical simulations, the time evolution of $\langle r^2(t)\rangle$ depends on the initial separation. Hence, it is not possible to conclude whether it obeys the Richardson–Obukhov prediction $\langle r^2(t)\rangle \propto \varepsilon t^3$ (for e.g., [15, 19] for the 3D case and [25, 56] for the 2D inverse energy-cascade case). The

same is applicable to the second-order moment of relative velocity, $\langle v_l^2(t)\rangle$ for which the K41 dimensional analysis yields $\langle v_l^2(t)\rangle \propto \varepsilon t$ (for e.g., [126] for the 3D case). In the 2D simulation at moderate Reynolds numbers, the initial-separation dependence is clearly confirmed for both $\langle r^2(t)\rangle$ shown in Fig. 2.2(a) and (c) and $\langle v_l^2(t)\rangle$ shown in Fig. 2.2(b) and (d) where $t_f = (l_f^2/\varepsilon)^{1/3}$ denotes the forcing time scale. We examine the results by varying the initial separations below the forcing scale, namely $r_0 < l_f$. Thus, the initial separations are in the scales lower than the inertial range. If we set the initial separation in the inertial range, the graphs of $\langle r^2(t)\rangle$ and $\langle v_l^2(t)\rangle$ are located (they are not shown) above the curves plotted in Fig. 2.2. Thus, we normalize all quantities by l_f and t_f unless there is some particular reason. This is because l_f and t_f approximately define the lowest length and time scale of the inertial range, respectively.

The data with the initial-separation dependence indicates that it is possible to select a special value corresponding to r_0 for which $\langle r^2(t)\rangle$ becomes consistent with the Richardson–Obukhov law $\langle r^2(t)\rangle = g\varepsilon t^3$. Further, we include the Richardson constant, g, which is non-dimensional and possibly universal. We show the squared separation of the special case in the inset of Fig. 2.2(a) as a logarithmic local slope. However, it should be noted that (even for the special case) agreement of the squared velocity with the K41 prediction, $\langle v_l^2(t)\rangle \propto \varepsilon t$ is not as good as that of the squared separation. This is observed in the inset of Fig. 2.2(b).

Given the apparent failures of the K41, in this study, we still argue that a certain bulk of the particle pairs starting from each initial separation r_0 shown in Fig. 2.2 obey the Richardson–Obukhov law of the squared separation even at the moderate Reynolds numbers. Thus, we perform conditional sampling of particle pairs. The qualitative condition is that we remove particle pairs that prevent from separating too fast. In the following section, we demonstrate that this type of a conditional average $\langle r^2(t)\rangle_c$ becomes independent of the initial separation and that $\langle r^2(t)\rangle_c$ is the same as the unconditioned $\langle r^2(t)\rangle$ commencing from the special initial separation (see Fig. 2.4). Hence, the conditional sampling recovers the Richardson–Obukhov law, $\langle r^2(t)\rangle_c = g\varepsilon t^3$, including the Richardson constant and flux. Thus, we term the special initial separation as the proper initial separation, which we denote as $r_0^{(p)}$

Evidently, our conditional sampling is contrived. It has several tuning parameters as we will specify them. We determine their values empirically by ensuring that $\langle r^2(t)\rangle_c \propto t^3$ holds. In order to demonstrate the extent to which it is contrived, we examine the manner in which conditional statistics change by varying tuning parameters. Furthermore, we demonstrate that the number of removed pairs decreases when the Reynolds number increases. The details of the conditional sampling are given in the next subsection.

2.3.2 Conditional sampling via mean exit time

Figure 2.2(a) plots nine cases of the different initial separations. To develop the conditional sampling, we first focus on initial separations that satisfy $r_0 > r_0^{(p)}$, where $r_0^{(p)}$ denotes the proper initial separation. Thus, we consider three cases from above in In

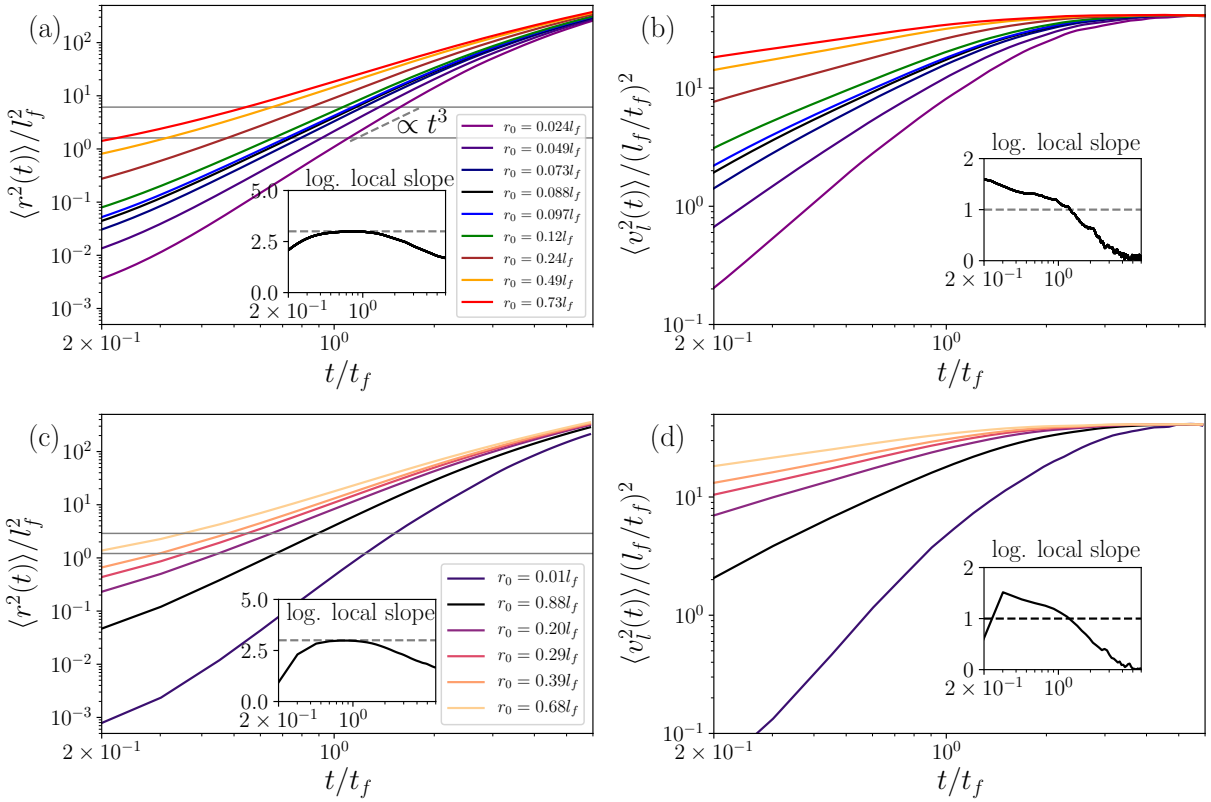

Figure 2.2: (a) Mean squared separation for the hyperviscous case with $Re_\alpha = 40$ as a function of time for various initial separations. Here, $t_f = (l_f^2/\varepsilon)^{1/3}$ denotes the forcing time scale. The ranges between the two horizontal lines correspond to the inertial range determined by the region of the mean exit time that is proportional to $r^{2/3}$, which is discussed later. Inset: the logarithmic local slope for the special initial separation, $r_0 = 0.088l_f \sim r_0^{(p)}$, where ε denotes the mean energy flux in the inertial range. The gray dashed line corresponds to the Richardson scaling exponent, 3. (b) mean squared relative velocity for various initial separations. Inset: the logarithmic local slope for the special initial separation, $r_0 = 0.088l_f$. The gray dashed line corresponds to the Kolmogorov scaling exponent, 1. (c) Same as (a) albeit for the normal viscous case. (d) Same as (b) albeit for the normal viscous case.

Fig. 2.2(a). Our estimate of the proper initial separation is empirical: we examine the compensated plot of the unconditional moment $\langle r^2(t)\rangle$ as shown in Fig. 2.2(a) by changing r_0. Subsequently, we select r_0 for which the compensated plot exhibits the widest plateau. We evaluate the proper initial separation in this manner as $r_0^{(p)} = 0.088l_f, 0.101l_f$, and $0.121l_f$ for $Re_\alpha = 40, 80$, and 160, respectively.

With respect to the initial separations $r_0 > r_0^{(p)}$, the graphs of the mean squared separation $\langle r^2(t)\rangle$ are situated above the graph starting from $r_0^{(p)}$ as shown in Fig. 2.2. This indicates that it is necessary to remove particle pairs moving too fast to recover the t^3 scaling. Now, we pose two questions on the conditional sampling: (A) Is it possible to instantaneously determine whether it is excessively fast, i.e., exhibiting excessively large $r(t)$?; (B) How to draw a line between excessively fast pairs and not excessively fast pairs, i.e., the threshold level between the two sets? We handle both the questions with exit-time statistics that are proved as effective tools in the study of relative diffusion.

The exit time concerns the first passage time. The first passage time of the separation $r(t)$ for a given value R is defined by the first instance when the separation $r(t)$ becomes equal to R. (for the first passage time of a general stochastic process, see, e.g., [47]). We express the first passage time as $T_F(R)$. To define the exit time, it is necessary to set the domains. We denotes the domain as a series $R_0, R_1, R_2, \ldots$. The exit time of the j-th zone $R_{j-1} \le r(t) < R_j$ is then defined as $T_E^{(j)} = T_F(R_j) - T_F(R_{j-1})$ where $R_j = r_s\rho^j$ with parameters r_s and $\rho > 1$ for $j = 1, 2, \ldots$. In the relative diffusion problem, exit-time statistics are introduced to solve the finite-size problems [3, 21, 25, 99]. By selecting thresholds R_js in the inertial range, it is possible to exclusively extract information of the inertial range. It is known that exit-time statistics are insensitive to the Reynolds number(for e.g.,[89]). It is also known that the mean exit time is consistent with the K41 prediction, $\langle T_E^{(j)}\rangle \propto R_j^{2/3}$ when R_j is in the inertial range. Furthermore, the scaling behavior holds independent of the initial separations [15, 25]. In our simulation with $r_s = 1.3l_f$ and $\rho = 1.1$, the K41 scaling of the mean exit time is observed for $1 \le j \le 7$ for the hyperviscous $Re_\alpha = 40$ case and $1 \le j \le 14$ for the hyperviscous $Re_\alpha = 80$ case as shown in Fig. 2.3. Typical value of ρ as used in the previous studies corresponded to 1.1 or 1.2 [3, 21, 25, 89, 99] and the properties of exit-time statistics as mentioned above do not change in the range of ρ.

Now, we describe how we address the two questions of conditional sampling with the exit time. For the first question (A), we assume that it is not possible to instantaneously determine excessively-fast pairs. This is performed over certain consecutive zones in the inertial range. We express the number of the zones by N_Q (at the end of Sec. 2.3.2. We change the parameter N_Q and discuss question (A).).

With respect to the second question (B), evidently small exit time $T_E^{(j)}$ corresponds to pairs separating fast. Hence, to remove the excessively-fast pairs, we set an upper threshold, τ, in terms of the exit time over the zones $j = 1, 2, \ldots, N_Q$. Hence, if the exit time of the particle pair satisfies

$$\frac{T_E^{(j)}}{\langle T_E^{(j)}\rangle} \le \tau \tag{2.5}$$

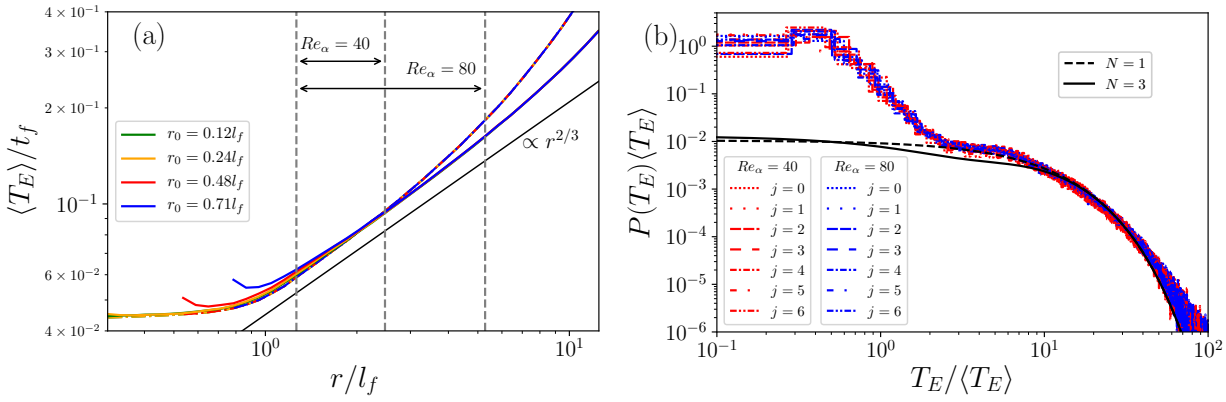

Figure 2.3: (a) Mean exit time for the hyperviscous cases with $Re_\alpha = 40$ (dash-dotted line) and $Re_\alpha = 80$ (solid line). Black solid line denotes $r^{2/3}$ power law. The ranges between the two gray dashed lines denote the inertial range estimated with the exit time at $Re_\alpha = 40$ and $Re_\alpha = 80$. (b) The PDFs of exit time normalized by the mean at $Re_\alpha = 40$ (red) and 80 (blue) for $j = 0$ to 6. Black dashed line and solid line denote longtime asymptotic forms for the PDF of exit times, i.e., $P(T_E)\langle T_E \rangle \sim C \sum_{i=1}^{N} j_{2,i} J_2'(j_{2,i}) \exp[-\frac{j_{2,i}^2}{12} \frac{\rho^{2/3}-1}{\rho^{2/3}} \frac{t}{\langle T_E \rangle}]$ [25], at $N = 1$ and $N = 3$, respectively. Here, C denotes the normalized factor, J_2 denotes the Bessel function, and $j_{2,i}$ denotes the i-th zero point of J_2 and $\rho = 1.1$.

in *all* of the zones, $j = 1, 2, \ldots, N_Q$, then this type of a pair is removed from the Lagrangian average. It should be noted that the threshold τ is independent of j. The condition implies that the removed pairs spend a short time when compared to the average in any of the N_Q zones. Thus, the removed pair separate too fast in all of the monitored zones. Conversely, the remaining pairs in the conditional sampling generally spend a sufficiently long time such that $T_E^{(j)}/\langle T_E^{(j)} \rangle > \tau$. However, they can become excessively-fast in several (but not all) of the N_Q zones. It should be noted that the conditional sampling includes two parameters: N_Q and τ.

Our physical picture of the conditional sampling is as follows: The pair separation $r(t)$ is given by the time integral of the relative velocity from time 0 to t. The accumulating nature of $r(t)$ suggests that it is necessary to consider the history of a pair in conditional sampling. We consider it in terms of the N_Q zones starting from the lowest scale of the inertial range. An actual value of N_Q will be determined empirically. With respect to τ, it is noted that the right part of the PDF of the exit time is given by the Richardson PDF of the separation, $P(r,t) \propto \varepsilon^{-1} t^{-3} \exp[-(\text{const.})\varepsilon^{-1/3} t^{-1} r^{2/3}]$, which denotes the self-similar solution to the Richardson's diffusion (Fokker-Plank) equation [25]. The correspondence of the PDFs shown in Fig. 2.3(b) indicates that the pairs in the left part in the exit-time PDF should be removed in the conditional sampling, thereby leading to the criterion, Eq. (2.5). This picture is only qualitative in nature.

We then describe the determination of parameter values in practice. In the case of $Re_\alpha = 40$, the inertial range is covered by 7 zones. Hence, we set the number of the

monitored zones to $N_Q = 7$. Subsequently, we tune the threshold τ's based on the initial separation r_0 to recover the Richardson–Obukhov law by examining whether the compensated plot $\langle r^2(t)\rangle_c/(\varepsilon t^3)$ exhibits a plateau. We empirically determine that the τ values correspond to 0.40, 1.2, 3.4, and 4.6 for the initial separations $r_0/l_f = 0.12, 0.24, 0.48$, and 0.71, respectively. Given the parameters, we present the results of the conditional average of the squared separations in Fig. 2.4(a). With respect to the hyperviscous $Re_\alpha = 80$ case, the inertial range is covered by 14 zones. However, we demonstrate the result with the same $N_Q = 7$ as that in the lower Reynolds number case to enable a better comparison in Fig. 2.4(b). The thresholds are observed as $\tau = 0.25, 0.50, 1.4$ and 3.0 for the same set of the initial separations $r_0/l_f = 0.12, 0.24, 0.48$ and 0.71, respectively. In the normal-viscous case, $N_Q = 7$ and the thresholds correspond to $\tau = 0.45, 1.05, 2.4$, and 4.4 for the initial separations $r_0/l_f = 0.20, 0.29, 0.39$ and 0.68, respectively.

As shown in Fig. 2.4, the conditioned curves $\langle r^2(t)\rangle_c$ collapse in the inertial range and beyond the unconditioned curve for proper initial separation. It should be noted that the width of the collapsed region increases as we increase Re_α. When we compare τ between the two Reynolds number cases for the same normalized initial separation r_0/l_f, it approximately decreases by a factor of 1/2. The fraction of the remaining pairs in the conditional sampling corresponds to 41 % for $Re_\alpha = 40$ and 65 % for $Re_\alpha = 80$. Qualitatively, the increase in the fraction is interpreted as follows. We assume that we compare each pair's distance $r(t)$ at the same time t for the two Reynolds numbers. Given the wider inertial range at higher Re_α, pairs with larger separation $r(t)$ (i.e., pairs separating fast) are tolerated in the higher Re_α case to recover the Richardson–Obukhov law. The increase in the fraction supports the working hypothesis that a certain bulk of particle pairs obey the Richardson–Obukhov law even at moderate Reynolds numbers.

We then examine changes in the results of the conditional sampling when we vary parameters N_Q and τ's for various initial separation r_0. For the purpose of simplicity, we limit ourselves to the two hyperviscous cases with $Re_\alpha = 40$ and 80. With respect to the reference exit-time statistics, we do not change the parameters $r_s = 1.30 l_f$ and $\rho = 1.1$. At $Re_\alpha = 40$, we use $N_Q = 7$ as the number of monitored zones independent of the initial separation r_0. The N_Q zones, $R_1 = r_s\rho \le R \le R_7 = r_s\rho^7$, cover almost the entire inertial range. We consider the initial separations satisfying $r_0^{(p)} < r_0 < r_s$. We then reduce N_Q to $6, 5, 4, 3, 2$, and 1 although we use the same set of τ's determined with $N_Q = 7$. The results indicate that further tuning of τ for the change in N_Q is not necessary. The reduction of N_Q does not alter the behavior of $\langle r^2(t)\rangle_c$ as shown in Fig. 2.4(a). The same is applicable to the higher $Re_\alpha = 80$ case shown in Fig. 2.4(b). In this case, we change N_Q to $14, 13, \ldots, 1$ although we use the same τ for each N_Q. Therefore, the result of the conditional sampling is robust relative to changes in the parameters. An important result obtained in the examination is that $N_Q = 1$ is sufficient. This answers question (A) on the conditional sampling, namely it is not possible to instantaneously determine if a given pair is excessively fast (consequently exhibiting excessively high $r(t)$). However, it can be performed in terms of the exit time of the first zone in the inertial range. Thus, it is possible to locally remove excessively-

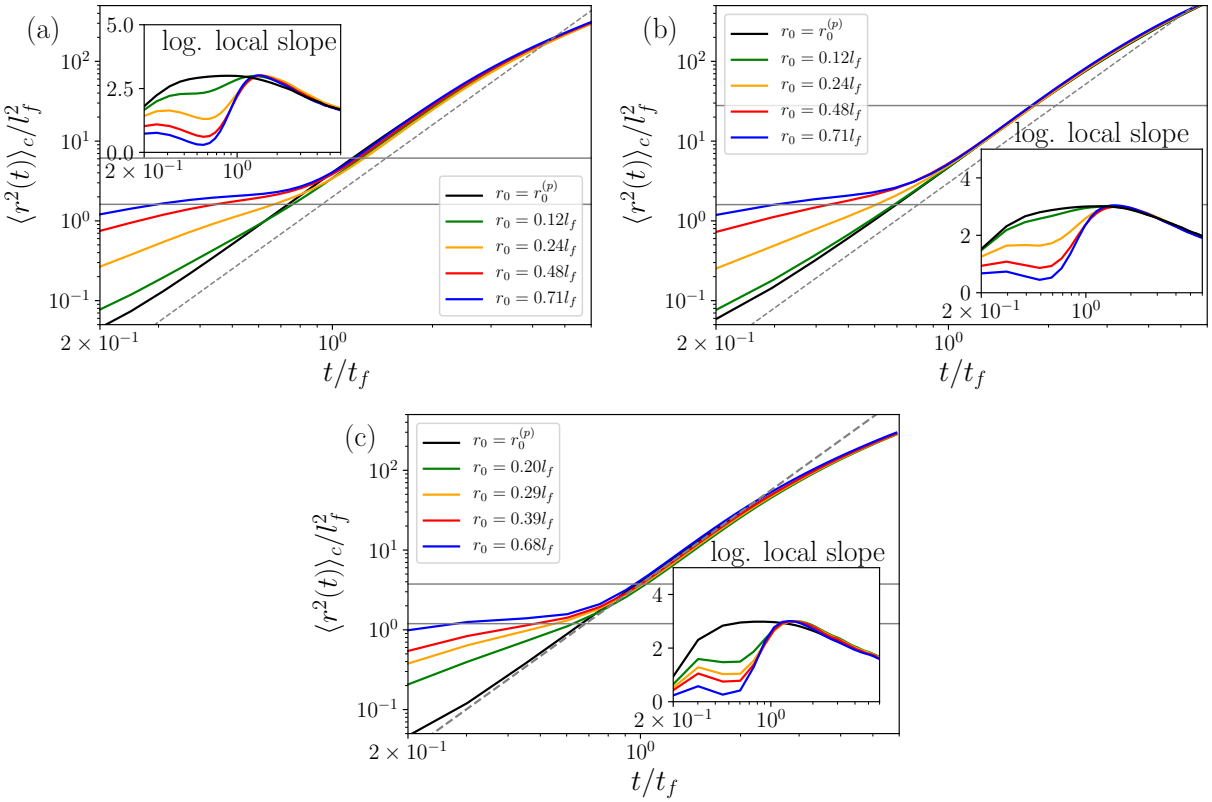

Figure 2.4: Conditionally sampled second-order moments of relative separations. The initial separations exceed the proper initial separation $r_0^{(p)}$. (a) Conditional sampling for the hyperviscous $Re_\alpha = 40$ case starting from various initial separations. (b) Conditional sampling for the hyperviscous $Re_\alpha = 80$ starting from various initial separations. (c) Conditional sampling for the viscous $Re_\alpha = 39$ case starting from various initial separations. Inset shows the logarithmic local slopes of the conditionally sampled $\langle r^2(t)\rangle$. Black solid curve shows the second-order moment of the relative separation without any conditional sampling starting from the proper initial separation, $r_0 = r_0^{(p)}$. The gray dashed line denotes t^3 power law. The range between the two horizontal gray solid lines denotes the inertial range estimated with the exit time.

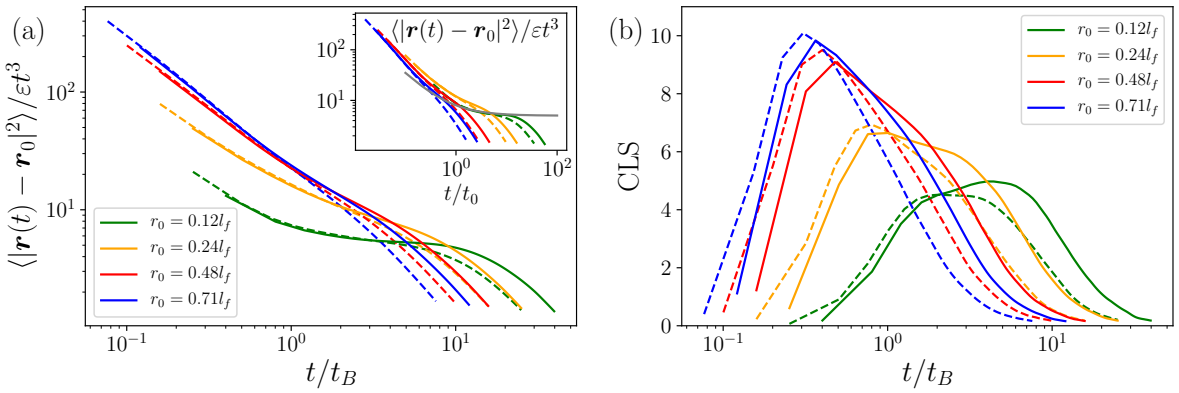

Figure 2.5: (a) Mean squared separations for the hyperviscous case with $Re_\alpha = 40$ (dashed line) and $Re_\alpha = 80$ (solid line), although the initial separation is subtracted for various initial separations. This is compensated by the scaling εt^3. Inset shows the same plots as the main panel although the horizontal axis is compensated by the Bitane time scale, $t_0 = S_2(r_0)/2\varepsilon$. Gray line denotes the scaling law, $\langle \boldsymbol{r}(t) - \boldsymbol{r}_0 \rangle = g\varepsilon t^3(1 + Ct_0/t)$ as suggested by Bitane *et al.* [18]. Here, $C = 0.6$. (b) Cubed-local slopes of $\langle r^2(t) \rangle$ for various initial separations at the hyperviscous $Re_\alpha = 40$ (dashed line) and $Re_\alpha = 80$ (solid line). In panel (a) and (b), the time is normalized with the Batchelor time, $t_\mathrm{B} = r_0^{2/3}\langle\varepsilon\rangle^{-1/3}$. In the inset of panel (a), the time is normalized with Bitane time, $t_0 = S_2(r_0)/2\varepsilon$.

fast pairs to recover the Richardson–Obukhov law in space at the entry of the inertial range. Evidently, this is not locally in time. This implies that evolution of a pair in the inertial range is somewhat monotone after the entry. As shown in the next section, this is observed as a self-similar evolution of the relative velocity.

Other methods are developed to remove the initial separation dependence. For the purpose of comparison, we apply two methods used for 3D turbulence [18, 19, 32] to 2D data without utilizing conditional sampling. A method involves subtracting the initial-separation vector $\boldsymbol{r}_0$ from the separation vector $\boldsymbol{r}(t)$. In Fig. 2.5 (a), we plot $\langle|\boldsymbol{r} - \boldsymbol{r}_0|^2\rangle/(\varepsilon t^3)$ of our data for the $Re_\alpha = 80$ case with the hyperviscosity. The Richardson–Obukhov law appears as a plateau in the region $t/t_B \gg 1$ or $t/t_0 \gg 1$. Although the range of t/t_B in our data is comparable to that in the 3D study [32], the degree of collapse of our 2D data is worse than that of the 3D result. The other method involves extracting the possibly subdominant t^3 term in $r(t)$ with a suitable exponentiation and temporal finite difference. In Fig. 2.5 (b), we plot the cubed local-slope (CLS), $\left\{(d/dt)[\langle r^2(t)\rangle^{1/3}]\right\}^3/\varepsilon$, [32] of our 2D data. The Richardson–Obukhov law appears as a plateau in the CLS in $t/t_B \gg 1$. However, the degree of the collapse for the 2D result is worse. The discrepancy between the 2D and 3D cases can be ascribed to the difference in the physics of turbulence in 2D and 3D. Conversely, the plateau is unclear irrespective of the dimensions. This can be due to finite Reynolds number effects. However, in order to evaluate the effects, it is necessary to add the

tuning parameter to the Richardson–Obukhov law. A physical meaning of the tuning parameter is obscure in many cases. Although the scaling law suggested by Bitane *et al.* [18] approximately corresponds to data for finite Reynolds number at small time, $t \lesssim t_0$, by tuning the parameter, C, it does not correspond to the data at large time, $t \gtrsim t_0$. Hence, it is necessary to add another tuning parameter for large time. Furthermore, the cause for the difference between $\langle r^2(t) \rangle$ and $\langle |\boldsymbol{r}(t) - \boldsymbol{r}_0|^2 \rangle$ is not clarified. Hence, it is insufficient to only investigate statistical moments of all particle pairs. Thus, it is necessary to investigate the PDF of particle pairs. We should consider extreme events of particle pairs that can affect even lower moments such as $\langle r^2(t) \rangle$. It is intrinsically necessary to consider conditional statistics on a special part of particle pairs.

So far, we restricted the conditional sampling for the cases of $r_0 > r_0^{(p)}$. For lower initial separations, $r_0 < r_0^{(p)}$, we can also recover t^3 scaling with the same conditional statistics. However, we found that the results indicate the condition for the threshold, τ, changes from the inequality (2.5) to

$$\tau_1 \leq \frac{T_E^{(j)}}{\langle T_E^{(j)} \rangle} \leq \tau_2, \tag{2.6}$$

where $\tau_1 \neq 0$. For example, we empirically determine $(\tau_1, \tau_2) = (0.16, 7.5), (0.2, 1.0)$ and $(0.18, 0.50)$ for initial separations $r_0/l_f = 0.024, 0.049$, and 0.073, respectively at $Re_\alpha = 40$. Although t^3 scaling law is recovered via conditional sampling, the Richardson constant, $g = \langle r^2(t) \rangle_c / \varepsilon t^3$, for the conditional data is extremely sensitive to the initial separations (figure not shown). The sensitivity considerably differs from the cases of $r_0 > r_0^{(p)}$. This indicates that for $r_0 < r_0^{(p)}$ cases, we fail to construct conditional statistics that remove the initial separation dependence. We infer that in these cases the bulk of particle pairs do not obey the Richardson–Obukhov law in the aforementioned cases. The initial separations are extremely small such that the pairs experience effects from the dissipation range and the small-scale forcing is longer than that of the cases with $r_0 > r_0^{(p)}$. Hence, two parameters are required for conditional sampling. We do not focus on cases with $r_0 < r_0^{(p)}$ in the remaining part of the section. However, the failure implies that $r_0^{(p)}$ corresponds to the border line of the initial separation, beyond which the bulk of the particle pairs becomes consistent with the Richardson–Obukhov law.

2.4 Scaling of the relative velocity

2.4.1 Conditional sampling

Using the conditional sampling described in the previous section, we show conditional averages of the squared longitudinal relative velocity, $\langle v_l^2(t) \rangle_c$ in Fig. 2.6. Conditional velocity statistics exhibit a collapse similar to that of the conditional separations. Hence, the second-order and first-order conditional moments, $\langle v_l^2(t) \rangle_c$ and $\langle v_l(t) \rangle_c$,

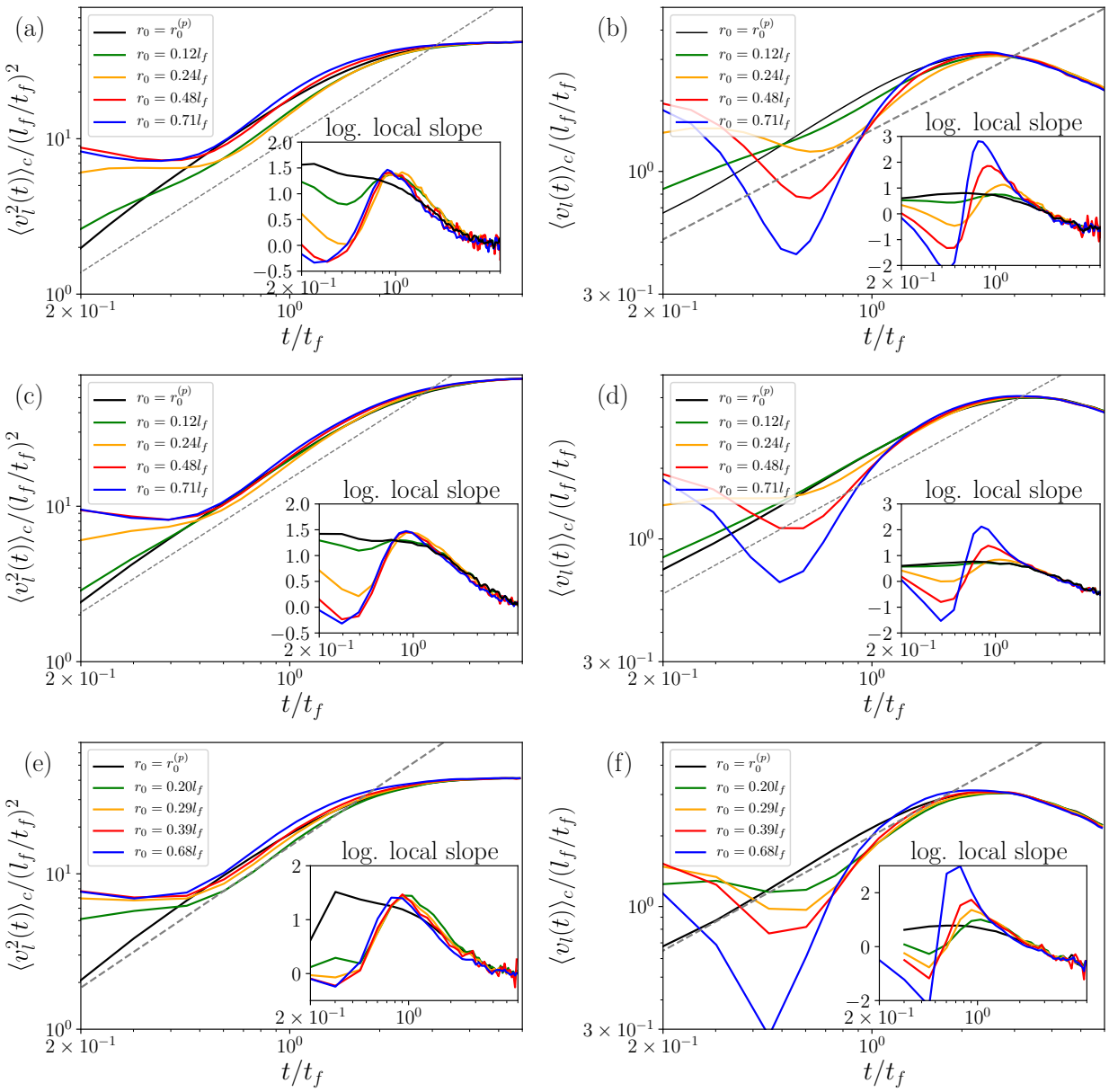

Figure 2.6: Second-order (left panels) and first-order (right panels) moments of the longitudinal relative velocity for conditionally sampled data starting from various initial separations and for the unconditioned data starting from the proper initial separation, $r_0^{(p)}$. Inset: Logarithmic local slope. (a) (b) $Re_\alpha = 40$ with hyperviscosity. (c) (d) $Re_\alpha = 80$ with hyperviscosity. (e) (f) $Re_\alpha = 39$ with normal viscosity. Dashed line denotes $t^{1.23}$ and $t^{0.7}$ scalings for second-order and first-order moments, respectively.

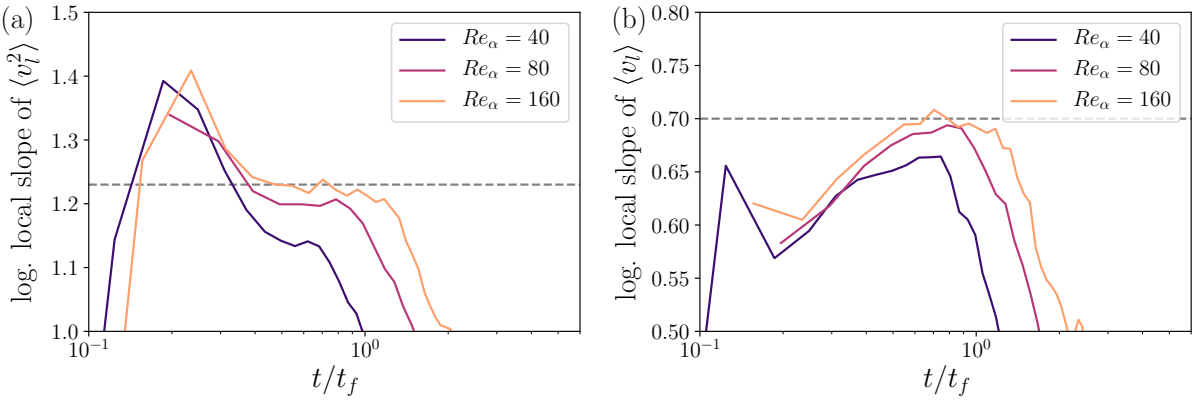

Figure 2.7: Re_α-dependence of the logarithmic local slope of (a) $\langle v_l^2(t) \rangle$, and (b) $\langle v_l(t) \rangle$, for unconditioned data at the proper initial separation, $r_0^{(p)}$ at $Re_\alpha = 40, 80$, and 160. Gray dashed lines correspond to (a) 1.23 and (b) 0.70, respectively.

respectively, starting from various initial separations become almost identical to the unconditioned moments starting from the proper initial separation. However, the degree of collapse of the velocity data is worse at the hyperviscous $Re_\alpha = 40$ and normal viscous $Re_\alpha = 39$ although it improves at $Re_\alpha = 80$ with hyperviscosity. The results indicate that the second-order conditional moment $\langle v_l^2(t) \rangle_c$ and conditional average $\langle v_l(t) \rangle_c$ deviate from their K41 power-law predictions, t^1 and $t^{1/2}$, respectively. This contrasts with the conditional relative separation $\langle r_l^2(t) \rangle_c$ that is driven as consistent with the K41 prediction or the Richardson–Obukhov law.

We observe the deviation from the Kolmogorov scaling exponents and then measure the exponents from the logarithmic local slopes of $\langle v_l^2(t) \rangle$ and $\langle v_l(t) \rangle$ shown in the insets of Fig. 2.6. At large times, the converging behavior of the local slopes to that of the proper initial separation is observed. However, a plateau is absent in the converged part. We then assume that at higher Re_α, the converged part corresponds to plateau and that the level of the converged (hypothetical) plateau is identical to that of the proper initial separation. We then plot the logarithmic local slopes of the data starting from the proper initial separation with three Re_αs in Fig. 2.7. We observe that increases in Re_α widen the plateau and that the levels of the plateaus do not approach the K41 scaling exponents, which correspond to the bounds of vertical axis in Fig. 2.7. Furthermore, it should be noted that the differences between the neighbor levels decreases when Re_α increases. This indicates that asymptotic exponent values are present. As shown in Fig.2.7, given our assumptions of the converged behavior, we infer that the scaling exponents of the velocity statistics are

$$\langle v_l(t) \rangle \propto t^{0.7}, \tag{2.7}$$
$$\langle v_l^2(t) \rangle \propto t^{1.23}. \tag{2.8}$$

The scaling exponents are visually determined from Fig.2.7. The values increase with increases in Re_α.

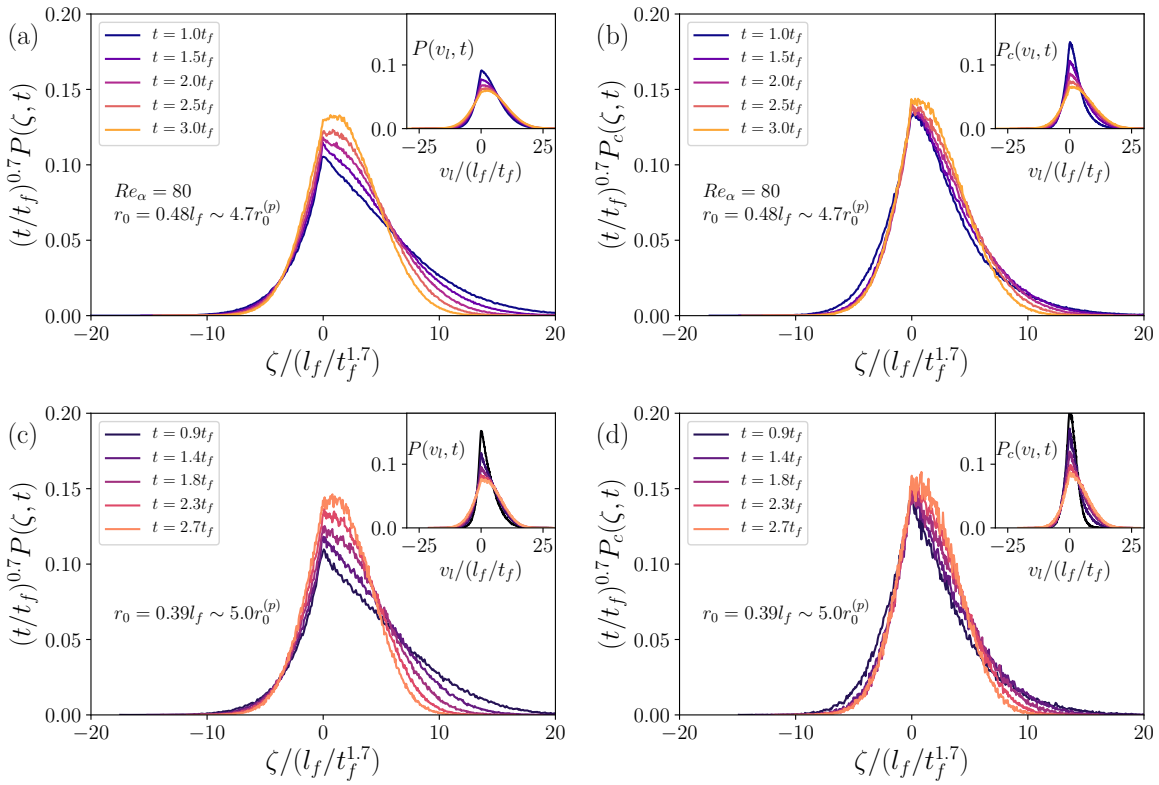

Figure 2.8: (a) PDFs of the rescaled longitudinal relative velocity, $\zeta(t) = v_l(t)/t^{0.7}$ for unconditioned data at different instances $t/t_f = 1.0, 1.5, 2.0, 2.5, 3.0$ for $Re_\alpha = 80$ with hyperviscosity. Here, the initial separation corresponds to $r_0 = 0.48l_f$ which is different from the proper initial separation. It should be noted that ζ is non-dimensionalized as it is divided by $l_f/t_f^{1.7}$. Inset: PDFs without re-scaling of the longitudinal relative velocity for the unconditioned data with the initial separation $r_0 = 0.48l_f$. (b) Same as (a) albeit for the conditionally sampled data. (c) Same as (a) albeit for $Re_\alpha = 39$ with normal viscosity at different instances $t/t_f = 0.9, 1.4, 1.8, 2.3, 2.7$. Here, the initial separation corresponds to $r_0 = 0.39l_f$. (d) Same as (c) albeit for conditionally sampled data.

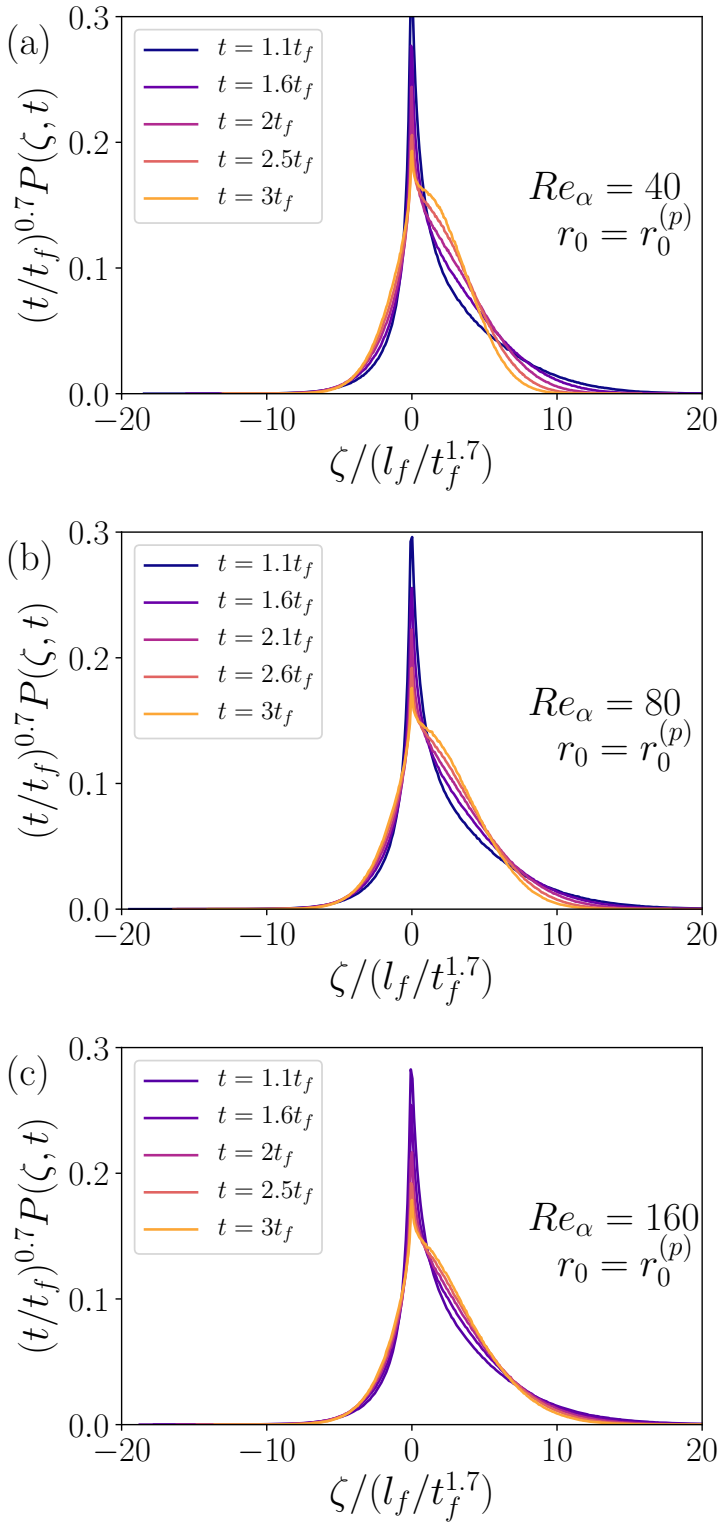

Figure 2.9: Evolution of PDFs of the rescaled longitudinal relative velocity, $\zeta(t) = v_l(t)/t^{0.7}$, of the unconditioned pairs starting from the proper initial separation, $r_0^{(p)}$. The PDFs are for (a) $Re_\alpha = 40$. (b) $Re_\alpha = 80$. (c) $Re_\alpha = 160$.

Furthermore, by normalizing with temporal scaling in Eq. (2.7), the time evolution of the PDF of the conditionally sampled v_l becomes self-similar as shown in Fig. 2.8(b). Here, $P_c(A,t)$ corresponds to the conditional PDF for a quantity, A. The collapse among different instances does not appear perfect. The collapse around the peak is important because the probability in the tails decays faster than the exponential decay (we compare the degree of the collapse around the peak of the scaled PDF to that of the PDF in the inset). Conversely, the unconditional v_l scaled with the same scaling in Eq. (2.7) does not exhibit the self-similar evolution as shown in Fig. 2.8(a). Even if we scale the relative velocity with $t^{a/2}$, where the exponent a is measured from $\langle v_l(t)^2\rangle \propto t^a$ shown in Fig. 2.2(b) for each r_0, the head parts of the PDFs do not collapse each other as shown in the inset of Fig. 2.8(a). This implies that the evolution becomes self-similar only for conditionally sampled relative velocity with scaling relations (2.7). We obtained similar results for the normal viscous case as shown in Fig. 2.8(c) and (d). It should be noted that in the instances plotted in Fig. 2.8, the conditional separation, $\langle r^2(t)\rangle_c$, is forced to agree with the Richardson–Obukhov law. The self-similar evolution of the PDF of $v_l(t)$ also holds for unconditioned data starting from the proper initial separation as shown in Fig. 2.9 for three cases of Re_α with hyperviscosity.

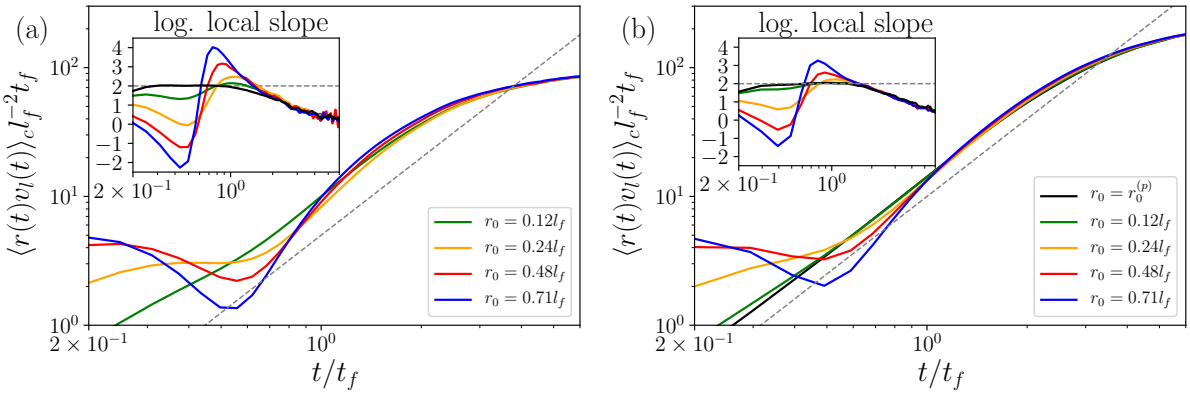

Figure 2.10: (a) Mean separation rate, $\langle r(t)v_l(t)\rangle_c$ for conditioned data at various initial separations and for unconditioned data at the proper initial separation, $r_0^{(p)}$ for $Re_\alpha = 40$ with hyperviscosity. Dashed line denotes t^2 scaling. Inset: The logarithmic local slopes of the data shown in the outset. Dashed line denotes t^2 scaling. (b) Same as (a) but for $Re_\alpha = 80$ with hyperviscosity.

Now, we obtain two evidently incompatible results via conditional sampling and selecting the proper initial separation. The second-order moment of the separation, $r(t)$, obeys the K41 scaling (although this is enforced). Conversely, the statistics of relative velocity, $v_l(t)$, deviate from the K41 scaling although its evolution is self-similar. As a soft argument in favor of the compatibility between the two results, we examine the mean of the product $r(t)v_l(t)$. It should be noted that it is directly related to the evolution of the mean squared separation as $d\langle r^2(t)\rangle/dt = 2\langle r(t)v_l(t)\rangle$, and thus it is

termed as the separation rate. As shown in Fig. 2.10(a), the conditional mean separation rate obeys $\langle r(t)v_l(t)\rangle_c \propto t^2$ as expected given that we enforced the Richardson–Obukhov law. The same t^2 scaling also holds for the unconditioned mean separation rate starting from the proper initial separation (figure not shown). Evidently, $r(t)$ and $v_l(t)$ are statistically dependent, and this is also evident from the kinematics. Hence $\langle r(t)v_l(t)\rangle_c \neq \langle r(t)\rangle_c\langle v_l(t)\rangle_c$. This indicates that $\langle v_l(t)\rangle_c \sim t^{0.7}$ does not affect the t^2 law of the mean separation rate. We observe that the mean separation rate differs from scaling $\langle r(t)\rangle_c\langle v_l(t)\rangle_c \sim t^{3/2+0.7} = t^{2.2}$, as shown in the insets of Fig. 2.10(a) and (b), if we consider proper initial separation data as the truly asymptotic data. Therefore, non-Kolmogorov scaling $\langle v_l(t)\rangle_c \sim t^{0.7}$ is not ruled out due to the dependence despite the Richardson–Obukhov law $\langle r^2(t)\rangle_c \sim t^3$ or, equivalently, the scaling of its time derivative $\langle r(t)v_l(t)\rangle_c \sim t^2$.

2.4.2 Quasi-steady state simulation

The non-K41 scaling of the relative velocity as shown in Fig. 2.6 is not convincing due to the limited scaling range. Here, we increase the scaling range by using the quasi-steady state of the inverse energy-cascade turbulence [75].

Specifically, we solve the Navier–Stokes equation, Eq. (2.3), without the hypodrag term, i.e., $\alpha = 0$ by maintaining the other parameters as identical to those in Table 2.1 with hyperviscosity ($h = 8$). With respect to averaging, we generate ten random initial data with flat energy spectra extending up to the truncation wavenumber $k_{\max} = (N+2)/3$ with kinetic energy corresponding to 0.010. Over the ten runs, we take the ensemble average. We perform the simulation with the three resolutions corresponding to $N = 1024, 2048$, and 4096. We use the statistically quasi-steady velocity field obtained in time $24.0 \leq t \leq 26.5$ for advecting the particle pairs. In the time window, the energy spectrum shows the $k^{-5/3}$ scaling extending down to approximately $k = 1$ and the energy grows linearly in time as εt. Here, we do not use conditional sampling and consider only the particle pairs starting from the proper initial separation estimated as $r_0^{(p)} = 0.60 \times (2\pi/N)$ for each resolution, which amounts to $0.145 l_f$. The value exceeds those of the statistically steady state, $r_0^{(p)} = 0.078 l_f$ at $Re_\alpha = 39$ with normal viscosity and, $r_0^{(p)} = 0.089 l_f$ at $Re_\alpha = 40$, $r_0^{(p)} = 0.104 l_f$ at $Re_\alpha = 80$, and $r_0^{(p)} = 0.122 l_f$ at $Re_\alpha = 160$ with hyperviscosity. This indicates that $r_0^{(p)}$ is affected by the cut-off scale of the inertial range because small-scale quantities are expected to be identical to steady-state simulations.

Figure 2.11(a) shows $\langle r^2(t)\rangle$ satisfying the t^3 scaling law for longer duration than statistically steady-state cases. In Fig. 2.11(b), we present $\langle v_l^2(t)\rangle$ that confirms the non-K41 power-law scaling observed in the statistically steady-state simulations. In more precise terms, from the logarithmic local slope in the inset of Fig. 2.11(b), we estimate that the scaling exponent is approximately 1.2. This is consistent with the relation (2.8). We note that the slopes in the inset of Fig. 2.11(b) do not exhibit well-developed plateaus.

To summarize Sec. 2.4, we find the non-K41 scaling law of the relative velocity, $v_l(t) \propto t^{0.7}$, and self-similar evolution of the PDFs of $v_l(t)$ in the two selected ensembles of the particle pairs. An ensemble corresponds to pairs starting from the proper initial separation $r_0^{(p)}$. The other ensemble corresponds to the conditional sampling of the pairs starting from $r_0 > r_0^{(p)}$. For both ensembles, the Richardson–Obukhov law, $\langle r^2(t)\rangle = g\varepsilon t^3$, is designed to hold.

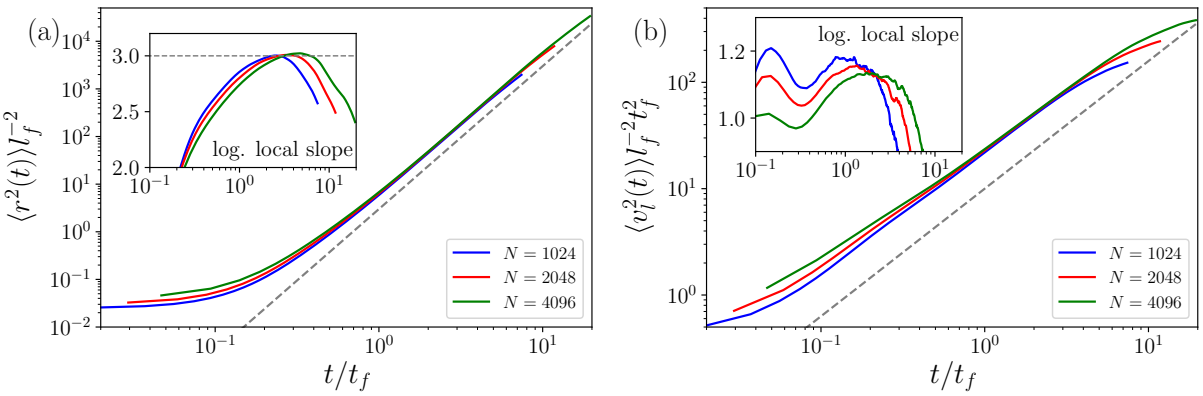

Figure 2.11: (a) Second-order moments of the relative separations, $\langle r^2(t)\rangle$, starting from the proper initial separations in the quasi-steady simulations with resolution $N = 1024, 2048$, and 4096. Dashed lines denote t^3 scaling. Inset: the logarithmic local slope of $\langle r^2(t)\rangle$. (b) Same as (a) albeit for the second-order moments of the longitudinal relative velocity, $\langle v_l^2(t)\rangle$. Dashed line denotes $t^{1.2}$ scaling. Inset: the logarithmic local slope of $\langle v_l^2(t)\rangle$.

2.5 Concluding Remarks

In the 2D inverse energy-cascade turbulence, we developed conditional sampling to recover the Richardson–Obukhov law by using the relation between the exit-time PDF and Richardson PDF. Here, Eq.(2.5) and Eq.(2.6) are the conditions for the conditional sampling to remove the particle pairs at $r_0 > r_0^{(p)}$ and $r_0 < r_0^{(p)}$, respectively. Here, $r_0^{(p)}$ is the proper initial separation as defined in Sec. 2.3.1. The conditional squared separation obeys the Richardson–Obukhov law, $\langle r^2(t)\rangle_c = g\varepsilon t^3$, irrespective of the initial separation r_0. It is noted that we mainly considered $r_0 > r_0^{(p)}$. The fraction of the particle pairs remaining in the conditional sampling increased with increases in Re_α. This supports our assumption that a bulk of the particle pairs for various initial separations at the moderate Reynolds numbers are in agreement with the Richardson–Obukhov law. As $Re_\alpha \to \infty$, deviation in $\langle r^2(t)\rangle$ from the Richardson–Obukhov law $g\varepsilon t^3$ is likely to vanish. This leads to a conclusion similar to that in a study of the Richardson–Obukhov law in 3D [32]. Furthermore, conditional sampling indicated that the relative velocity exhibits a different temporal scaling from the prediction of

the K41. The results are also obtained for the normal viscous and hyperviscous cases. Therefore, we conclude that the hyperviscosity does not affect the statistical properties of particle pairs.

Evidently, it is always possible to devise conditional sampling to obtain any desired result. To avoid the pitfall, we showed that the conditional statistics are weakly dependent on the parameters, number of the monitored zones N_Q, and the thresholds of the exit time τ's. An important finding is that $N_Q = 1$ is sufficient. This implies that the deviation from the Richardson–Obukhov law is caused in the dissipation range and also by the forcing. It implies that a major deviation is not produced later in the inertial range. The latter implication can result from the intermittency-free Eulerian velocity field of the 2D inverse energy-cascade turbulence.

However, the implications can overlook the behavior of pairs starting from the proper initial separation for which the deviation is negligible. The results indicated that the self-similar evolution of the longitudinal relative velocity is a common feature between the conditionally sampled pairs and unconditional pairs staring from $r_0^{(p)}$. This self-similarity is not observed in the unconditional pairs starting from $r_0 > r_0^{(p)}$. It should be noted that the self-similarity emerges only with the non-K41 power law of the equal-time relative velocity correlation, namely the relation (2.8). Furthermore, the self-similarity among the PDFs of various instances indicates that the non-K41 scaling differs from the intermittency observed in the Eulerian velocity increments of 3D turbulence. We argued that the non-K41 velocity scaling is not immediately ruled out by the enforced Richardson–Obukhov law.

The non-K41 power-law scaling obtained here, $\langle v_l^2(t)\rangle \propto t^{1.23}$, exhibits an exponent that differs from the K41 prediction, $\langle v_l^2(t)\rangle \propto \varepsilon t$. This can be qualitatively explained by the following behavior of the two-time correlation function of the Lagrangian relative velocity, $\langle \delta\boldsymbol{v}(s_1)\cdot\delta\boldsymbol{v}(s_2)\rangle$, where $\delta\boldsymbol{v}(t) = \boldsymbol{v}(t|\boldsymbol{a}+\boldsymbol{r}_0) - \boldsymbol{v}(t|\boldsymbol{a})$. We use DNS data starting from the proper initial separation and plot the correlation function in the 2D space (s_1, s_2). This type of a plot is presented for the 3D case in [55]. The two-time correlation is characterized by two functional forms as follows: one along the diagonal line and the other along the line perpendicular to the diagonal line. The preliminary study suggests that the two functional forms exhibit distinct self-similar functions. Specifically, we speculate that the self-similarity of the latter one along the line normal to the diagonal line leads to the deviation from the K41 scaling of the relative velocity. Thus, the non-K41 behavior of the velocity can be ascribed to the temporal correlation, which is ignored in the K41 argument [42, 88]. A future study will detail the two-time correlation.

The results obtained with the enforced Richardson–Obukhov law lead us to conclude that self-similarity of the relative velocity with the non-K41 scaling plays an indispensable role in the Richardson–Obukhov law of the squared separation. The condition is fulfilled for the pairs starting from the proper initial separation, $r_0^{(p)}$. An explanation for this is absent. It can be cautiously stated that quantitative aspects of the proper initial separation depend on the forcing because $r_0^{(p)} < l_f$.

We qualitatively discuss the characteristics of the special particle pairs initially sep-

arated by $r_0^{(p)}$ with respect to conditional sampling. The conditional sampling classifies particle pairs into three groups as follows: (i) removed particles for $r_0 > r_0^{(p)}$, (ii) removed particles for $r_0 < r_0^{(p)}$, and (iii) unremoved particles. It should be noted that we here include the result of the conditional sampling for $r_0 < r_0^{(p)}$. We argue that the nature of each group can be different. For $r_0 > r_0^{(p)}$, the power-law exponent of the unconditional $\langle r^2(t)\rangle$ is lower than the Richardson–Obukhov exponent 3 as shown in Fig. 2.2(a). In the conditional sampling, we remove particle pairs in which the exit time per the mean is lower than the threshold, τ. Subsequently, the power-law exponent of $\langle r^2(t)\rangle_c$ rises to 3. This implies that the removed pairs for $r_0 > r_0^{(p)}$ lower the power-law exponent of $\langle r^2(t)\rangle$.

A physical interpretation can be as follows. The removed pairs in the group (i) typically either hardly expand and consequently stay at around the initial separation or exit from the inertial range and then behave as standard Brownian particles while the unremoved particle pairs are still in the inertial range. Conversely, for $r_0 < r_0^{(p)}$, the power-law exponent of $\langle r^2(t)\rangle$ is larger than 3 as shown in Fig. 2.2(a). In the conditional sampling, we remove the particle pairs in which the exit time per the mean is within the interval, $[\tau_1, \tau_2]$, i.e., Eq. (2.6). Subsequently the power-law exponent of $\langle r^2(t)\rangle_c$ decreases to 3. This implies that the removed pairs for $r_0 < r_0^{(p)}$ increase the power-law exponent of $\langle r^2(t)\rangle$. A physical interpretation is as follows. The removed pairs for $r < r_0^{(p)}$ in the group (ii) typically expand anomalously fast through the inertial range while the unremoved particle pairs are still in the inertial range. The pairs in the group (iii), namely, the unremoved pairs in the conditional sampling regardless of the initial separation, are typically those that satisfy the Richardson–Obukhov law. The results indicated that the fraction of the pairs belonging to the groups (i) and (ii) significantly depend on the initial separation. Groups (i) and (ii) are potentially related to the extreme events [16, 105]. We now return to the proper initial separation. It is inferred that the effects of the two removed groups on $\langle r^2(t)\rangle$ are balanced at the proper initial separation. Hence, the Richardson–Obukhov law recovers for $r_0^{(p)}$ without the conditional sampling because contamination from the two groups is cancelled. Additionally, the cancelling also supports the dependence of the proper initial separation on the width of the inertial range mentioned in Sec.IVB, i.e., $r_0^{(p)}$ increases with Re_α. The number of particle pairs in the group (i) that exit the inertial range relatively fast and separate based on the t^2 law decreases inversely with the width of the inertial range, and the value of $r_0^{(p)}$ should be increased to cancel the anti-effects of groups (i) and (ii) on the scaling exponent.

We observed the non-Kolmogorov scaling law of the Lagrangian velocity. Evidently, an important question is whether or not the deviation from the K41 exponent persists when the Reynolds number increases. The trend shown in Fig.2.7(a) indicates that the deviation persists. However, it is not possible to eliminate the possibility that the Kolmogorov scaling law $\langle v_l^2(t)\rangle \propto t$ prevails at significantly higher Reynolds numbers. To address the question, an approach that differs from numerical simulation such as Lagrangian two-point closure theory, is preferable.

Our conditional sampling method can be easily adopted to 3D turbulence. However, the insights gained in 3D should significantly differ from those obtained here in the 2D inverse energy-cascade turbulence. Physics of the 2D energy inverse-cascade turbulence considerably differs from that of the 3D turbulence although the scaling argument using the dissipation rate (i.e., the mean energy flux) leads to the same prediction of scaling exponents of various statistics. The main difference is that it is necessary to add the forcing at a small scale for the 2D case. This implies that Lagrangian particles in 2D turbulence are more directly affected by the forcing than those in 3D turbulence. A future study will present a detailed analysis of the 3D problem.

Chapter 3

Two-time Lagranian velocity correlation function

3.1 Introduction

Velocity correlation function is fundamental to characterize turbulence. We can understand dynamical couplings between two points and two times in turbulence through the correlation function [51]. Eulerian and Lagrangian velocity correlation functions have different characteristic time scales from each other, which is essential to develop two-point closure approximations to the Navier-Stokes equations without ad-hoc parameters [58, 71, 73]. These direct-interaction approximations or Lagrangian renormalized approximations provide consistent results with Kolmogorov's 1941 (K41) phenomenology [70] and also with the 2D analog [11, 75, 78]. In particular, the success of these closures lies in adopting the approximation to the Lagrangian velocity correlation, not to the Eulerian velocity correlation.

The most general form of the second-order Lagrangian velocity correlation function can be written in terms of Kraichnan's generalized velocity notation [73] as

$$Q_{ij}^{L}(\boldsymbol{a}, s_1|t_1; \boldsymbol{b}, s_2|t_2) \equiv \langle v_i(\boldsymbol{a}, s_1|t_1) v_j(\boldsymbol{b}, s_2|t_2)\rangle. \tag{3.1}$$

Here $v_i(\boldsymbol{a}, s|t)$ is the i-th component of the Lagrangian velocity measured at time t of a Lagrangian particle passed through a point $\boldsymbol{a}$ at time s and $\langle\cdot\rangle$ denotes an ensemble average. Since the general form, Eq.(3.1), is too hard to tackle, majority of theoretical, numerical and experimental investigations on the Lagrangian velocity correlation is devoted to the abridged form of Eq.(3.1) by setting $s_1 = s_2$ and $t_2 = s_2$ [49, 50, 52, 59, 60, 61, 74], namely,

$$Q_{ij}^{L}(\boldsymbol{a}, s|t; \boldsymbol{b}, s|s) = \langle v_i(\boldsymbol{a}, s|t) v_j(\boldsymbol{b}, s|s)\rangle. \tag{3.2}$$

It should be noticed that $v_j(\boldsymbol{b}, s|s)$ coincides with the Eulerian velocity at a point $\boldsymbol{b}$ at time s. Thus, the correlation Eq.(3.1) is between the Lagrangian velocity and the Eulerian velocity.

An abridged form of Eq.(3.1) but involving only the Lagrangian velocity can be

$$Q_{ij}^{L}(\boldsymbol{a}, s|t_1; \boldsymbol{b}, s|t_2) = \langle v_i(\boldsymbol{a}, s|t_1) v_j(\boldsymbol{b}, s|t_2) \rangle, \tag{3.3}$$

where the measuring times t_1 and t_2 are different from the labeling time s. There are few studies on the Lagrangian correlation function Eq.(3.3) that is an essential ingredient to solve unsteady problems of turbulence such as turbulent diffusion and turbulent mixing [34]. In a notable study of the correlation Eq.(3.3) [55], the authors have performed a direct numerical simulation (DNS) to obtain the Lagrangian velocity correlation function Eq.(3.3). However, to analyze the computed correlation function, they had to resort to the theory developed for the Lagrangian-Eulerian correlation Eq.(3.2). This may be not only because a theory for the Lagrangian correlation Eq.(3.3) is not developed, but also because simple characterization of it remains to be done. By simple characterizations, we mean answers to the following cascading questions: does the Lagrangian correlation function Eq.(3.3) have a self-similar form?; if this is so, what is the self-similar form?; if the self-similar form is a power-law function, what are scaling exponents? In this section, we address these questions with phenomenological theory beyond the dimensional analysis and direct numerical simulations. Our simulation here is limited to two-dimensional energy inverse cascade turbulence, but the theory is applicable both to two and three dimensions.

One of the difficulties in these questions is that the Lagrangian velocity correlation function Eq.(3.3) is intrinsically dependent on both two times, t_1 and t_2. To illustrate our approach, let us show a color map of the Lagrangian correlation function as a function of t_1 and t_2 in Fig.3.1. For reasons described shortly, we do not consider the Lagrangian correlation Eq.(3.3). In stead, we study the Lagrangian velocity increment or, equivalently, the relative velocity between two Lagrangian particles

$$\delta v_i(\boldsymbol{a}, \boldsymbol{r}_0, s|t) \equiv v_i(\boldsymbol{a} + \boldsymbol{r_0}, s|t) - v_i(\boldsymbol{a}, s|t) \tag{3.4}$$

and its correlation

$$C_{ij}^{L}(r_0, t_1, t_2) = \langle \delta v_i(\boldsymbol{a}, \boldsymbol{r}_0, s|t_1) \delta v_j(\boldsymbol{a}, \boldsymbol{r}_0, s|t_2) \rangle, \tag{3.5}$$

where $r_0 = |\boldsymbol{r}_0|$. We call the Lagrangian correlation Eq.(3.5) as two-time Lagrangian correlation function in this section (on the left hand side of Eq.(3.5), we suppress to write dependence on $\boldsymbol{a}, s$). The two-time Lagrangian correlation function shown in Fig.3.1 is numerically computed in two-dimensional energy inverse-cascade turbulence. The details will be explained in Sec.3.3 in this section.

To characterize the two-time correlation function shown in Fig.3.1, one way is to look at it along the diagonal line through the origin, $t_1 = t_2$. The line is parallel to the "T" axis written in Fig.3.1. The other way is obviously to study it along the lines perpendicular to the diagonal line, i.e, $t_1 + t_2 = c_p$, where c_p is a positive constant. These lines are parallel to the "τ" axis written in Fig.3.1. Accordingly, a correlation time can be defined for each line. From Fig.3.1, it can be observed that a correlation time along

a perpendicular line grows as we increase the constant c_p. This sort of non-stationary behavior is not present in the two-point Eulerian velocity correlation, whose correlation time is constant due to the statistical stationarity. Unlike the Eulerian one, the two-time Lagrangian velocity correlation function has more than one degree of freedom. It implies that the scaling law of the two-time Lagrangian correlation function cannot be obtained by dimensional analysis. For this kind of problems, the incomplete similarity [6] provides a framework to specify possible self-similar forms. In this study, by using both the incomplete similarity and DNS, we propose a self-similar form of the two-time correlation function shown in Fig.3.1

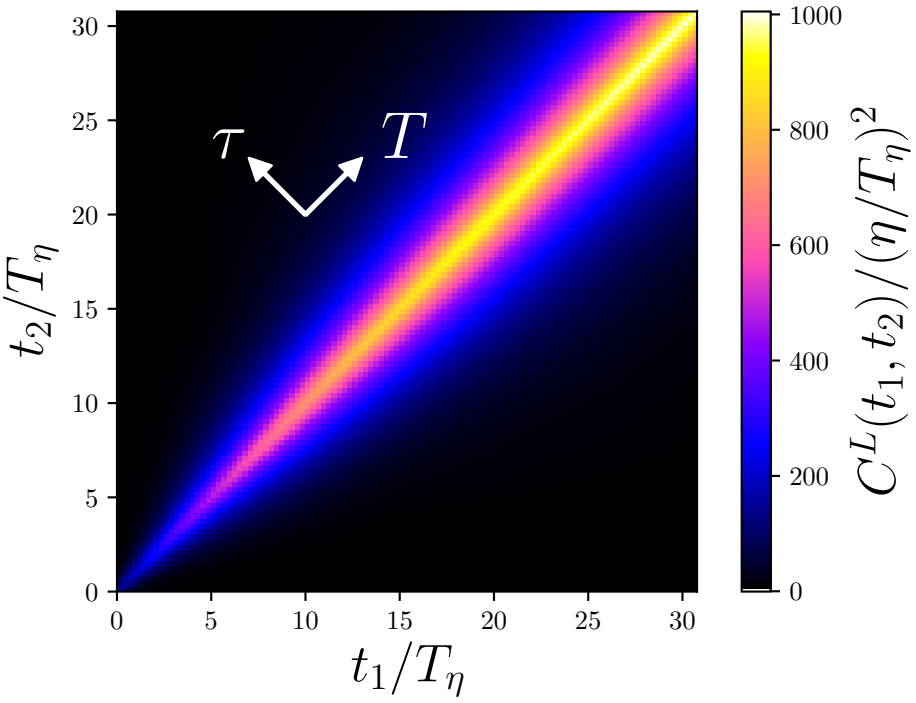

Figure 3.1: Color map of the two-time Lagrangian velocity correlation function, Eq.(3.5), with $T_B = 3.4T_\eta$ for $\mathrm{Re}_\alpha = 160$, where T_B and T_η are the Batchelor time and the Kolmogorov dissipation time scale, respectively. The infrared Reynolds number Re_α is defined in the main text. See Sec. 3.3 for details.

Now let us explain why we consider the correlation of the Lagrangian velocity increment, Eq.(3.4). The two-time Lagrangian velocity correlation function is directly related to relative dispersion as follows. The relative separation of a particle pair, whose Lagrangian labels are $\boldsymbol{a}$ and $\boldsymbol{r}_0$ at time 0, is written as

$$\boldsymbol{r}(t) = \boldsymbol{r}_0 + \int_0^t \delta\boldsymbol{v}(t')\, dt'. \tag{3.6}$$

The squared separation can then be written in terms of the two-time Lagrangian velocity

correlation function as

$$\langle r^2(t)\rangle = r_0^2 + 2\int_0^t \boldsymbol{r_0}\cdot\langle\delta\boldsymbol{v}(t_1)\rangle\, dt_1 + 2\int_0^t\int_0^t \langle\delta\boldsymbol{v}(t_1)\delta\boldsymbol{v}(t_2)\rangle\, dt_1 dt_2. \tag{3.7}$$

The turbulent relative dispersion has been widely investigated since the pioneering work by Richardson [98], who first predicted that the left hand side (lhs) of Eq.(3.7) grows as $\langle r^2(t)\rangle \propto t^3$ over an appropriate time interval, see Ref. [103] as a review. The t^3 prediction can be also derived by naively using the K41 dimensional analysis in the inertial subrange [9, 87] and therefore, the t^3 law is referred to as the Richardson–Obukhov law.

In the K41 framework, statistics on the relative separation, whose best studied quantity is the second moment $\langle r^2(t)\rangle$, is considered to be independent of the initial separation, r_0, as long as $r(t)$ is in the sufficiently wide inertial subrange. This implies that, when we plot $\langle r^2(t)\rangle$ starting from various r_0's, the curves become independent of r_0 and eventually collapses to the only one curve independent of r_0, which is proportional to t^3. Indeed, such an asymptotic state is indicated by DNS in three dimensions at high Reynolds numbers [32, 33, 104]. By contrast, one has never clearly observed the r_0-independence in laboratory experiments in three dimensions [90, 91] and in two dimensions [56, 99, 100, 119]. The situation is similar in numerical simulations of the 3D turbulence [15, 19, 32, 104, 126] and of the 2D inverse energy-cascade turbulence [25, 26, 65]. In this sense, the Richardson–Obukhov law is not verified satisfactorily by observations. Of course, with much higher Reynolds number, a cleaner t^3 law irrespective of r_0 may be observed. In this section, we parametrize finite Reynolds-number effect on the Richardson–Obukhov law by analyzing the two-time Lagrangian correlation function Eq.(3.5). Specifically, we will study Reynolds-number dependence of the correlation function. Then, through Eq.(3.7), we argue dependence of $\langle r^2(t)\rangle$ on r_0 at finite Reynolds numbers and infer its asymptotic form at infinite Reynolds number.

In particular, with moderate Reynolds numbers it is known that the t^3 scaling behavior of $\langle r^2(t)\rangle$ is observed for a certain selected initial separation, see Refs. [25, 63, 65] for further discussion. This special initial separation is around the Kolmogorov dissipation length for both 2D and 3D and thus dependent on the Reynolds number. Our argument on the r_0-dependence reveals nature of this special initial separation.

We organize this section as follows. In Sec. 3.2, we make ansatz of the scaling laws of the two-time Lagrangian velocity correlation function shown in Fig.3.1 by adopting the incomplete similarity [6]. The method enables us to explore qualitatively scaling laws that deviate from the K41 dimensional analysis. In particular, we take the finite Reynolds number effect and the dependence on r_0 into consideration.

Next, in Sec.3.3, we verify the ansatz and determine quantitatively scaling exponents involved by comparing with DNS data of 2D energy inverse-cascade turbulence. We estimate the scaling exponents as a function of Reynolds number by using DNSs with four different Reynolds numbers. Subsequently, we infer asymptotic values of the scaling exponents at infinite Reynolds number by extrapolating those at finite Reynolds numbers. There are several reasons for selecting the 2D system; detailed numerical

study is more feasible; the Eulerian velocity is intermittency free [22, 94] and therefore we factor out the intermittency effects on the Lagrangian statistics. Of course, careful discussion and further investigation are required when one applies the method used here to the 3D system.

In Sec.3.4, we discuss implications of the self-similar ansatz of the Lagrangian velocity correlation on the Richardson–Obukhov law. Furthermore, we explain why t^3 scaling law of $\langle r^2(t)\rangle$ is observed for a selected initial separation at moderate Reynolds numbers. Concluding remarks are made in Sec.3.5.

3.2 Incomplete self-similarity of the Lagrangian correlation and scaling exponents

In this section, we present a scaling ansatz of the two-time Lagrangian velocity correlation function for particle pairs. It should be noted that the argument below is independent of specific dimensions. Therefore, we expect that the ansatz is meaningful for both 2D and 3D turbulence.

As we discussed in Sec.3.1, we consider the Lagrangian correlation function, $C^L_{ii}(r_0, t_1, t_2)$, of the velocity difference Eq.(3.4), where we use the Einstein summation convention of the repeated indices. We write $C^L_{ii}(r_0, t_1, t_2)$ as $C^L(r_0, t_1, t_2)$ below.

We consider a statistically steady, homogeneous, and isotropic turbulent Eulerian velocity field, and therefore we deal with an external forcing which leads to such a state. In the following scaling argument, we ignore effects of the external forcing on the Lagrangian correlation function. Later, in Sec. 3.5, we discuss the effects when we analyze the DNS data of the correlation function.

Let us first change time variables from t_1 and t_2 to an average time, T, and a relative time, τ as

$$T \equiv \frac{t_1 + t_2}{2}, \quad \tau \equiv t_1 - t_2. \tag{3.8}$$

The new variables are useful because the correlation function is symmetrical with respect to the T-axis as shown in Fig.3.1.

Now we present the scaling ansatz for the Lagrangian correlation function. Our arguments are given thereafter. The Lagrangian correlation function can be this form:

$$C^L(r_0, T, \tau) = \varepsilon T \Phi(r_0, T, \tau), \tag{3.9}$$

which we assume to be valid at an appropriate time interval. Here ε is the energy dissipation rate. The non-dimensional function $\Phi(r_0, T, \tau)$ includes deviation from the dimensional analysis. By using the idea of incomplete similarity [6], we argue that $\Phi(r_0, T, \tau)$ can be written as

$$\Phi(r_0, T, \tau) = G\left(\frac{T_B}{T}\right)^{\gamma} g^L\left(\frac{\tau}{T_B^{\beta} T^{1-\beta}}\right), \tag{3.10}$$

where G is a non-dimensional, non-zero constant, T_B is the Batchelor time as we will define later, and $g^L(\xi)$ is a non-dimensional self-similar function with $g^L(0) = 1$. Here the two scaling exponents, β and γ, appear. They are not determined by dimensional analysis. With the ansatz Eq.(3.10), the width of the ridge along the diagonal line $t_1 = t_2$ shown in Fig. 3.1 is given by $T(T_B/T)^\beta$. Later in Sec.3.3, by comparing with DNS data, we will show that the exponents take the following functional form

$$\beta = \beta_0 + \tilde{\beta}\left(\frac{T_\eta}{T_B}, \frac{T_L}{T_B}\right), \tag{3.11}$$

$$\gamma = \gamma_0 + \tilde{\gamma}\left(\frac{T_\eta}{T_B}, \frac{T_L}{T_B}\right). \tag{3.12}$$

Here, we introduce three time scales, T_B, T_η, and T_L, which are given by

$$T_B \equiv \left(\frac{r_0^2}{\varepsilon}\right)^{1/3}, T_\eta \equiv \left(\frac{\eta^2}{\varepsilon}\right)^{1/3}, T_L \equiv \left(\frac{L^2}{\varepsilon}\right)^{1/3}, \tag{3.13}$$

where T_B is the Batchelor time associated with the initial separation r_0 [8], T_η is the smallest time scale of turbulence associated with the smallest length scale, η, such as Kolmogorov dissipation length, and T_L is the largest time scale of turbulence associated with the largest length scale, L, such as the integral scale.

Now let us explain how we reach the scaling ansatz, (3.9)–(3.12), of the Lagrangian correlation function. Our argument here follows the self-similar analysis of Ref. [6]. First, we specify a system of all the governing parameters of the correlation function, $C^L(r_0, T, \tau)$. It depends on the average time, T, the relative time, τ, which are defined in Eqs. (3.8), the initial separation of particle pairs, r_0, the energy dissipation rate or the average energy flux in the inertial subrange, ε, the smallest length scale of turbulence such as the Kolmogorov length, η, and the largest length scale of turbulence such as the integral scale, L. Taking them into account, we rewrite arguments of the two-time correlation function of the relative Lagrangian velocity as

$$C^L(r_0, T, \tau, \varepsilon, \eta, L) = \langle \delta v_i(\boldsymbol{a}, \boldsymbol{r}_0, s = 0|t_1)\delta v_i(\boldsymbol{a}, \boldsymbol{r}_0, s = 0|t_2)\rangle \tag{3.14}$$

Here we take average over the Lagrangian marker $\boldsymbol{a}$. Hence we omit dependence on $\boldsymbol{a}$. We set the labeling time to zero, i.e., $s = 0$ and t_1 and t_2 are measured from this time origin. We also omit dependence on s on the left hand side of Eq.(3.14). For the 2D energy inverse-cascade turbulence, we can use the characteristic length of the drag as L instead of the integral scale and use the energy flux cascading inversely in the inertial range as ε. In this case, we can explicitly write down L dimensionally by using the drag coefficient and the energy dissipation rate. This may be an advantage of the 2D turbulence.

Second, we apply the Buckingham Π-theorem [6] to Eq.(3.14) by assuming that independent dimensions are ε and T. This means that all the other governing parameters

are non-dimensionalized by ε and T. This leads to an expression with a dimensionless function, C_*^L, as

$$C^L(r_0, T, \tau, \varepsilon, \eta, L) = \varepsilon T \; C_*^L \left(\frac{\tau}{T}, \frac{r_0}{\varepsilon^{1/2} T^{3/2}}, \frac{\eta}{\varepsilon^{1/2} T^{3/2}}, \frac{L}{\varepsilon^{1/2} T^{3/2}} \right). \tag{3.15}$$

This is rewritten by using the time scales (3.13) as

$$C^L(r_0, T, \tau, \varepsilon, \eta, L) = \varepsilon T C_*^L \left(\frac{\tau}{T}, \frac{T_B}{T}, \frac{T_\eta}{T}, \frac{T_L}{T} \right). \tag{3.16}$$

Third, we consider intermediate asymptotics of the time scales, T_η, T, and T_L, and reduce the number of the arguments on the right hand side of Eq.(3.16). As is clear from our choice of the independent dimensions, we assume that T_η and T_L, are sufficiently separated and that

$$T_\eta \ll T \ll T_L. \tag{3.17}$$

This intermediate time interval for T is a Lagrangian counterpart of the inertial subrange of the Eulerian velocity statistics. We call the time interval the inertial subrange in this section. In this inertial subrange, we assume that the correlation function becomes independent of T_η and T_L. This implies that the complete similarity holds for T_η and T_L. Hence, with a dimensionless function $C_{**}^L(\zeta, \xi)$, Eq.(3.16) is simplified as,

$$C^L(r_0, T, \tau, \varepsilon) = \varepsilon T C_{**}^L \left(\frac{\tau}{T}, \frac{T_B}{T} \right). \tag{3.18}$$

Fourth, let us also assume that the initial separation, r_0, is sufficiently small. Namely, we consider that the average time is much larger than T_B ($\propto r_0^{2/3}$):

$$(T_\eta \ll) \quad T_B \ll T \quad (\ll T_L) \tag{3.19}$$

To discuss behavior of C^L in this time range, for simplicity, we rewrite the dimensionless times as

$$\zeta \equiv \frac{\tau}{T}, \quad \xi \equiv \frac{T_B}{T}. \tag{3.20}$$

instead of τ, T in Eqs (3.8) and T_B in Eqs (3.13). The additional asymptotics (3.19) implies $\xi \to 0$. Now there are two possibilities for the asymptotic behavior of $C_{**}^L(\zeta, \xi)$ as $\xi \to 0$ [6]:

(i) the limit of $C_{**}^L(\zeta, 0)$ exists and is finite and non-zero,

(ii) no finite limit of $C_{**}^L(\zeta, 0)$ exists, or the limit is zero if it exists.

We do not know a priori which case holds unless the full functional dependence of $C^L(r_0, T, \tau, \varepsilon)$ was obtained theoretically from the Navier-Stokes equations. It is necessary to study data for small ξ, which is obtained from DNS or laboratory experiment in order to conclude which case is valid [6].

Now let us discuss implications of each case. In the case (i), a scaling law for $C^L(\zeta, 0)$ is consistent with the K41 phenomenology. In other words, we can determine the scaling relations for $C^L(\zeta, 0)$ by dimensional analysis (complete similarity). In this case, we can estimate ξ-dependence by the Taylor series

$$C^L_{**}(\zeta, \xi) = C^L_{**}(\zeta, 0) + A_1(\zeta)\xi + O(\xi^2), \tag{3.21}$$

where $A_1(\zeta) = (\partial C^L_{**}/\partial\xi)_{\xi=0}$. Therefore, in the case (i), the scaling law for $C^L(r_0, T, \tau)$ is as follows:

$$C^L(r_0, T, \tau) = \varepsilon T A_0\left(\frac{\tau}{T}\right) + \varepsilon T_B A_1\left(\frac{\tau}{T}\right) + O(\xi^2), \tag{3.22}$$

where $A_0(\tau/T) = C^L_{**}(\tau/T, 0)$.

Furthermore, when the intermediate asymptotics (3.17) is insufficient, we assume that there were still complete similarity but no similarity in T_η and T_L [7]. Under this assumption, in the inertial range, Eq.(3.22) may be modified as

$$C^L(r_0, T, \tau) = \varepsilon T A_0\left(\frac{\tau}{T}, \frac{T_\eta}{T_L}\right) + \varepsilon T_B A_1\left(\frac{\tau}{T}, \frac{T_\eta}{T_L}\right) + O(\xi^2). \tag{3.23}$$

It should be noted that the width of ridge along the diagonal line $t_1 = t_2$ shown in Fig.3.1 is given by T in the inertial range for any Reynolds number.

On the other hand, in the case (ii), a scaling law for $C^L(\zeta, \xi)$ has non-trivial scaling exponents which cannot be determined by dimensional analysis (incomplete similarity). When ξ is sufficiently small, as a natural self-similar form suggested in [6], we propose

$$C^L_{**}(\zeta, \xi) = G\xi^\gamma g^L\left(\frac{\zeta}{\xi^\beta}\right), \tag{3.24}$$

where $g^L(X)$ is a dimensionless function and $g^L(0) = 1$. Here G is a non-zero constant factor and independent of T_B. It should be noticed that Eq.(3.24) is consistent with the case (ii) since the function $g^L(X)$ is bounded. The scaling exponents, β and γ, are determined either by the Navier-Stokes equations (or, more precisely, closure equations for the Lagrangian correlation function) or by comparison with experimental data.

As we will show in Sec.3.3, the case (ii) yields a better agreement with DNS data of 2D energy inverse-cascade turbulence than for the case (i). Therefore, we conclude that the case (ii) holds for the 2D turbulence. Finally, we arrive at the following form for the Lagrangian correlation function:

$$C^L(r_0, T, \tau, \varepsilon) = G\varepsilon T\left(\frac{T_B}{T}\right)^\gamma g^L\left(\frac{\tau}{T\left(\frac{T_B}{T}\right)^\beta}\right), \tag{3.25}$$

which is supposed to hold under the conditions (3.17) and (3.19).

Having obtained the ansatz for the temporal inertial range, we now consider finite-Reynolds number effect. The argument below is very much heuristic and should be

justified experimentally. At finite Reynolds numbers, we assume that the above self-similar form (3.25) is applicable. However, we assume that the scaling exponents, β and γ, are dependent on T_η and T_L in such a way that

$$\beta = \beta_0 + \tilde{\beta}\left(\frac{T_\eta}{T_B}, \frac{T_L}{T_B}\right), \quad \gamma = \gamma_0 + \tilde{\gamma}\left(\frac{T_\eta}{T_B}, \frac{T_L}{T_B}\right). \tag{3.26}$$

Here β_0 and γ_0 are asymptotic values for infinite Reynolds number, and are therefore independent of T_η and T_L. In addition, the constant factor, G, may also depend on T_η and T_L at finite Reynolds numbers. In the next section we show that these hypothetical formula of the exponents are useful to fit the DNS data obtained at finite Reynolds numbers and to infer the asymptotic behavior of C^L.

It should be noted that an undetermined scaling exponent such as β or γ does not appear in a scaling relation for the Eulerian two-time correlation function $C^E(r, t_1, t_2)$ of the velocity increments, which is defined by

$$C^E(r, t_1, t_2) = \langle \delta u_i(\boldsymbol{x}, \boldsymbol{r}, t_1) \delta u_i(\boldsymbol{x}, \boldsymbol{r}, t_2) \rangle. \tag{3.27}$$

Here the Eulerian velocity increment is given by

$$\delta u_i(\boldsymbol{x}, \boldsymbol{r}, t_1) = u_i(\boldsymbol{x} + \boldsymbol{r}, t_1) - u_i(\boldsymbol{x}, t_1) \tag{3.28}$$

and $r = |\boldsymbol{r}|$. We used spatial homogeneity and isotropy.

Because of the statistically steady state, $C^E(r, t_1, t_2)$ does not depend on T and can be written with all the governing parameters by

$$C^E(r, t_1, t_2) = C^E(r, \tau, \varepsilon, \eta, L). \tag{3.29}$$

According to the Π-theorem, there exists a dimensionless function, C^E_*, by regarding ε and r as the independent parameters, such that C^E has the form,

$$C^E(r, \tau, \varepsilon, \eta, L) = \varepsilon^{2/3} r^{2/3} C^E_* \left(\frac{\tau}{\varepsilon^{-1/3} r^{2/3}}, \frac{\eta}{r}, \frac{L}{r}\right). \tag{3.30}$$

Furthermore, when we consider that r is in the inertial subrange,

$$\eta \ll r \ll L, \tag{3.31}$$

we can assume that, as $\eta \to 0$ and $L \to \infty$, the dependence on η and L can be ignored. Then C^E has a reduced form,

$$C^E(r, \tau, \varepsilon) = C_2 \varepsilon^{2/3} r^{2/3} g^E\left(\frac{\tau}{\varepsilon^{-1/3} r^{2/3}}\right), \tag{3.32}$$

where C_2 is a universal constant related to the Kolmogorov constant and the function $g^E(X)$ satisfies $g^E(0) = 1$. This is consistent with Kolmogorov phenomenology. In this way, the scaling law of the Eulerian velocity correlation function can be determined by the dimensional analysis thanks to the statistical stationarity. This is different from the Lagrangian velocity correlation function. However, it should be noted that the sweeping effect by large-scale advection of eddies [72, 111] may be more dominant than the Kolmogorov time scale $\varepsilon^{-1/3} r^{2/3}$. If that is the case, the Eulerian correlation function may be different from the the scaling law given in Eq.(3.32), see Refs. [51, 120] for review.

3.3 Numerical experiments

3.3.1 Numerical details

We perform DNS of the 2D inverse energy-cascade turbulence in order to numerically verify the ansatz made in Sec.3.2. We suppose that the Eulerian velocity field, $\boldsymbol{u}(\boldsymbol{x},t)$, follows the two-dimensional Navier-Stokes equation with forcing, hyperviscous, and hypodrag terms. We numerically solve the equation in terms of the vorticity,

$$\frac{\partial\omega}{\partial t}+(\boldsymbol{u}\cdot\nabla)\,\omega=(-1)^{h+1}\nu\Delta^{h}\omega+\alpha\Delta^{-1}\omega+f, \tag{3.33}$$

where ω is vorticity filed, $\omega(\boldsymbol{x},t)=\partial_x u_y(\boldsymbol{x},t)-\partial_y u_x(\boldsymbol{x},t)$. The hyperviscous, and hypodrag terms are the first and second terms on the right hand side of Eq.(3.33) and f is an external forcing term. For the 2D inverse energy-cascade turbulence, the smallest and largest time scale can be explicitly described by the viscous coefficient, ν, and the drag coefficient, α, respectively as below:

$$T_\eta\equiv\left(\frac{\nu}{\varepsilon^h}\right)^{\frac{1}{3h-1}},\quad T_L\equiv\left(\frac{1}{\alpha\varepsilon}\right)^{\frac{1}{4}}.$$

This is an advantage of the 2D turbulence, because the integral time scale of the 3D turbulence cannot be explicitly described.

The forcing term, $f(\boldsymbol{x},t)$, is given in terms of the Fourier coefficients, $\hat{f}(\boldsymbol{k},t)=k^2\varepsilon_{in}/[n_f\hat{\omega}^*(\boldsymbol{k},t)]$, where $\hat{f}$ denotes the Fourier transform of the function $f(\boldsymbol{x},t)$. The energy input rate is denoted by ε_{in}, and n_f denotes the number of the Fourier modes in the following forcing wavenumber range. We select the coefficients, $\hat{f}(\boldsymbol{k},t)$, as non-zero only in high wave numbers, $\boldsymbol{k}$, satisfying $k_f-1<|\boldsymbol{k}|<k_f+1$. Thus, the energy input rate is maintained as constant in time. Numerical integration of Eq. (3.33) is performed via the pseudospectral method with the 2/3 dealiasing rule in space and the 4-th order Runge–Kutta method in time. The setting and our numerical method are identical to those used in [85, 122]. In this DNS, the maximum wavenumber is $k_{max}=\sqrt{2}N/3$, where N^2 is the number of grid points. Here, $k_{max}\eta\simeq 1.8$, where η is the Kolmogorov length. Here we use the infrared Reynolds number, $\mathrm{Re}_\alpha\equiv k_f/k_\alpha$, as proposed by Vallgren [116] in order to quantify the span of the inertial subrange. In Table 3.1 we list the parameters of simulations used in the study.

To obtain the Lagrangian statistics, we employ a standard particle tracking method. The flow is seeded with a large number of tracer particles. The number of particles, N_p^2, for each simulation is described in Table 3.1. The particles are tracked in time via integrating the advection equation,

$$\frac{\mathrm{d}}{\mathrm{d}t}\boldsymbol{x}_p(t)=\boldsymbol{u}(\boldsymbol{x}_p(t),t), \tag{3.34}$$

where $\boldsymbol{x}_p(t)$ denotes the particle position vector. The numerical integration of Eq. (3.34) is performed using the Euler method. The velocity value at an off-grid particle position

Table 3.1: Parameters of numerical simulations: N^2, $\delta x = 2\pi/N$, δt, ν, h, α, k_f, ε_{in}, and N_p^2 denote the number of grid points, grid spacing, size of the time step, hyperviscosity coefficient, order of the Laplacian of the hyperviscosity, hypodrag coefficient, forcing wavenumber, energy input rate of the forcing, and, number of the Lagrangian particles, respectively. Turbulent characteristics: ε, σ_ε, L, $u_{\rm rms}$, Re_α, T_η, and T_L denote mean of the resultant energy flux in the inertial subrange, standard deviation of the resultant energy flux, integral scale, root-mean-square velocity, infrared Reynolds number, viscous time scale, and, drag time scale, respectively.

N^2	δx	δt	ν	h	α	k_f	ε_{in}	N_p^2	ε	σ_ε	L	$u_{\rm rms}$	Re_α	T_η	T_L
1024^2	0.006	0.002	1.82×10^{-38}	8	35	249	0.1	2048^2	0.019	2.9×10^{-4}	0.38	0.5	40	0.091	1.1
2048^2	0.003	0.001	4.664×10^{-43}	8	35	496	0.1	2048^2	0.019	2.9×10^{-4}	0.37	0.5	80	0.057	1.1
4096^2	0.0015	0.001	1.05×10^{-47}	8	35	997	0.1	4096^2	0.019	2.6×10^{-4}	0.36	0.5	160	0.036	1.1

is estimated by the fourth-order Lagrangian interpolation of the velocity calculated on the grid points.

In Eq.(3.33), we use hyperviscosity, $h = 8$, rather than normal viscosity, $h = 1$, for DNSs. This is because the hyperviscosity extends the inertial subrange for a given spatial resolution. We confirmed that the hyperviscosity does not affect the particle-pair statistics in Ref. [65].

First of all, let us consider to what extent the assumptions on the time separations, $T_\eta \ll T \ll T_L$ (Eq.(3.17)) and $T_B \ll T$ (Eq.(3.19)), made in Sec.3.2 holds in our DNS. In the DNS, $T_L/T_\eta \lesssim 10^2$. Certainly, this poses limitations on studying whether the asymptotic behavior of the Lagrangian correlation function, Eq.(3.25), is valid. In theory, if $T_\eta \ll T_B \ll T_L$, then the particle pairs may be hardly influenced by neither the viscosity nor the large scale drag from the beginning of the relative diffusion. However, in practice, due to the limited scale separation, $\xi = T_B/T$ may not become sufficiently small in our DNS, as $T = (t_1 + t_2)/2$ increases while satisfying $T_\eta < T_B < T < T_L$. Therefore, it is inevitable to consider that the numerically obtained correlation function, $C^L(r_0, T, \tau, \varepsilon)$, depends on T_η and T_L even if the large T_B condition, $T_\eta < T_B < T_L$, is satisfied.

Given this practical limitations, it is useful to relax the large T_B condition and to consider the case $T_B < T_\eta$, which we call the small T_B condition. Obviously in the small T_B condition, we cannot ignore viscous effects on particle-pair statistics. However, the value of $\xi = T_B/T$ can become smaller as the average time T increases in $T_\eta \ll T \ll T_L$ than in the large T_B condition. Some previous studies investigate particle-pair statistics in the small T_B condition [16, 26, 56, 105]. Of course, it is not obvious that the two different conditions give the same asymptotic behavior of $C^L(r_0, T, \tau, \varepsilon)$ as $\xi = T_B/T \to 0$. Therefore, we investigate dependencies on T_η, T_L and T_B for both conditions in the following subsections.

More specifically, we investigate the two scaling exponents, β and γ, appeared in our anzats (3.9). For this purpose, we decompose the Lagrangian velocity correlation

function $C^L(r_0, T, \tau, \varepsilon)$ into two parts:

$$C^L(r_0, T, \tau, \varepsilon) = C_d^L(T, T_B) C_p^L(T, \tau, T_B), \tag{3.35}$$

where $C_d^L(T, T_B)$ corresponds to the two-time Lagrangian correlation function along the diagonal line $t_1 = t_2$, that is, $C_d^L(T, T_B) \equiv C^L(r_0, T, \tau = 0, \varepsilon)$. The other part $C_p^L(T, \tau, T_B)$ corresponds to the two-time correlation along a line $t_1 + t_2 = 2T$, which is perpendicular to the diagonal line. Its value at $\tau = 0$ is normalized: $C_p^L(T, \tau = 0, T_B) = 1$. If the ansatz is correct, $C_p^L(T, \tau, T_B) = g^L(\tau/[T^{1-\beta} T_B^{\beta}])$.

In what follows, the values of the exponents, γ and β, are estimated from numerically calculated $C_d^L(T, T_B)$ and $C_p^L(T, \tau, T_B)$, respectively, as we vary T_B and T_η. We consider first the large T_B condition ($T_B > T_\eta$) and then the small T_B condition.

3.3.2 Large T_B condition: $T_\eta \ll T_B \ll T \ll T_L$

Let us consider the scaling laws of $C^L(r_0, T, \tau, \varepsilon)$ under the large T_B condition. In DNS, although this condition, $T_\eta < T_B < T_L$ is satisfied, the scale separations, $T_\eta \ll T \ll T_L$ and $T_B \ll T$, are not sufficient even in our largest simulation with $\mathrm{Re}_\alpha = 160$. Figure 3.2 shows color maps of $C^L(r_0, T, \tau, \varepsilon)$ in terms of the original time variables t_1 and t_2 with $T_B = 3.5 T_\eta$ for the three cases of Re_αs. We observe that the width of the ridge along the diagonal line (the region where the correlation $C^L(r_0, T, \tau, \varepsilon)$ remains large) becomes wider as the average time $T = (t_1 + t_2)/2$ increases. We also observe that qualitatively this tendency appears to be independent of Re_α.

Now we focus on the behavior of the correlation function along the diagonal line. Figure 3.3(a) shows time evolution of $C_d^L(T, T_B) = C^L(r_0, T, \tau = 0, \varepsilon)$ for various T_Bs. Obviously, it indicates that a scaling exponent, if it exists, is dependent on T_B. Figure 3.3(b) shows logarithmic local slopes (LLSs) of $C_d^L(T, T_B)$. If the ansatz (3.9) is valid, the LLS becomes $1 - \gamma$ (constant). We see that a narrow plateau region for each LLS. For the plateau, as T_B approaches T_η from above, we observe that the plateau region becomes wider and that the value of the plateau region becomes closer to 1 which corresponds to $\gamma = 0$. For further quantification, we infer the value of γ for each curve from the maximum value of the LLS. In the argument given in Sec.3.2, we assumed that the exponent γ is independent of T_B, T_η, and T_L. However, the data shown here indicate that it is not the case. To circumvent this, we now use the empirical form for γ given in Eq.(3.26).

Figure 3.3(c) shows the maximum values of the LLSs, which we regard as γ in Eq.(3.26), which is dependent on T_B, T_η and T_L. The horizontal axis of Fig.3.3(c) is set to $(T_B - T_\eta)/T_L$. We find empirically this combination of the independent variables, $(T_B - T_\eta)/T_L$, to make the data points collapse onto a single curve. The first observation concerns the behavior as $(T_B - T_\eta)/T_L \to 0$ (when T_B approaches T_η from above): the exponent γ seems to approach 0. However, this limit $T_B \to T_\eta$ violates the large T_B condition, $T_\eta \ll T_B \ll T_\eta$. The second observation is about the behavior at the large $(T_B - T_\eta)/T_L$ range, which is consistent with the large T_B condition. In this range, we

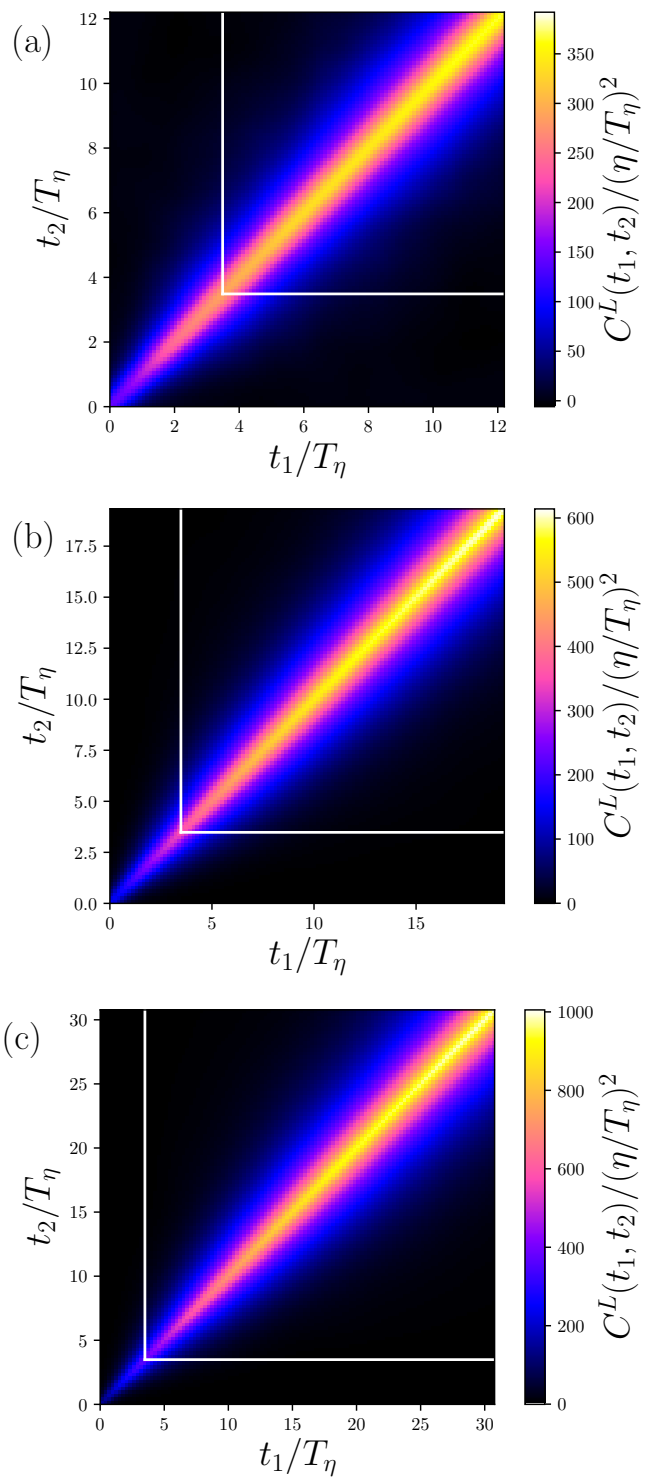

Figure 3.2: Color maps of time evolution of the Lagrangian velocity-increment correlation $C^L_{ii}(r_0, t_1, t_2)$ defined in Eq.(3.5) with $T_B = (r_0^2/\varepsilon)^{1/3} = 3.5T_\eta$. (a) $\mathrm{Re}_\alpha = 40$, (b) $\mathrm{Re}_\alpha = 80$, (c) $\mathrm{Re}_\alpha = 160$. The white lines indicate $t_i = T_B$ $(i = 1, 2)$. Here the time axes, t_i/T_η $(i = 1, 2)$, span from 0 to T_L/T_η.

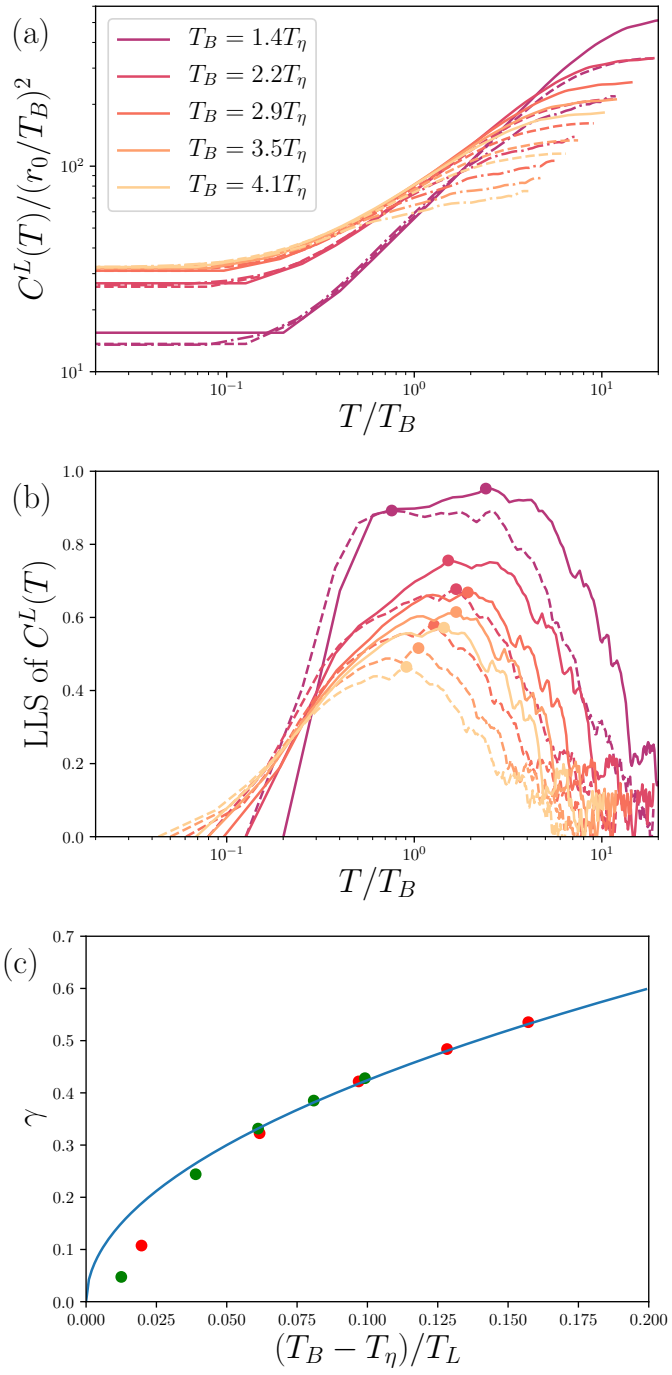

Figure 3.3: (a) Time evolution of $C_d^L(T, T_B)$ for various T_Bs at $\mathrm{Re}_\alpha = 40$ (dashed dotted), 80 (dashed), and 160 (solid). (b) Logarithmic local slope (LLS) of $C_d^L(T, T_B)$ at $\mathrm{Re}_\alpha = 40$ (dashed) and 160 (solid). The filled circle on each line indicates the position of the maximum. (c) Value of the exponent γ suggested by the maximum value of the LLS plotted as a function of $(T_B - T_\eta)/T_L$ at $\mathrm{Re}_\alpha = 40$ (red) and 160 (green). The blue solid line corresponds to $1.34[(T_B - T_\eta)/T_L]^{0.5}$, which is determined by the least square fit in the range $0.039 \leq (T_B - T_\eta)/T_L \leq 0.16$.

observe that the master curve becomes independent of Re_α as shown in Fig.3.3(c). Our best fit function to the curve for the exponent γ is

$$\gamma\left(\frac{T_\eta}{T_B}, \frac{T_L}{T_B}\right) = \overline{\gamma}_0 \left(\frac{T_B - T_\eta}{T_L}\right)^{1/2}, \tag{3.36}$$

which is plotted as a solid line in Fig.3.3(c). Here $\overline{\gamma}_0$ is a constant estimated about 1.34 ± 0.01 by the fitting.

Now we come back to the ansatz (3.9) leading to $C^L(r_0, T, \tau = 0, \varepsilon) \propto T^{1-\gamma}$. The functional form of the exponent (3.36) indicates that $\gamma \to 0$, when the scale separation (3.19) is sufficient. This implies that the K41 scaling, $C^L(r_0, T, \tau = 0, \varepsilon) = C_d^L(T, T_B) \propto T$, is recovered under the sufficient scale separation. However, for this recovery, the exponent 1/2 in Eq.(3.36) suggests that we need an enormously large Re_α. For example, in order to get the value of γ valid for one effective figure, $\gamma \sim 0.01$, we may need $T_L/T_\eta \sim 10^5$ (in our DNS here $T_L/T_\eta \sim 30$ at most), which may correspond to $\mathrm{Re}_\alpha \sim 10^6$.

On the other hand, at small values of $(T_B - T_\eta)/T_L$, γ deviates from the relation (3.36) as shown in Fig. 3.3(c). Let us suppose that the deviation persists at larger Reynolds numbers. Then γ may have a negative limit value as $T_B \to T_\eta$ (approaching T_η from above). We extrapolate the deviation to $(T_B - T_\eta)/T_L = 0$ and obtain the limit value of γ about -0.25. We cannot conclude whether the deviation remains at sufficient large Reynolds numbers from our DNS. In summary of the result for the correlation function along the diagonal line, our simulation data suggest that the scaling law of $C_d^L(T, T_B)$ at sufficiently large Re_α is,

$$C^L(r_0, T, \tau = 0, \varepsilon) = C_d^L(T, T_B) = G\varepsilon T_B^{\overline{\gamma}_0\sqrt{\frac{T_B - T_\eta}{T_L}}} \; T^{1-\overline{\gamma}_0\sqrt{\frac{T_B - T_\eta}{T_L}}}. \tag{3.37}$$

where G, which is the constant appeared in Eq.(3.9), is estimated as $G \sim 80$ from the compensated plot of Fig.3.3(a) by $T_B^\gamma T^{1-\gamma}$ (the compensated plot is not not shown).

Next, we consider the behavior of the correlation function along the lines perpendicular to the diagonal line, which is given by $C_p^L(T, \tau, T_B)$. Figure 3.4 shows sectional views of the color map shown in Fig.3.2 for various sections given by the lines $t_1 + t_2 = 2T$. It should be noted that the curves shown in Fig.3.4 are normalized by $C_d^L(T, T_B)$. Hence they are the graphs of $C_p^L(T, \tau, T_B)$ as a function of the relative time $\tau = t_2 - t_1$ for a fixed average time T.

We first notice that the typical width of the peak of $C_p^L(T, \tau, T_B)$ centered at zero relative time $\tau = 0$ is given by the dissipation time scale T_η initially, i.e., for small average time T. Then, the width becomes larger and larger as the average time increases. At large average times, $T \lesssim T_L$, the function $C_p^L(T, \tau, T_B)$ decreases exponentially as shown in the insets of Fig. 3.4. Moreover, the data indicate that $C_p^L(T, \tau, T_B)$ decreases faster than exponential at $\tau \sim T_L$.

To quantify the decay of $C_p^L(T, \tau, T_B)$, we use a n-th decay time scale, $\tau_{1/n}(T)$, defined as

$$C_p^L(T,\ \tau = \tau_{1/n}(T),\ T_B) = \frac{1}{n}. \tag{3.38}$$

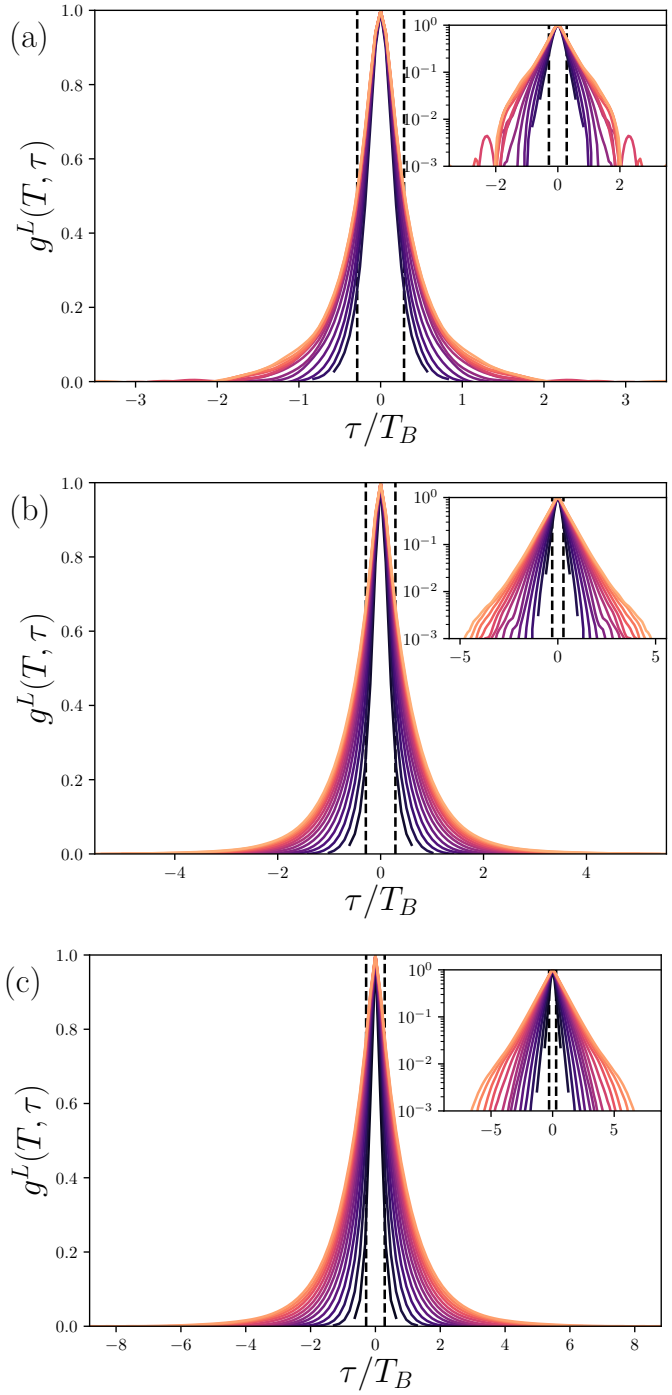

Figure 3.4: Normalized correlation function, $C_p^L(T,\tau,T_B)$, defined in Eq.(3.35) as a function of the relative time τ with $T_B = 3.5T_\eta$ for various Ts. The average time varies in $T_\eta < T < 0.54T_L$ and the corresponding curves are colored from black to yellow. The three panels corresponds to (a) $\mathrm{Re}_\alpha = 40$, (b) $\mathrm{Re}_\alpha = 80$, (c) $\mathrm{Re}_\alpha = 160$. Two vertical dashed lines in each panel show $\tau/T_B = \pm T_\eta/T_B$, respectively. The horizontal axis spans in $-T_L/T_B \leq \tau/T_B \leq T_L/T_B$. The insets show the same plots as the outsets but in the lin-log coordinates.

If $\tau_{1/n}(T)$ is power-law such as $\tau_{1/n}(T) \propto T^{1-\beta}$ and the scaling exponent, β, is independent of the value of n, then $C_p^L(T, \tau, T_B)$ has the self-similar form of the ansatz (3.9), that is, $C_p^L(T, \tau, T_B) = g^L(\tau/[T_B^\beta T^{1-\beta}])$.

If β depends on n, which we denote by $\beta_{1/n}$, we can still expect that $C_p^L(T, \tau, T_B)$ has a self-similar form in a certain interval of τ. The interval is determined by the value of $\tau_{1/n}(T)$.

Figure 3.5 shows $\tau_{1/n}(T)$ with $n = 2, 8$, and 32 for various T_Bs. With a small n such as $n = 2$, we probe the behavior in the vicinity of the peak of $C_p^L(T, \tau, T_B)$, and on the other hand, with a large n such as $n = 32$, we characterize the behavior in the tail region of $C_p^L(T, \tau, T_B)$. For $n = 2$ as shown in Fig. 3.5(a), $\tau_{1/2}(T)$ strongly depends on T_B. This is because $\tau_{1/2}(T)$ is smaller than T_B for almost all Ts. Nevertheless, there may be a power-law behavior in a certain range of T. On the other hand, for larger n such as $n = 8$ and 32, as shown in Fig.3.5(b) and (c), the power law behavior of $\tau_{1/n}(T)$ becomes clearer and $\tau_{1/n}(T) \propto T^{1-\beta_{1/n}}$ holds at a certain time interval of T. The scaling exponents, $\beta_{1/n}$ appears to become independent of T_B and the scaling region becomes larger as increasing Re_α. These observations lead us to conclude that the ansatz (3.9) is a reasonable description of the function $C_p^L(T, \tau, T_B)$.

However, as shown in the insets of Fig. 3.5, the LLSs are too noisy to determine a value of $\beta_{1/n}$ accurately. The noise may be suppressed as we increase massively the number of particle-pair samples. Instead, here we use compensated plots of Fig. 3.5 to estimate the value of the scaling exponent $\beta_{1/n}$. The compensation is based on the self-similar variable ζ/ξ^β in Eq.(3.24), which is the argument of the function g^L. If the self-similarity is valid at $\tau = \tau_{1/n}(T)$ with the exponent $\beta_{1/n}$, the self-similar variable

$$\left.\frac{\zeta}{\xi^{\beta_{1/n}}}\right|_{\tau=\tau_{1/n}(T)} = \frac{\tau_{1/n}(T)}{T_B^{\beta_{1/n}} T^{1-\beta_{1/n}}} \equiv D_{n,\beta_{1/n}}(T) \tag{3.39}$$

becomes constant which neither depends on T nor T_B. Here, ζ and ξ are the dimensionless times as defined in Eqs (3.20). For each n, we plot $D_{n,q}(T)$ by varying q and find q_* that gives the widest flat region as a function of T. We regard this q_* as $\beta_{1/n}$. We show $D_{n,\beta_{1/n}}(T)$ in Fig. 3.6 for $n = 2, 8$, and 32. These compensated plots are less noisy than the LLSs, but they still have tiny oscillations. As increasing Re_α, we observe that $D_{n,\beta_{1/n}}(T)$ becomes independent of T_B except for $T_B = 1.4T_\eta$, in particular, for $n = 32$ as shown in Fig. 3.6 (c). The results indicate that the ansatz (3.25) is reasonable for $C_p^L(T,\ \tau, T_B)$, albeit that the numerical data is noisy.

Now let us specify the empirical form of the exponent β given in Eq.(3.11). Figure 3.7 shows the measured values of $\beta_{1/n}$ with $n = 2, 8$ and 32 as a function of $(T_B - T_\eta)/T_L$ that is the same independent variable used in Fig.3.3 (c) for the other exponent γ.

For $n = 2$, the outset of Fig. 3.7(a) indicates that $(T_B - T_\eta)/T_L$ is not appropriate since the data points are still scattered. This leads us to search for a more suitable self-similar variable for $\beta_{1/2}$, which is found to be T_B/T_L as shown in the inset of Fig. 3.7(a). This implies that $\beta_{1/2}$ depends only on T_B and T_L, but not on T_η. The dependence is consistent with the strong T_B dependence of $\tau_{1/2}(T)$ observed in Fig.

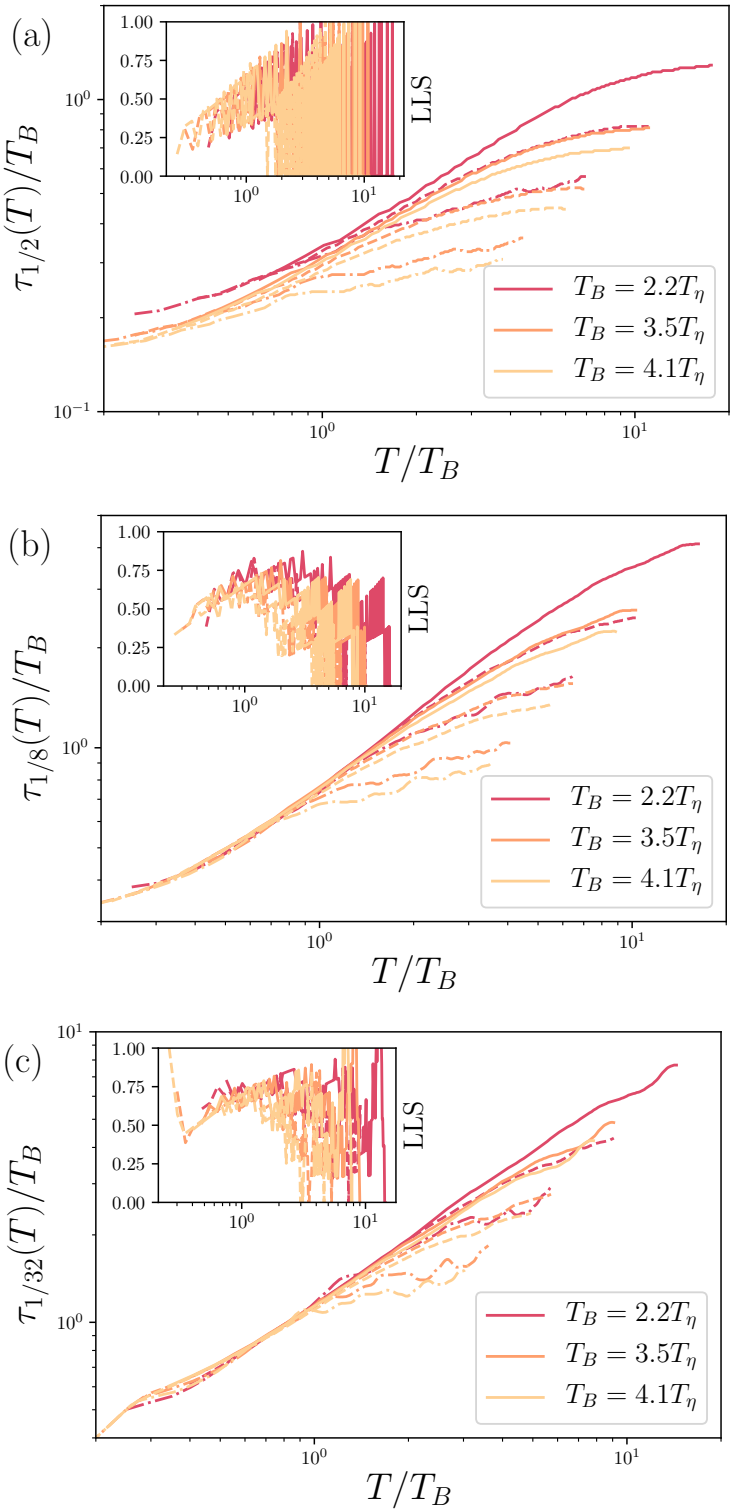

Figure 3.5: n-th decay time scale, $\tau_{1/n}(T)$ as a function of the average time T for (a) $n = 2$, (b) $n = 8$, (c) $n = 32$ at $\mathrm{Re}_\alpha = 40$ (dashed dotted), $\mathrm{Re}_\alpha = 80$ (dashed), and $\mathrm{Re}_\alpha = 160$ (solid). The insets show the LLS of $\tau_{1/n}(T)$ shown in the ousets.

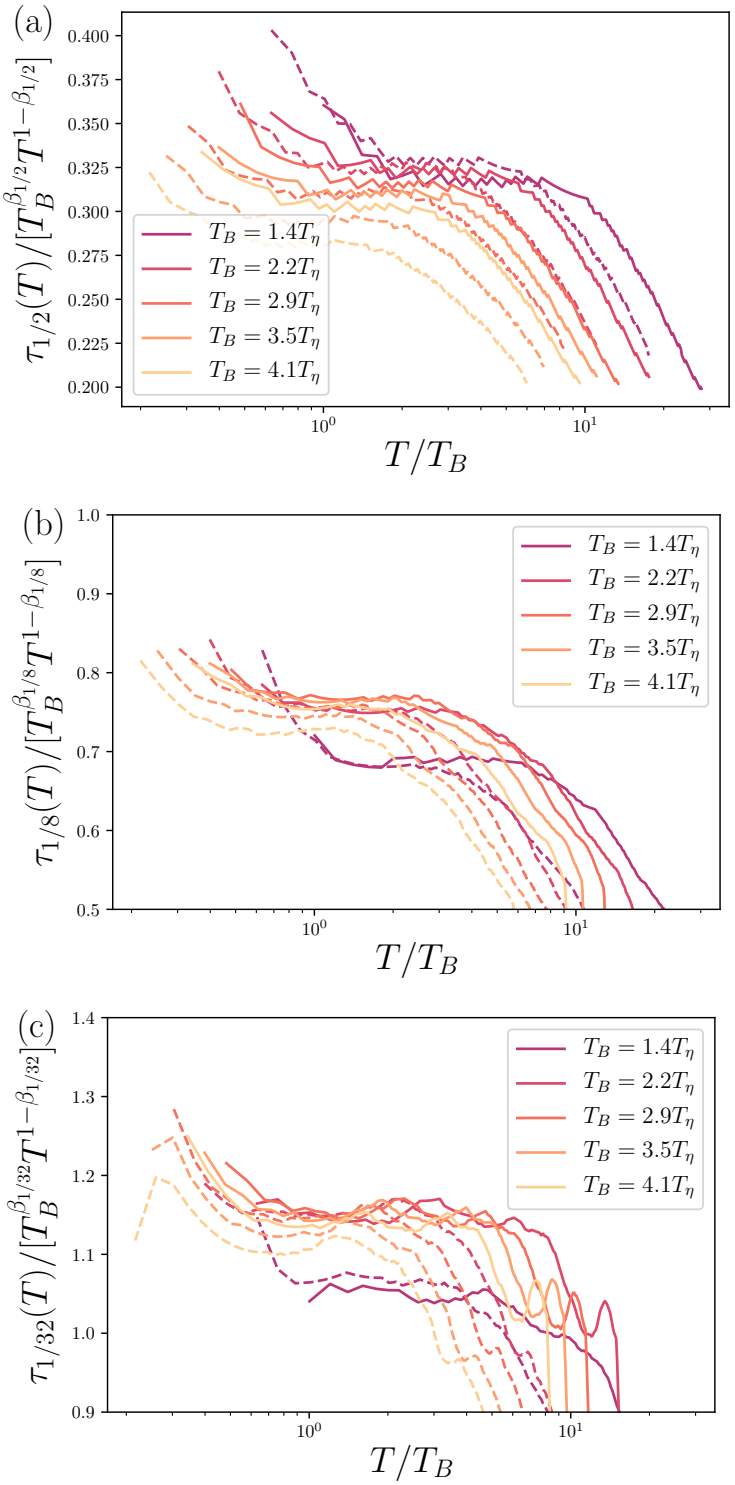

Figure 3.6: Compensated plots of $\tau_{1/n}(T)$ by $T^{1-\beta_{1/n}}$ for (a) $n = 2$, (b) $n = 8$, (c) $n = 32$ at $\mathrm{Re}_\alpha = 80$ (dashed), and $\mathrm{Re}_\alpha = 160$ (solid). The values of $\beta_{1/n}$ are determined in such a way that the compensated graphs have the widest flat region.

3.5(a). Empirically we now fit the collapsed curve obtained in the inset of Fig. 3.7(a) with a function $\check{\beta}(T_B/T_L+a)^b$ with constants $\check{\beta}, a$, and b. Our result is $\beta_{1/2} \propto [T_B/T_L+\omega_1]^{0.4}$, where the constant ω_1 takes zero or a non-zero small value possibly in a range, $0 \le \omega_1 \lesssim 0.01$. The fitted functions are shown in the inset of Fig. 3.7(a).

On the other hand, for $n = 8$ and 32, the exponents $\beta_{1/8}$ and $\beta_{1/32}$ are dependent on T_B, T_η, and T_L. Our best fit by a single parameter ω_2 is $\beta_{1/n} \propto [(T_B - T_\eta)/T_L + \omega_2]^{0.4}$ for $n = 8, 32$, as shown in Fig. 3.7(b) and (c). Here, ω_2 is a constant in a range $0 \le \omega_2 \lesssim 0.01$. The accurate values of ω_1 and ω_2 cannot be determined from the data shown in Fig. 3.7. This is because the data are noisy and also the Reynolds numbers are not sufficiently large for studying the behavior in $T_B/T_L \to 0$. Nevertheless, it is obvious that the behavior of $\beta_{1/2}$ is different from the others. On the other hand, for larger n's such as $n = 8$ or 32, the behaviors of $\beta_{1/n}$ are similar to each other. Therefore, these results suggest that the exponent β in the ansatz has two different self-similar forms depending on $\tau \lesssim T_B$ and $\tau \gg T_B$ at sufficiently large Reynolds numbers. Specifically, we infer from the data

$$\beta\left(\frac{T_\eta}{T_B}, \frac{T_L}{T_B}\right) = \begin{cases} \left(\dfrac{T_B}{T_L} + \omega_1\right)^{0.4} \equiv \beta_1 & \text{for} \quad \tau \lesssim T_B, \\ \left(\dfrac{T_B - T_\eta}{T_L} + \omega_2\right)^{0.4} \equiv \beta_2 & \text{for} \quad \tau \gg T_B, \end{cases} \tag{3.40}$$

where ω_1 and ω_2 are Re_α independent constants, which may be zero. Accordingly, the function g^L in the ansatz (3.25) can be given by

$$g^L\left(\frac{\tau}{T_B^\beta T^{1-\beta}}\right) = \begin{cases} g_1^L\left(\dfrac{\tau}{T_B^{\beta_1} T^{1-\beta_1}}\right) & \text{for} \quad \tau \lesssim T_B, \\ g_2^L\left(\dfrac{\tau}{T_B^{\beta_2} T^{1-\beta_2}}\right) & \text{for} \quad \tau \gg T_B, \end{cases} \tag{3.41}$$

where g_1^L and g_2^L are self-similar functions.

Now we discuss the limit of β as $T_\eta \to 0$ and $T_L \to \infty$. Here, $\omega_1^{0.4}$ in Eq.(3.40) is the limit of β_1 as $T_B/T_L \to 0$. Similarly, $\omega_2^{0.4}$ is the limit of β_2 as $(T_B - T_\eta)/T_L \to 0$. These limits correspond to β_0 in Eq.(3.11). Let us suppose $\omega_2 = 0$. Then the K41 scaling law is recovered at $\tau \gg T_B$ at sufficiently large Reynolds numbers. It is impossible to determine an accurate value of ω_2 from Fig. 3.7. It appears that $\omega_2 = 0.01$ is the best fitted value judging from Fig. 3.7(c) though $\omega_2 = 0$ is not ruled out. On the other hand, even if $\omega_1 = 0$, the K41 scaling law may be not recovered at $\tau \lesssim T_B$ because β_1 may be dependent on T_B at all Reynolds numbers. Both values $\omega_1 = 0.01$ and $\omega_1 = 0$ seem equally good as in the case for ω_2. In order to determine the accurate values of ω_1 and ω_2, we need to perform DNSs with much larger Reynolds numbers and with much larger number of the particle pairs. It is noted that T_L does not change when Re_α is

increased in our DNS. Only T_η changes. Therefore we cannot study T_L-dependency of β in this study.

In Eq.(3.41), the two different behaviors of g^L are inferred from those of β. We now demonstrate that the two forms are consistent with the DNS data. Figure 3.8 shows $C_p^L(T,\tau,T_B)$ as a function of $\tau/[T^{1-\beta_{1/n}}T_B^{\beta_{1/n}}]$ for $n=2$ in Fig.3.8(a) and $n=32$ in Fig.3.8(b). Figure 3.8(a) for $n=2$ is plotted in lin-lin coordinates, which means that we mainly observe regions where $C_p^L(T,\tau,T_B)$ is large. On the other hand, figure 3.8(b) for $n=32$ is plotted in lin-log coordinates, which means that we mainly observe regions where $C_p^L(T,\tau,T_B)$ is small. The master curve in Fig.3.8(a) corresponds to g_1^L and the one in Fig.3.8(b) corresponds to g_2^L in Eq.(3.41). Here we assume $\beta_1=\beta_{1/2}$ and $\beta_2=\beta_{1/32}$. Compare the collapsed curves in Fig.3.8 to those shown in Fig.3.4 without taking an appropriate similarity variable. Furthermore, let us assume that the rescaled functions are exponential, namely $g_1^L(X)=\exp(-k_1X)$ and $g_2^L(X)=\exp(-k_2X)$. This assumption is consistent with Fig.3.8. We can estimate the constants as $k_1\sim 2.3$ and $k_2\sim 3.0$ from Fig.3.8, though these values are also slightly dependent on T_η, T_L, and T_B. The exponential forms will be used to estimate the Richardson constant in Sec.3.4.

3.3.3 Small T_B condition: $T_B < T_\eta$

Now, we consider scaling laws of $C^L(r_0,T,\tau,\varepsilon)$ under the small initial separation condition, $T_B<T_\eta$. Under this condition, particle pairs may be strongly influenced by small scale effects caused by the viscosity and the forcing. On the other hand, the condition $T_B \ll T_L$ is met more easily than in the large T_B condition, which we considered in the previous subsection. Hence, we can expect that $C^L(r_0,T,\tau,\varepsilon)$ is independent of large scale effects such as the drag. Moreover, the t^3 scaling law for $\langle r^2(t)\rangle$ has been observed under the small T_B condition in many previous studies for both 2D and 3D as mentioned in Sec.3.1. We also investigate the reason why the t^3 scaling is observed even at moderate Reynolds numbers for a tuned initial separation r_0.

First we study the correlation along the diagonal line. Figure 3.9(a) shows $C_d^L(T,T_B)$ as a function of T/T_B for various T_B's. Figure 3.9(b) shows the corresponding LLSs. Plateau regions of the LLSs are observed at large T_B such as $T_B=0.87T_\eta$, though the smaller T_B is, the narrower the plateau region is. In the same way as we did in Fig. 3.3(b) for the large T_B condition, we determine the exponent γ from the maximum value of the LLSs. In what follows we write the exponents with check in the small T_B condition. In the inset of Fig. 3.9(c), we show the measured $\check{\gamma}$ as a function of T_B/T_η. This yields a curve independent of Re_α. As a functional form of the curve, we propose the following form:

$$\check{\gamma}(T_B,T_\eta)=\ln\left(\frac{T_B}{T_\eta}\right)-\upsilon, \tag{3.42}$$

where the constant υ is 0.25 ± 0.02 which is determined by a least-square method.

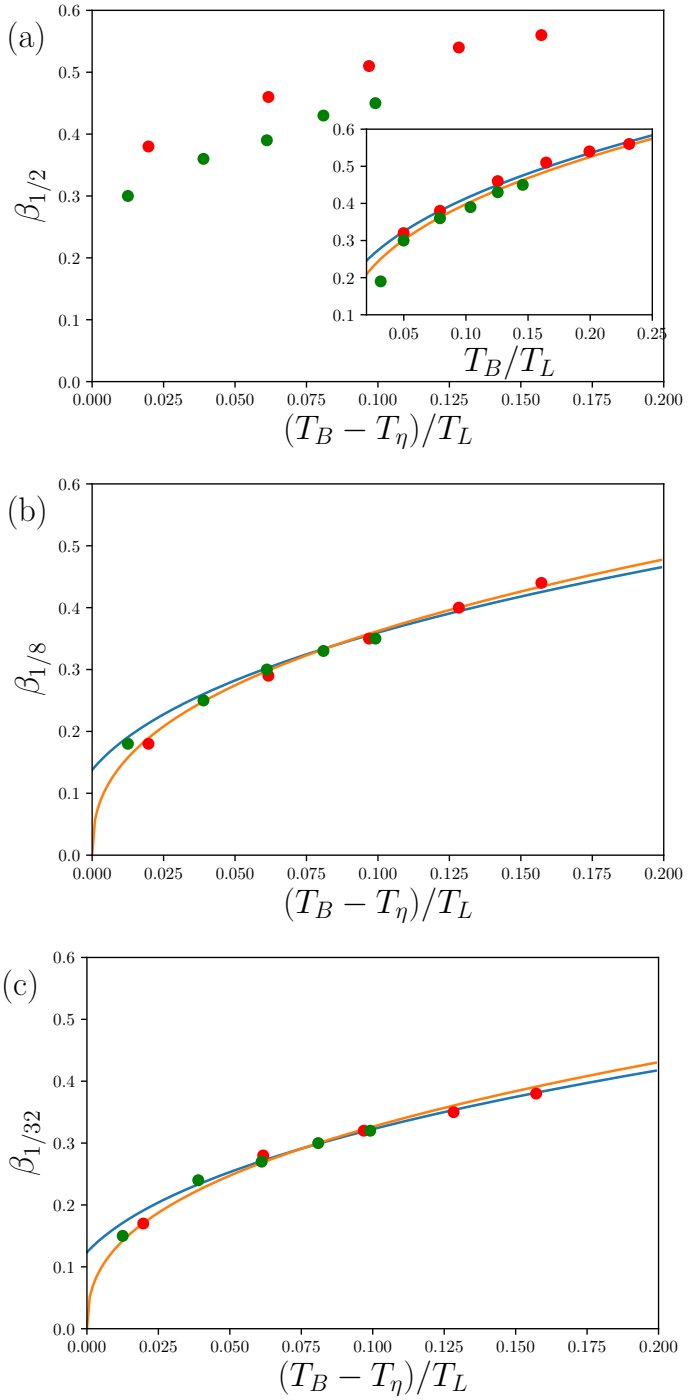

Figure 3.7: Scaling exponents, $\beta_{1/n}$, evaluated from the compensated plots of Fig. 3.5 for (a) $n = 2$, (b) $n = 8$, and (c) $n = 32$ at $\mathrm{Re}_\alpha = 80$ (red) and $\mathrm{Re}_\alpha = 160$ (green). The inset of (a) shows the same plots in the outset, but the horizontal axis is changed to T_B/T_L from $(T_B - T_\eta)/T_L$. The orange solid line shows $[T_B/T_L]^{0.4}$. The blue solid line shows $[T_B/T_L + 0.01]^{0.4}$. For (b) and (c), the orange solid line shows $[(T_B - T_\eta)/T_L]^{0.4}$. The blue solid line shows $[(T_B - T_\eta)/T_L + 0.01]^{0.4}$.

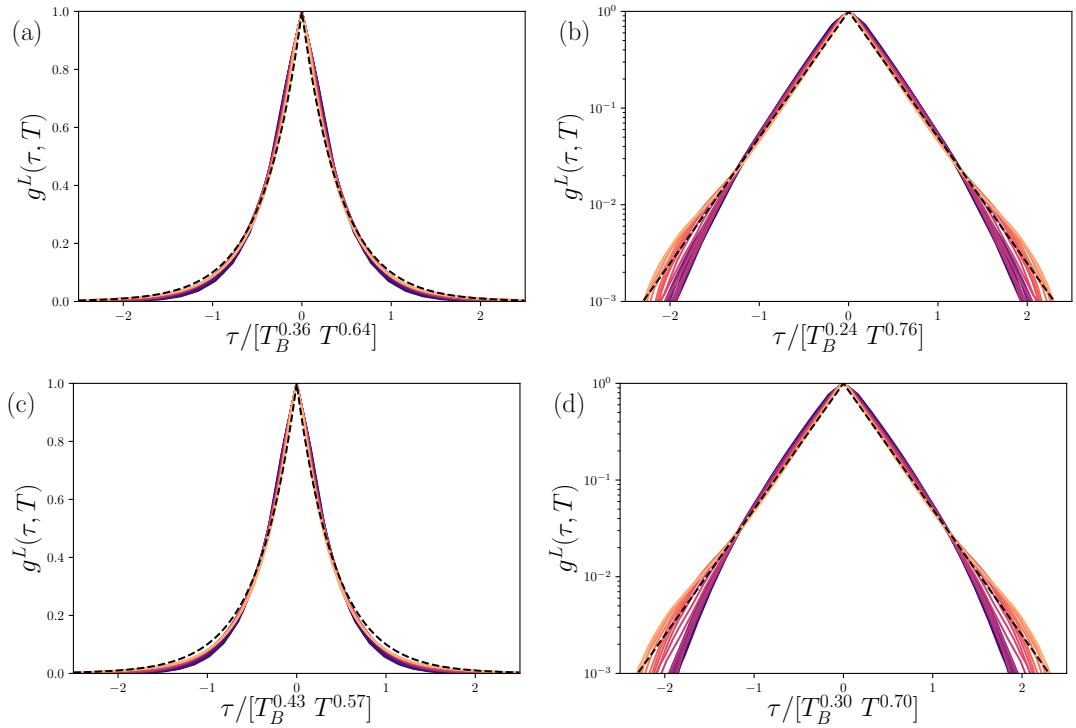

Figure 3.8: Normalized correlation function, $C_p^L(T, \tau, T_B)$ for $T_B = 2.2T_\eta$ rescaled as a functions of (a) $\tau/[T_B^{1-\beta_{1/2}}\ T^{\beta_{1/2}}]$ and (b) $\tau/[T_B^{\beta_{1/32}}\ T^{1-\beta_{1/32}}]$, where $\beta_{1/2} = 0.64$ and $\beta_{1/32} = 0.76$, for $T_B < T < 0.54T_L$ at $\mathrm{Re}_\alpha = 160$. The colors of the curves change from black to yellow as the average time T increases, which is similar to Fig.3.4. Black dashed lines show (a) $\exp(-2.3|\tau|/[T_B^{\beta_{1/2}}\ T^{1-\beta_{1/2}}])$ and (b) $\exp(-3.0|\tau|/[T_B^{\beta_{1/32}}\ T^{1-\beta_{1/32}}])$. (c) Same as (a) but for $T_B = 3.5T_\eta$, where $\beta_{1/2} = 0.57$. (d) Same as (b) but for $T_B = 3.5T_\eta$, where $\beta_{1/32} = 0.70$.

Therefore, at $T_B < T_\eta$, the scaling law of $C_d^L(T, T_B)$, can be,

$$C_d^L(T, T_B) = G\varepsilon T \left(\frac{T_B}{T}\right)^{\check{\gamma}} = GT^{1-\ln\left(\frac{T_B}{T_\eta}\right)+\upsilon}, \tag{3.43}$$

Next we focus on the other part of the correlation $C_p^L(T, \tau, T_B)$ defined in Eq.(3.35) and the scaling exponent, β. Figure 3.10 shows the n-th decay time scale, $\tau_{1/n}(T)$ as a function of T/T_B with $n = 2, 8, 32$ for various T_Bs. Unlike $T_B > T_\eta$ cases, the value of $\tau_{1/2}(T)$ becomes larger than T_B in a small average time T. Figure 3.11 shows compensated plots of Fig. 3.10 by $T^{1-\beta_{1/n}}$, where the exponent $\beta_{1/n}$ is selected in the same way as in the previous large T_B case. It should be noted that what we show in Fig.3.11 is not $D_{n,\beta_{1/n}}(T)$ defined in Eq.(3.39), but $\tau_{1/n}(T)/T^{1-\beta_{1/n}}$.since $\tau_{1/n}(T)/T^{1-\beta_{1/n}}$ is found to be more appropriate as a self-similar variable than $D_{n,\beta_{1/n}}(T)$. The plotted variable $\tau_{1/n}(T)/T^{1-\beta_{1/n}}$ is less dependent of T_B than $D_{n,\beta_{1/n}}(T)$, which is consistent with the T_B independent behavior of the n-th decay time shown in Fig.3.10.

Although the compensated data shown in Fig.3.11 have oscillations and they become stronger for large n, we observe a plateau region for each graph. It is noticeable that the values of the plateaus depend on Re_α. This tendency is not present in the large T_B case as shown in Fig.3.6 (ignoring data for the smallest T_B). If self-similarity of the kind written as Eq.(3.25) is valid for $C_p^L(T, \tau, T_B)$, the values of the plateaus should become independent of Re_α. Therefore, Fig.3.11 suggests two possibilities: one is that $C_p^L(T, \tau, T_B)$ is not self-similar; the other is that $C_p^L(T, \tau, T_B)$ is self-similar but with yet another time scale, T_X.

Here we consider that the second possibility is more likely, although numerical evidence is marginally convincing as we will see. With the hypothetical time scale T_X, a similarity variable for $C_p^L(T, \tau, T_B)$ can be made as $\tau/[T_X^\beta T^{1-\beta}]$. We just replace T_B in the similarity variable of g^L in Eq.(3.25) by T_X. The numerical value of T_X can be determined empirically by removing the Re_α dependence shown in Fig.3.11. More specifically, if we can make plateau values of $\tau_{1/n}/[T_X^{\beta_{1/n}} T^{1-\beta_{1/n}}]$ being independent of Re_α, such T_X is the hypothetical time scale. The time scale T_X should have the following properties: $T_X^{\beta_{1/n}}$ is independent of T_B, that is T_X itself is dependent on T_B, and T_X is dependent on T_η or Re_α. We notice that T_X may be affected by the external forcing added in the high wavenumber region. We do not pursue the origin of T_X further.

We next study the similarity function g^L for $C_p^L(T, \tau, T_B)$, assuming that T_X exists. Let us write the variable in the vertical axis of Fig.3.11 as $E_{n,\beta_{1/n}}(T) = \tau_{1/n}(T)/T^{1-\beta_{1/n}}$. As we discussed with Fig.3.11, the levels of the plateaus of $E_{n,\beta_{1/n}}$ are independent of T_B. Regarding change in the numerical values of the plateau levels as we vary n, we observe $E_{2,\beta_{1/2}} \simeq (1/3)E_{8,\beta_{1/8}} \simeq (1/5)E_{32,\beta_{1/32}}$, yielding $\tau_{1/n}(T) = \tau_{1/2}(T)\log_2 n$. This implies that $C_p^L(T, \tau, T_B)$ for $T_B < T_\eta$ decays exponentially in all the range of τ. On the other hand, the numerical value of $\beta_{1/n}$ depends on n. Specifically, $\beta_{1/2}$ is different from those of $\beta_{1/8}$ and $\beta_{1/32}$, as read from the insets of Fig.3.11. The latter two exponents $\beta_{1/8}$ and $\beta_{1/32}$ have similar values. Therefore, g^L in the small T_B condition is likely to

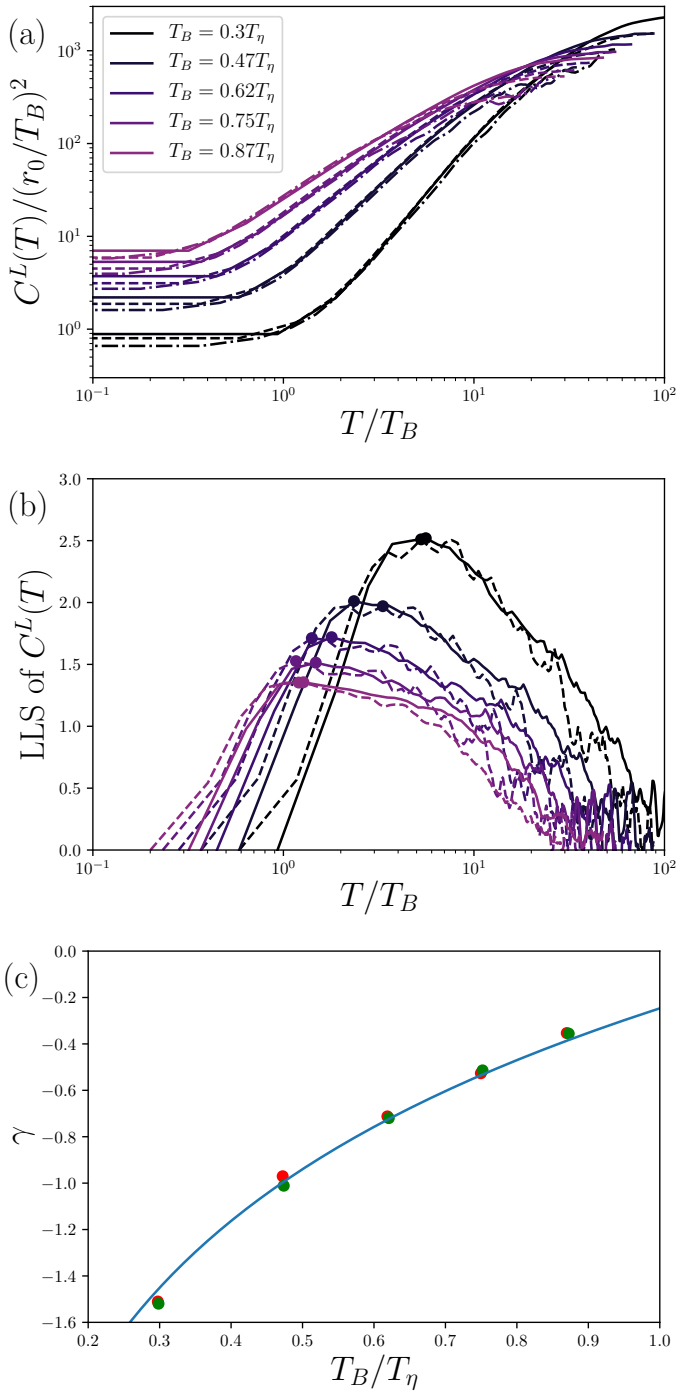

Figure 3.9: (a) Time variation of $C_d^L(T, T_B)$ for various T_Bs at $\mathrm{Re}_\alpha = 40$ (dashed dotted), 80 (dashed), and 160 (solid). (b) LLSs of $C_d^L(T, T_B)$ at $\mathrm{Re}_\alpha = 40$ (dashed) and 160 (solid). Filled circles on the curves show positions of their maximum value. (c) Values of the exponent $\check{\gamma}$ as a function of T_B/T_η, which are measured by the maximum value of the LLSs at $\mathrm{Re}_\alpha = 40$ (red) and 160 (green). The blue solid line shows $\ln(T_B/T_\eta) - 0.25$.

have two self-similar forms such as

$$g^L\left(\frac{\tau}{T_X^{\beta}T^{1-\beta}}\right) = \begin{cases} \exp\left[-\check{k}_1\left(\dfrac{\tau}{T_X^{\check{\beta}_1}T^{1-\check{\beta}_1}}\right)\right] & \text{for} \quad \tau \lesssim T_B, \\ \exp\left[-\check{k}_2\left(\dfrac{\tau}{T_X^{\check{\beta}_2}T^{1-\check{\beta}_2}}\right)\right] & \text{for} \quad \tau > T_B, \end{cases} \tag{3.44}$$

where $\check{\beta}_1$ and $\check{\beta}_2$ are exponents for the two self-similar regimes of τ and $\check{k}_1$ and $\check{k}_2$ are constants. We consider that the exponent $\check{\beta}_1$ for small τ is represented by $\beta_{1/2}$ and $\check{\beta}_2$ for large τ is by $\beta_{1/8} \simeq \beta_{1/32}$. Equation (3.44) is analogous to Eq.(3.41) in the large T_B condition. However, in the present small T_B condition, numerical distinction between the two regimes, $\tau \lesssim T_B$ ($< T_\eta$) and $\tau > T_B$, is harder to make than that in the large T_B condition with the limited scale separation of our DNS.

The dependence of the exponent $\beta_{1/n}$ on T_B, T_η, and T_L is also more complicated than in the previous condition. Compare the insets of Fig. 3.11 to Fig.3.7 for the large T_B condition. We fail to collapse data points of $\beta_{1/n}$ by taking a suitable self-similar variable with T_B, T_η and possibly T_X. The difficulty lies in the peculiar (non-monotonic) behavior of $\beta_{1/n}$ as T_B approaches to T_η, as shown in the inset of Fig. 3.11. We cannot find a simple form of $\beta_{1/n}$ analogous to Eq. (3.40) for the large T_B condition.

We show now that the two different scaling behaviors given in Eq.(3.44) are consistent to the DNS data. Figure 3.12 shows $C_p^L(T, \tau, \varepsilon)$ as a functions of $\tau/T^{\beta_{1/n}}$ with $n = 2$ and $n = 32$. More precisely, since we do not know T_X, we use T_B to non-dimensionalize $\tau/T^{\beta_{1/n}}$ in the horizontal axis of Fig.3.12. We can see that all the curves in each panel collapse to one curve with each way to rescale τ. However, it should be noted that the two rescalings may be not very different from each other since the exponents $\check{\beta}_1 = \beta_{1/2}$ and $\check{\beta}_2 = \beta_{1/32}$ are rather close. Furthermore, as shown in Fig.3.12, the similarity function g^L can be fitted with an exponential curve.

Let us summarize the results in this section. We have considered numerically scaling behavior of $C^L(r_0, T, \tau, \varepsilon)$ in comparison with the ansatz (3.25) under two conditions, $T_B > T_\eta$ and $T_B < T_\eta$. The DNS data of $C^L(r_0, T, \tau, \varepsilon)$ are consistent to the ansatz for both conditions. The difference between the two conditions is in the functional forms of the exponents, $\gamma\left(\frac{T_\eta}{T_B}, \frac{T_L}{T_B}\right)$ (Eqs.(3.36) and (3.42)), and $\beta\left(\frac{T_\eta}{T_B}, \frac{T_L}{T_B}\right)$ (Eq.(3.40)), although β for the latter case was not identified. Furthermore, γ and β are probably continuous at $T_B = T_\eta$. In particular, in the large T_B condition, our DNS data indicates that γ and β do not approach zero as $T_B \to T_\eta$. If this is not a finite Reynolds number effect, the non-zero limits of the exponents imply that the two-time Lagrangian velocity-increment correlation function has exponents that deviate from the K41 dimesional analysys. Consequently, the squared relative separation $\langle r^2(t)\rangle$ disagrees with the Richardson–Obukhov law t^3, even if we take $r_0 \to 0$ at infinite Reynolds number. We will discuss this point in the next section.

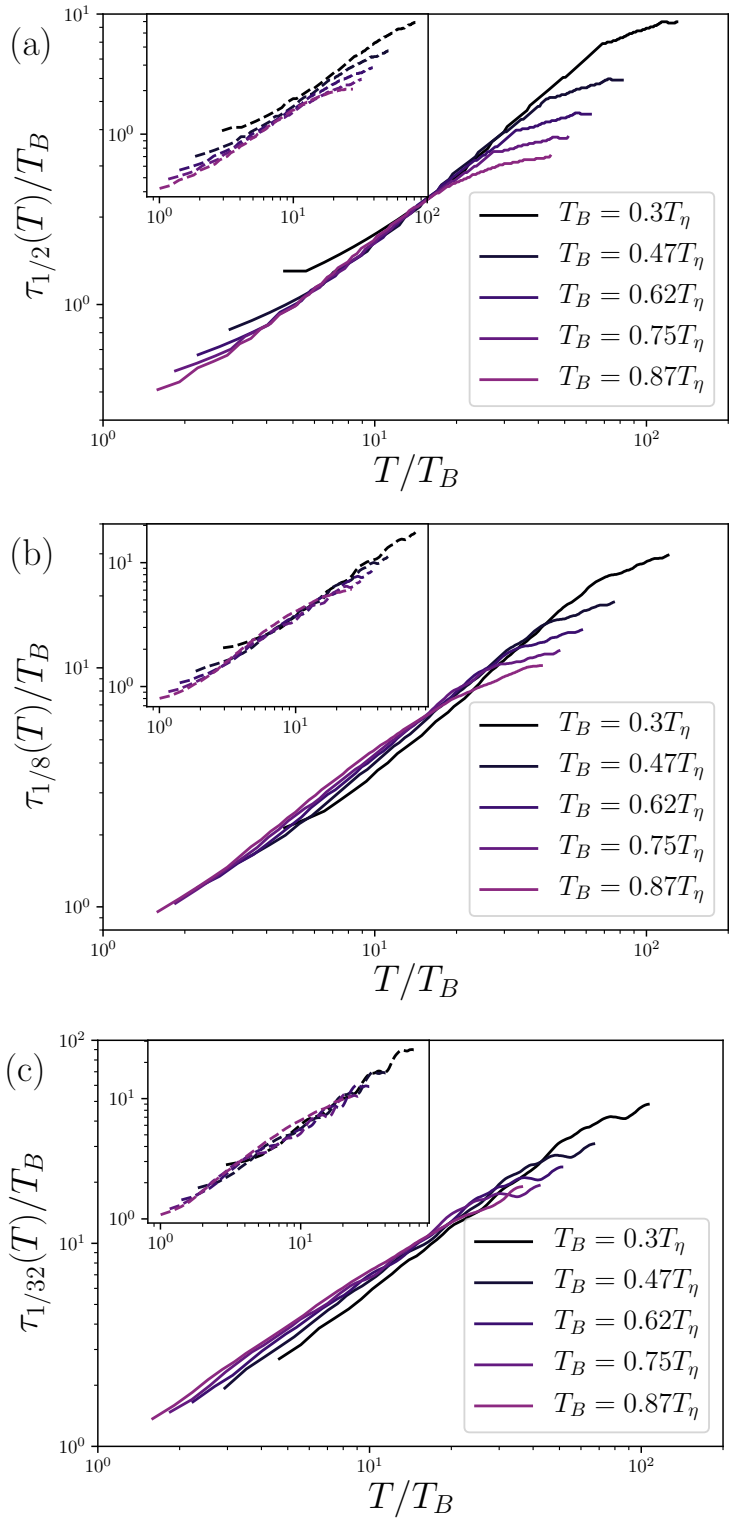

Figure 3.10: Time evolution of the n-th decay time scale, $\tau_{1/n}(T)$ for (a) $n = 2$, (b) $n = 8$, (c) $n = 32$ at $\mathrm{Re}_\alpha = 160$. The insets show the same plots as the outsets but at $\mathrm{Re}_\alpha = 80$.

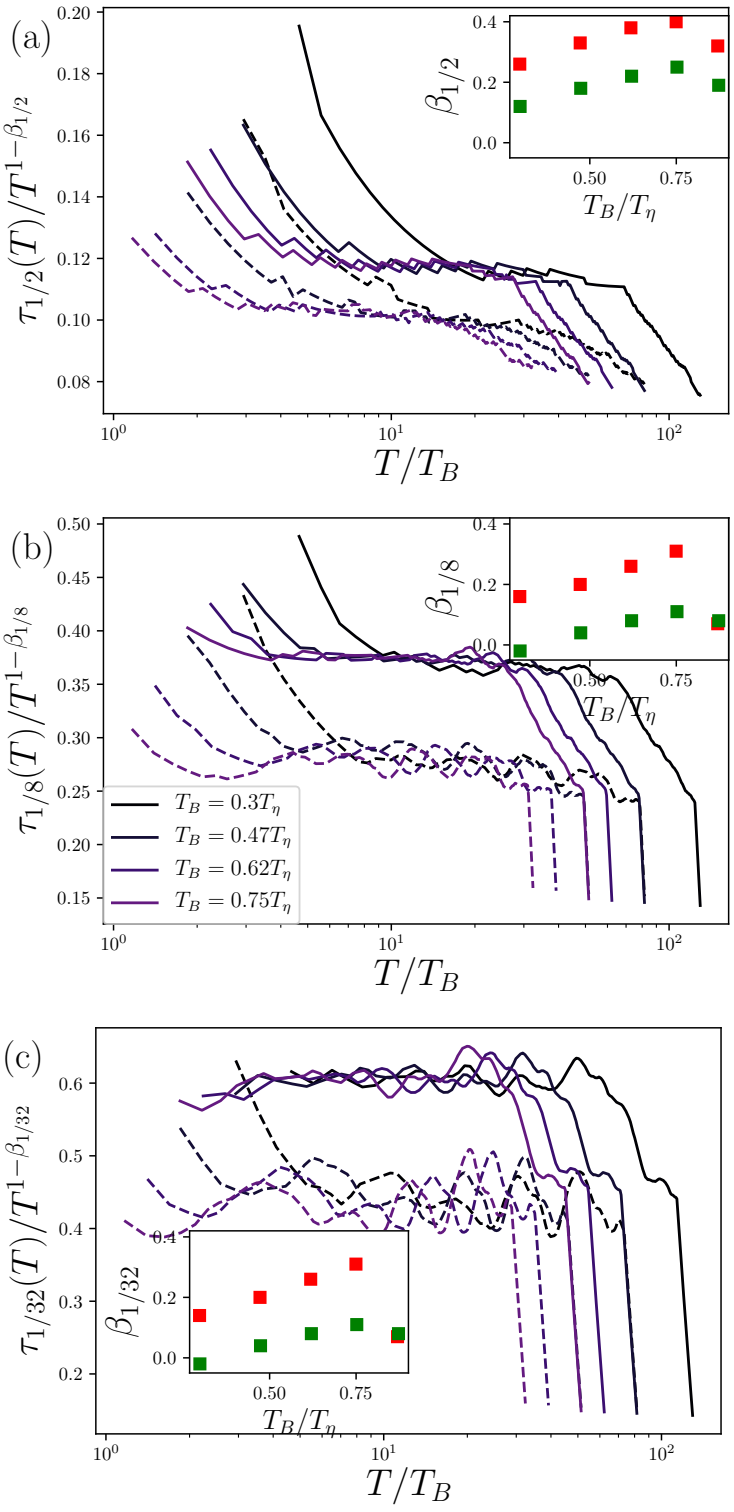

Figure 3.11: Compensated graphs of $\tau_{1/n}(T)$ by $\beta_{1/n}$ for (a) $n = 2$, (b) $n = 8$, and (c) $n = 32$ at $\mathrm{Re}_\alpha = 80$ (dashed) and $\mathrm{Re}_\alpha = 160$ (solid). The Insets show $\beta_{1/n}$ as a function of T_B/T_η at $\mathrm{Re}_\alpha = 80$ (red) and $\mathrm{Re}_\alpha = 160$ (green).

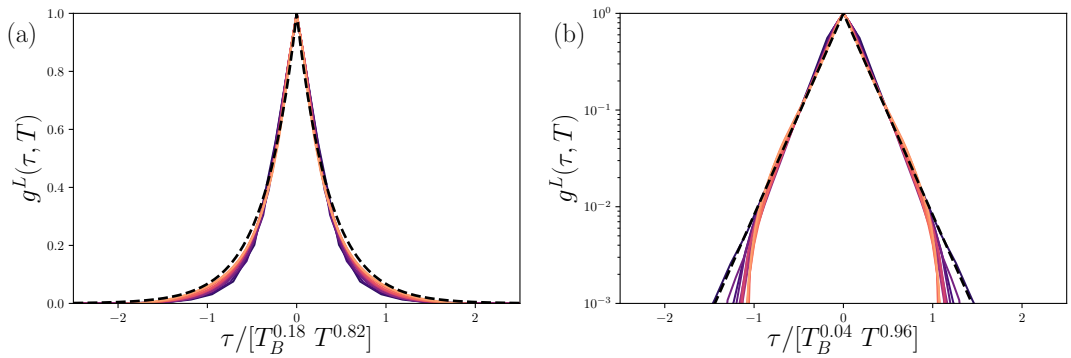

Figure 3.12: Normalized correlation function, $C_p^L(T, \tau, \varepsilon)$, with $T_B = 3.5T_\eta$ as a function of rescaled variable (a) $\tau/[T_B^{1-\beta_{1/2}}\ T^{\beta_{1/2}}]$ and (b) $\tau/[T_B^{1-\beta_{1/32}}\ T^{\beta_{1/32}}]$ in the small T_B condition. Here the exponents are $\beta_{1/2} = 0.82$ and $\beta_{1/32} = 0.96$. Different curves have different Ts in $T_B < T < 0.54T_L$ at $\mathrm{Re}_\alpha = 160$. The black dashed lines correspond to (a) $\exp(-2.7|\tau|/[T_B^{\beta_{1/2}}\ T^{1-\beta_{1/2}}])$ and (b) $\exp(-4.8|\tau|/[T_B^{\beta_{1/32}}\ T^{1-\beta_{1/32}}])$.

3.4 Implications on the Richardson–Obukhov law

Finally, we consider implications of the above scaling behaviors of $C^L(r_0, T, \tau, \varepsilon)$ on relative separations of particle pairs. The second moment of the relative separation $r(t)$ can be reduced to

$$\begin{aligned}\langle r^2(t)\rangle &= r_0^2 + 2\int_0^t \boldsymbol{r_0}\cdot\langle\delta\boldsymbol{v}(t_1)\rangle\ dt_1 + 2\int_0^t\int_0^t \langle\delta\boldsymbol{v}(t_1)\delta\boldsymbol{v}(t_2)\rangle\ dt_1dt_2 \\ &\sim r_0^2 + 4\int_0^t\int_0^{t/2} C^L(r_0, T, \tau, \varepsilon)\ d\tau dT, \end{aligned} \tag{3.45}$$

where the average time is $T = (t_1 + t_2)/2$ and the relative time is $\tau = t_2 - t_1$. We also assume $\boldsymbol{r}_0 \cdot \langle\delta\boldsymbol{v}(t)\rangle = 0$ by taking the direction of the initial separation $\boldsymbol{r}_0$ being randomly and isotropically distributed and use the symmetry of $C^L(r_0, T, \tau, \varepsilon)$ with respect to the diagonal line $t_1 = t_2$.

First, we consider the scaling law of $\langle r^2(t)\rangle$ under the large T_B condition, $T_\eta \ll T_B \ll T_L$, at sufficiently large Reynolds numbers. Under this condition, $C^L(r_0, T, \tau, \varepsilon)$ has the form,

$$C^L(r_0, T, \tau, \varepsilon) \sim T^{1-\gamma} g^L\left(\frac{\tau}{T_B^\beta T^{1-\beta}}\right), \tag{3.46}$$

where the exponent γ is given by Eq.(3.36). The self-similar function g^L and the other exponent β take two different forms as given in Eqs.(3.40)–(3.41), depending on $\tau \lesssim T_B$

or $\tau \gg T_B$. This allows us to split the integral over τ in Eq.(3.45) into two parts,

$$\langle r^2(t)\rangle \sim r_0^2 + \int_0^t dT\, T^{1-\gamma} \int_0^{T_B} d\tau\, g_1^L\left(\frac{\tau}{T_B^{\beta_1} T^{1-\beta_1}}\right) + \int_0^t dT\, T^{1-\gamma} \int_{T_B}^{t/2} d\tau\, g_2^L\left(\frac{\tau}{T_B^{\beta_2} T^{1-\beta_2}}\right). \tag{3.47}$$

When the Reynolds number is sufficiently large, the first interval $0 \le \tau \le T_B$ is much shorter than the second interval $T_B \le \tau \le t/2$. Nevertheless, the second term on the right hand side (rhs) of Eq.(3.47) cannot be neglected because the correlation is large for small τ. We should consider which term becomes dominant at large Reynolds numbers. To calculate it in more detail, we use the functional forms $g_1^L(x) = e^{-k_1 x}$ and $g_2^L(x) = e^{-k_2 x}$ observed in Fig.3.8. Thereby, we can calculate Eq.(3.47) as follows:

$$\langle r^2(t)\rangle \sim \; r_0^2 \;+\; t^{3-\gamma-\beta_1} - \Gamma\left(a_1, \frac{k_1 T_B}{t^{1-\beta_1}}\right) \;+\; \Gamma\left(a_2, \frac{k_2 T_B}{t^{1-\beta_2}}\right) \;-\; t^{3+\frac{2\beta_2-\gamma}{1-\beta_2}}\, \Gamma\left(a_2, \frac{k_2 t^{\beta_2}}{2}\right), \tag{3.48}$$

where we omit numerical constant in each term to highlight power law in t. Here $a_1 = \frac{-2+\gamma}{1-\beta_1} - 1$, $a_2 = \frac{-2+\gamma}{1-\beta_2} - 1$, and $\Gamma(a,x)$ is the upper incomplete gamma function defined by $\Gamma(a,x) = \int_x^\infty z^{a-1} e^{-z} dz$. The second and third terms on the rhs of Eq.(3.48) come from the second term on the rhs of Eq. (3.47) and the forth and fifth terms come from the third term of Eq. (3.47).

Now we consider conditions to recover the Richardson–Obukhov law, $\langle r^2(t)\rangle \propto t^3$. It is known that the upper incomplete gamma function, $\Gamma(a,x)$, has the following asymptotic series: $\Gamma(a,x) \sim x^{a-1}e^{-x}[1 + \frac{a-1}{x} + \frac{(a-1)(a-2)}{x^2} + \cdots]$ as $x \to \infty$ and $\Gamma(a,x) \sim -x^{a-1}/a$ as $x \to 0$ [1]. With these asymptotic formula, we have $\Gamma(a_1, k_1 T_B/(2t^{1-\beta_1})) \propto t^{3-\gamma-\beta_1}$, $\Gamma(a_2, k_2 T_B/(2t^{1-\beta_2})) \propto t^{3-\gamma-\beta_2}$, and $\Gamma(a_2, k_2 t^{\beta_2}/2)) \propto \exp(-k_2 t^{\beta_2}/2)$, as $t \to \infty$. Here we assume $\beta_2 \neq 0$ at infinitely large Reynolds number, i.e., $\omega_2 \neq 0$ in Eq.(3.40). Furthermore let us assume that $\beta_2 = \beta_1$ as $Re_\alpha \to \infty$ from the behavior shown in Fig.3.7. Therefore, the dominant power-law scaling at large t and large Re_α is given by

$$\langle r^2(t)\rangle \sim t^{3-\gamma-\beta_1}. \tag{3.49}$$

Here the power-law exponent of $\langle r^2(t)\rangle$ is related to those of the two-time correlation function $C^L(r_0, T, \tau, \varepsilon)$. In particular, it involves β_1, which implies that $\langle r^2(t)\rangle$ is affected by the correlation $C^L(r_0, T, \tau, \varepsilon)$ in the vicinity of the diagonal line. As is clear from Eq.(3.49), the Richardson–Obukhov t^3 law can be recovered, if γ and β_1 approach zero asymptotically at infinite Reynolds number.

We have found the empirical form of γ as a function of T_B, T_η, and T_L, which is given in Eq.(3.36). It suggests that $\gamma \to 0$ as $Re_\alpha \to \infty$. The similar form of β_1 given in Eq.(3.40) indicates that $\beta_1 \to \omega_1^{0.4}$ as $Re_\alpha \to \infty$. As we discussed in Sec.3.3.2, with our DNS data we are not able to conclude whether ω_1 vanishes or not. However, at the practically accessible Reynolds numbers, β_1 is not zero as indicated by Fig.3.7. Therefore, now including the constant factor, the Richardson–Obukhov law is modified

at finite Reynolds numbers to

$$\langle r^2(t)\rangle = \frac{4G\varepsilon}{k_1(3-\gamma-\beta_1)} T_B^{\gamma+\beta_1} t^{3-\gamma-\beta_1} + (\text{subleading terms}) \tag{3.50}$$

Although G and k_1 are slightly dependent on T_η, T_L, and T_B, they are estimated as $G\varepsilon \sim 1.5$ and $k_1 \sim 2.3$ from the DNS data.

Now let us consider the numerical value of the Richardson constant g_R involved in the Richardson–Obkuhov law $\langle r^2(t)\rangle = g_R \varepsilon t^3$. To evaluate g_R, we substitute the values of G, ε and k_1 in Eq.(3.50) by assuming that they do not change much at infinite Reynolds number. We also assume that the modified exponent $3-\gamma-\beta_1$ approach 3 at infinite Reynolds number, i.e., $\gamma \to 0$ and $\beta_1 \to 0$ as $Re_\alpha \to \infty$. Then the Richardson constant is estimated as $g_R = 4G/k_1 \sim 5.0 \times 10^1$, which is distinctly different from $g_R = 0.5$ and 3.8 obtained in previous experimental and numerical studies, respectively [26, 56]. This discrepancy of g_R is not surprising since the measurements in the previous studies were done in the small T_B condition.

We then consider the scaling law of $\langle r^2(t)\rangle$ under the small T_B condition. By doing an analogous calculation to that of the large T_B condition, we have

$$\langle r^2(t)\rangle = \frac{4G\varepsilon}{\check{k}_1(3-\check{\gamma}-\check{\beta}_1)} T_X^{\check{\gamma}+\check{\beta}_1} t^{3-\check{\gamma}-\check{\beta}_1} + (\text{subleading terms}), \tag{3.51}$$

at large t and large Re_α in the small T_B condition. This is similar to Eq.(3.50) for the large T_B condition. We assume here again that the exponent $\check{\beta}_2 \neq 0$ and that $\check{\beta}_1 = \check{\beta}_2$ at large Re_α. However, it is difficult to see whether the assumptions are valid from the numerically obtained exponents shown as a function of T_B/T_η in the insets of Fig.3.11. A crucial difference between Eqs.(3.51) and (3.50) is that the exponent $\check{\gamma}$ is negative as seen from Eq.(3.42). This enables one to tune T_B for given T_η such that $-\check{\gamma}(T_B, T_\eta) - \check{\beta}_1(T_\eta/T_B, T_L/T_B) = 0$ in the small T_B condition (our DNS data suggests that $\check{\beta}_1$ is generally positive). Consequently, we observe $\langle r^2(t) \propto t^3$, the same scaling exponent as the Richardson–Obukhov law. In contrast, this sort of tuning leading to t^3 is not possible in the large T_B condition since γ is always positive, see Eq.(3.36).

Indeed, it is known that $\langle r^2(t) \propto t^3$ can be observed even at moderate Reynolds number by tuning the initial separation r_0 which satisfies the small T_B condition $T_B \leq T_\eta$. See, for example, Refs. [26, 56, 63, 65, 99, 100] in the 2D energy inverse-cascade turbulence. Specifically, with the tuned initial separation r_0, T_B is close to T_η. In those circumstances, the equivalent of the Richardson constant can be given by $\check{g}_R = 4GT_X^{\check{\gamma}+\check{\beta}_1}/(3\check{k}_1)$ from Eq.(3.51). It is noted that the value of G in this range is strongly dependent on T_B and T_η. The Richardson constant measured in the previous experimental and numerical studies [26, 56] with the tuned initial separation should be therefore compared to $\check{g}_R$.

Let us now argue that the nature of the t^3 law with the tuned initial separation is different from that of the Richardson–Obukhov law. In general terms, by the Richardson–Obukhov t^3 law, it is understood that the t^3 law holds irrespective of the value of the

initial separation r_0, provided that the inertial range is sufficiently wide. Strictly speaking, one should add a condition that r_0 is inside the inertial range [8]. The large T_B condition which we have considered conforms to the added condition. From Eq.(3.50), the Richardson–Obukhov law corresponds to $\gamma = 0$ and $\beta_1 = 0$ and the resultant t^3 law does not depend on T_B, or equivalently r_0. For the sake of the argument, let us relax the added condition. Now we consider the small T_B condition. From Eq.(3.51), The t^3 law with the tuned initial separation corresponds to $-\check{\gamma} - \check{\beta}_1 = 0$ and the resultant t^3 law has a prefactor $T_X^{\check{\gamma}+\check{\beta}_1}$, which potentially depends on T_B. Therefore, the t^3 law observed at a given Reynolds number (however large) by tuning the initial separation is different from the Richardson–Obukuhov t^3 law. The agreement of the power-law exponents is coincidental.

It is interesting that such a coincidence do not occur in the large T_B condition. Then, in this condition, can we say anything about observability of the bona fide Richardson–Obukhov law? As far as our DNS data suggest, the exponents γ and β_1 do not vanish in the large T_B condition. Consequently, the Richardson–Obukhov law is not observable with the current Reynolds numbers. It should be noted that this is caused not by intermittency effects, but by correlation of the Lagrangian velocity. Extrapolation of the data indicates that γ and β_1 may vanish eventually at monstrously high Reynolds number as we discussed. This implies that the Richardson–Obukhov law is observable, if we are able to reach those high Reynolds numbers.

We presented here a framework to study the Richardson–Obukhov law by way of the self-similarity of the Lagrangian two-time correlation. It can be adopted to the 3D turbulence. The t^3 law with the tuned initial separation is also known in the 3D case, see, for example, Refs. [15, 19, 32, 90, 104]. Our analysis on the 3D case will be reported elsewhere. In this sense, the t^3 scaling of $\langle r^2(t)\rangle$ observed at moderate Reynolds numbers is a different state from the complete similarity for $\langle r^2(t)\rangle$, which is consistent with the dimensional analysis naively using the K41 phenomenology.

3.5 Concluding remarks

We have investigated the two-time Lagrangian velocity-increment correlation function for particle pairs with the incomplete self-similarity and the DNS of 2D energy inverse-cascade turbulence. First, we have made the self-similar ansatz (3.25) of the correlation function by using the idea of incomplete similarity. The ansatz includes the Bachelor time, the Kolmogorov dissipation length, and the integral length as a similarity variable, meaning that finite Reynolds number effects and the initial separation dependence are encoded. The ansatz is characterized by the two scaling exponents, β and γ, and the one-variable function g_L. The exponent γ concerns the equal-time correlation along the diagonal line through the origin shown in Fig.3.1. The other exponent β concerns how the correlation decreases along the direction perpendicular to the diagonal line. However, the ansatz is an example of the incomplete self-similarity, the two exponents cannot be determined by dimensional analysis.

In order to verify the ansatz, we have performed DNS of 2D energy inverse-cascade turbulence and calculated the two-time Lagrangian correlation functions by varying parameters such as the Batchelor time T_B and the dissipation time T_η. We split the DNS study into two parts: the large and small T_B conditions. For both conditions, we showed that the ansatz describes the DNS results reasonably well. Then we measured the values of the two exponents and the functional form of g_L from the DNS data which are in some cases too noisy to have reliable measurements. In particular, the measurements indicated that the exponents are weakly dependent on T_B and T_η. In theory, we assumed that they are independent. The dependence of the exponents are empirically determined as Eqs.(3.36), (3.40), and (3.42). The function g^L is determined as an exponential function.

We next considered the limit of these empirical relations at infinite Reynolds number. The extrapolation of the relations obtained at moderate Reynolds numbers was subject to uncertainty. Nevertheless, it suggest that the Lagrangian velocity correlation is consistent to the K41 dimensional analysis at infinite Reynolds number in the large T_B condition. However, at finite Reynolds numbers, our results indicate that the correlation in general has correction described by non-zero γ, non-zero β and the function g^L to the K41 dimensional analysis for both large and small T_B conditions.

Finally, we have considered relation between the scaling law of the Lagrangian velocity correlation and the Richardson–Obukhov t^3 law for the second moment of relative separation via the integral (3.45). With the asymptotic argument, we found that the Richardson–Obukhov law is probably not recovered for finite T_B at finite Reynolds numbers in the large T_B condition as shown in Eq. (3.50). Moreover, using the scaling law of the Lagrangian correlation, we explained why we, nevertheless, observe t^3 scaling at moderate Reynolds numbers with a special initial separation under the small T_B condition. This is because γ and β_B take a negative and positive values, respectively. Therefore, we concluded that the physics of this t^3-scaling behavior is different from that of the Richardson–Obukhov law.

In this section, we assumed that forcing effects are negligible. The external forcing is limited to small scales for 2D. In fact, the Eulerian statistics in the Fourier space such as the energy spectrum or the energy flux is influenced by the forcing only in the vicinity of the forcing scales [24, 85, 122]. Hence the influence is considered as local. This may be the reason why the empirically found functional forms of the scaling exponents, β and γ depend only T_η, T_L and T_B given by Eqs. (3.40) and (3.36) in the large T_B condition. Strictly speaking, we can neglect the forcing effects if correlation between the forcing and the Lagrangian velocity, $\langle f_i \delta v_j \rangle$, rapidly decays in time. Here f_i is the forcing increment between two Lagrangian particles and δv_j is the relative velocity between them. We speculate that the cross correlation rapidly decays because the characteristic time scales of the forcing and the velocity in the forcing scale are small.

Given the self-similar form Eq.(3.9 - 3.10) of the two-time Lagrangian velocity-increment correlation function, one would like to "derive" it from the Navier–Stokes equations using only plausible assumptions. More precisely, we propose to use it as an

input to a set of integro-differential equations (closure equations) for the Lagrangian correlation function obtained by a closure approximation such as direct-interaction approximation [58, 64, 71, 73]. One standard procedure in the last step of the closures is to substitute certain self-similar forms for the correlation function and the linear response function to those in the closure equations and then to study consistency of the self-similar forms with the closure equations. By input, we mean to input the ansatz studied here into closure equations of, for example, a direct-interaction approximation. This may give analytically functional forms of the scaling exponents, $\beta(T_\eta/T_B, T_L/T_B)$ and $\gamma(T_\eta/T_B, T_L/T_B)$ and their limits at infinite Reynolds number.

Closure approximations have been applied to study the Richardson–Obukhov t^3 law, see e.g., Refs. [55, 74]. However, these studies have used one-time Lagrangian velocity correlation function given by Eq.(3.2) in the Introduction, which is different from the two-time correlation function $C^L(r_0, T, \tau, \varepsilon)$ we have studied here. In fact, the two-time Lagrangian velocity correlation function is unexplored with the Lagrangian renormalization approximation [58] and perhaps any other closure approximation [1]. Therefore, the results in this study play an important role to develop a new avenue of closure theories.

Another approach can be to develop a stochastic model of turbulent relative dispersion using the ansatz we have obtained here. Recently, continuous time random walk (CTRW) models [29, 113] have developed for the relative dispersion. These models are constructed to be consistent with the Richardson–Obukhov law. It is possible to modify these models to have the self-similar properties of the two-time correlation function obtained in this section. Building such a model corresponds to incorporating effects of time correlations [41, 105] and finite propagation speed of the relative diffusion [57, 88]. We will report a stochastic modeling based on the ansatz elsewhere.

[1] Y. Kaneda (private communication)

Chapter 4

General Conclusions

4.1 Summary

We studied the turbulent relative dispersion in two ways: conditional sampling methods and two-time Lagrangian velocity correlation function. According to the experimental result that the mean square of the relative separations of particle pairs depends strongly on the initial separations beyond the Batchelor time scale, we investigated the origins of the initial separation dependence and improved the Richardson–Obukhov law to be consistent with the experimental data.

In Chapter 2, in the 2D inverse energy-cascade turbulence, we have developed a conditional sampling method to exhibit the t^3 scaling like the Richardson–Obukhov law by using the relation between the exit-time PDF and Richardson PDF. First of all, we observed that the mean squares of the relative separations of particle pairs strongly depend on the initial separations beyond the Bachelor time scale. The initial-separation dependence indicates that it is possible to select a special initial separation for which the mean square $\langle r^2(t)\rangle$ exhibits the t^3 scaling even at moderate Reynolds numbers. We call the special initial separation the proper initial separation. This terminology is based on the hypothesis that a certain bulk of the particle pairs starting from each initial separation obeys the Richardson–Obukhov law at moderate Reynolds numbers. Under this hypothesis, the proper initial separation is qualitatively interpreted as a state that only the bulk of particle pairs contributes to the mean square relative separations.

In order to investigate the validity of the hypothesis, and thus the validity of the Richardson–Obukhov law, we developed a conditional sampling method to recover the Richardson–Obukhov law for any initial separations. In this conditional sampling, We reject the particle pairs whose exit time is smaller than a given value, that is $T_E < \tau\langle T_E\rangle$, where T_E is the exit time of a particle pair and τ is a tuning parameter. The value of the tuning parameter is set for the resulted conditional mean square of the relative separation to exhibit the t^3 scaling in the inertial range. As a result, we showed that the initial separation dependence disappears for the conditional mean squares of the relative separations irrespective of the initial separations, and the conditional mean square collapses the curve of the unconditioned one for the proper initial

separation. Furthermore, the fraction of rejected particle pairs decreases with increasing the Reynolds numbers. Therefore, these results support the hypothesis described above.

On the other hand, in terms of the mean square of the relative velocity of particle pairs, we found that although the mean square of the relative velocity also collapses the curve of the unconditioned one for the proper initial separation irrespective of the initial separation, it deviates from the scaling law predicted by Kolmogorov phenomenology.

Based on these results, we qualitatively discuss the characteristics of the special particle pairs initially separated by the proper initial separation. According to the conditional sampling, we classify particle pairs into three groups as follows: (1) particle pairs which separate fast and exit immediately the inertial subrange. (2) particle pairs which expand anomalously fast through the inertial subrange but still stay at the inertial subrange. (3) a certain bulk of particle pairs which typically satisfy the Richardson–Obukhov law. Group (1) exhibits the scaling law with the exponent smaller than 3 while Group (2) exhibits the scaling law with the exponent larger than 3. Therefore, at the proper initial separation, the effects of the groups (1) and (2) on the mean square are balanced and canceled each other.

In Chapter 3, we have investigated the two-time Lagrangian velocity correlation function for particle pairs with incomplete similarity and DNS of 2D energy inverse-cascade turbulence. First, we have made the self-similar ansatz of the correlation function by using the idea of incomplete similarity as follows:

$$C^L(r_0, T, \tau, \varepsilon) = G\varepsilon T \left(\frac{T_B}{T}\right)^{\gamma} g^L\left(\frac{\tau}{T\left(\frac{T_B}{T}\right)^{\beta}}\right),$$

Here T_B is the Bachelor time, T_η is the Kolmogorov dissipation time, and T_L is the integral time. The ansatz means that the finite Reynolds number effects and the initial separation dependence are encoded. The exponent γ concerns the equal-time correlation along the diagonal line through the origin shown in Fig.3.1. The other exponent β concerns how the correlation decreases along the direction perpendicular to the diagonal line. However, the ansatz is an example of the incomplete similarity, and therefore the two exponents cannot be determined by dimensional analysis.

In order to verify the ansatz, we have performed DNS of 2D energy inverse-cascade turbulence and calculated the two-time Lagrangian correlation functions by varying parameters such as the Batchelor time T_B and the dissipation time T_η. We split the DNS study into two parts: the large and small T_B conditions. For both conditions, we showed that the ansatz describes the DNS results reasonably well. Then we measured the values of the two exponents and the functional form of g_L from the DNS data. Furthermore, we considered the limit of these empirical relations at infinite Reynolds number. The extrapolation of the relations obtained at moderate Reynolds numbers was subject to uncertainty. Nevertheless we proposed that the power-law properties of T_B, T_η, and T_L on the exponents β and γ appear only at the large T_B condition as

follows:

$$\beta\left(\frac{T_\eta}{T_B},\frac{T_L}{T_B}\right)=\begin{cases}\left(\dfrac{T_B}{T_L}+\omega_1\right)^{0.4}\equiv\beta_1 & (\text{for}\quad \tau\lesssim T_B),\\ \left(\dfrac{T_B-T_\eta}{T_L}+\omega_2\right)^{0.4}\equiv\beta_2 & (\text{for}\quad \tau\gg T_B),\end{cases}$$

$$\gamma\left(\frac{T_\eta}{T_B},\frac{T_L}{T_B}\right)=\overline{\gamma}_0\left(\frac{T_B-T_\eta}{T_L}\right)^{1/2}.$$

Moreover, the function g^L is determined as an exponential function. At the small T_B condition, these power-law properties of the exponents are not shown but the function g^L is also determined as an exponential function.

Our results indicate that at finite Reynolds numbers, the correlation in general has corrections described by non-zero γ, non-zero β and the function g^L to the Kolmogorov dimensional analysis for both large and small T_B conditions. Moreover, our data cannot deny the possibility that the scaling law for the two-time Lagrangian velocity correlation function deviates from Kolmogorov phenomenology at infinite Reynolds number, i.e., $\omega_1 \neq 0$ or $\omega_2 \neq 0$.

Finally, we have considered the relation between the scaling law of the Lagrangian velocity correlation and the Richardson–Obukhov law. With the asymptotic argument, we found that the Richardson–Obukhov law is probably not recovered for finite T_B at finite Reynolds numbers under the large T_B condition. Moreover, using the scaling law of the Lagrangian correlation, we explained why we, nevertheless, observe the t^3 scaling at moderate Reynolds numbers with a special initial separation under the small T_B condition. This is because γ and β_1 take negative and positive values, respectively. Therefore, we concluded that the physics of this t^3-scaling behavior is different from that of the Richardson–Obukhov law.

4.2 Main results of the thesis

Throughout the thesis, we have investigated the initial separation dependence of the mean square of the relative separations of particle pairs. We claim that the initial separation dependence always remains at no matter how large but finite Reynolds number. Furthermore, we have explained the properties of the special initial separation where the t^3 scaling law exhibits at moderate Reynolds numbers as follows. In terms of the incomplete similarity for the two-time Lagrangian velocity correlation function, the scaling exponent of the mean square of the relative separations is $3-\gamma-\beta_1$. Then, we observed that its exponents γ and β_1 are canceled each other at the special initial separation, i.e., $\gamma+\beta_1=0$ for $\gamma<0$ and $\beta>0$. We can interpret these values through the qualitative classification of particle pairs discussed in Chapter 2. The negative value of γ is due to particle pairs anomalously expanding fast in the inertial range, namely

groups (1) and (2), i.e., non-Kolmogorov scaling for mean square of relative velocity, while the positive value of β is due to long-time correlation between the particle pairs of these groups.

4.3 Some remarks

Although the concluding remarks are already made in each chapter, we would like to discuss once again the results in each chapter from a broader perspective. Here, by revisiting the results critically, we aim at gaining more insights about turbulent relative dispersion.

4.3.1 Conditional sampling method

The conditional sampling method via exit-time statistics, which is introduced in Chapter 2, has some tuning parameters, whose physical interpretations are difficult. Especially, the dimensionless parameter τ controls the scaling exponent of conditional moments of the relative separation of the particle pairs. It enables us to observe the t^3 scaling like the Richardson–Obukhov law at moderate Reynolds numbers. However, we could not interpret physically the tuned values of τ at which the t^3 scaling is observed. It seems to be a significant defect of the method.

On the other hand, the incomplete similarity for the two-time Lagrangian velocity correlation function, which is introduced in Chapter 3, reveals that the Richardson–Obukhov t^3 law is not observable at finite Reynolds numbers. In Chapter 3, we estimated the Richardson constant and it is larger than that estimated by the experiment [56]. This is because in the experiment the Richardson constant is estimated by the mean square of the relative separation at the proper initial separation. This is inconsistent with the idea that the Richardson–Obukhov law is "recovered" at finite Reynolds numbers by the conditional sampling method. This is because the Richardson constant of the conditional mean square of the relative separation corresponds to the unconditioned mean square at proper initial separation. This consideration leads us to conclude that the conditional sampling method do not recover the Richardson–Obukhov law.

Nevertheless, the conditional sampling method is still worth using for investigating the origins of the initial separation dependence. We stated in Chapter 3 that the initial separation dependence is crucial for the scaling law for the turbulent relative dispersion by means of the incomplete similarity of the two-time Lagrangian velocity correlation function. However, it is not yet clear why the initial separation dependence remains for such a long time. The conditional moments of the order p, which include the rational-order moments, of the relative separation as well as the relative velocity are almost independent of the initial separation in the inertial subrange, especially for $p \lesssim 3$. Therefore, it indicates that the initial separation dependence results from particle pairs rejected for the conditional sampling, whose exit times are small. As pointing out in Chapter 2, these pairs are classified into two groups (1) and (2). In

terms of the probability distribution function, these belong to the left and right tails, respectively. Thus, we can probably detect the rare events through the conditional sampling method [1]. Of course, it is not easy to define the rare events via the tuning parameters of the conditional sampling. However, if we could define such values of the tuning parameters, the conditional sampling as the rare-event detection system will give us more information on the rare events than the instantaneous probability distribution functions, which inform us about the information at a given scale r and a given time t, not for a rare particle-pair path.

4.3.2 Two-time Lagrangian velocity correlation function

The framework in terms of the intermediate asymptotics and incomplete similarity provides a few physical interpretations and unique values of scaling exponents which are not determined by dimensional analysis. In this thesis, we only obtain from the DNS data the values of the scaling exponents β and γ of the two-time Lagrangian velocity correlation function. The physical interpretations of β and γ remain unclear. The fact that the values of β and γ estimated by DNS are not rational numbers makes the physical interpretations difficult. This may be similar to the problem that the values of critical exponents in equilibrium systems deviate from those predicted by the dimensional analysis.

Here, we consider a physical interpretation of β and γ via the discussions by Goldenfeld [48] on Barenblatt's equation in one dimension [5] and the modified porous-medium equation [37]. These equations are not conservative, especially break the law of conservation of mass. Hence, information on the initial conditions are no longer available at an intermediate asymptotic time scale. Analogous to the critical phenomena in equilibrium systems, the anomalous dimensions of the above equations are derived by renormalization analysis, where the coarse-graining is performed in time. Barenblatt's equation and the modified porous-medium equation are simple enough to apply renormalization analysis. Furthermore, the values of the anomalous dimensions are calculated by perturbation methods.

We can in principle apply the renormalization idea to the two-time Lagrangian velocity correlation function. Of course, we cannot estimate the specific values of the exponents by perturbation methods because we do not have the closed equations for the two-time Lagrangian velocity correlation function. Here, we only aim to interpret physically the exponents through the renormalization idea. We define a renormalization constant Z as $A(t) = Z^{-1}A_{r_0}$, where $A_{r_0} = A(0)$ and $A(t)$ are quantities related to coarse graining. The quantity $A(t)$ is less clear than that for Barenblatt's equation and the modified porous-medium equation. Heuristically, we select the energy dissipation rate as the quantity $A(t)$. This is because the two-time Lagrangian velocity correlation

[1] Here, it is noted that the number of particle pairs for the (conditional) ensemble averages in our DNS data [65] in Chapter 2 may be not large enough to obtain converged higher-order statistics. Hence, it is necessary to verify that we actually detect the rare events through the conditional sampling method by numerical studies of higher-order statistics.

function is related to it at initial time as follows [42]:

$$\left.\frac{d}{dT}C^L(T,0)\right|_{T=0} = \begin{cases} -4\varepsilon & \text{for 3D turbulence,} \\ 4\varepsilon & \text{for 2D turbulence,} \end{cases} \tag{4.1}$$

at infinite Reynolds number. Furthermore, at finite Reynolds number, the right hand side may depend on the initial separations. Under these assumptions, we calculate the so-called (bare) renormalization group equation and obtain the relation between the exponents. However, the corresponding anomalous dimensions, i.e., β and γ are not derived from this renormalization analysis. This is because the variables T and τ are the same dimension, which is the condition different from Barenblatt's equation and the modified porous-medium equation. Hence, the corresponding conservation law is unclear. Therefore we should find out, if they exist, the conserved and initial-separation-dependent quantities for inviscid fluid in terms of the motions of particle pairs.

Next, we consider relations between the anomalous scaling of the two-time Lagrangian velocity correlation function and the breaking of self-similarity of the probability distribution function of the relative separations of particle pairs. In the case of generalized Lévy walk models [2, 27], the existence of rare events, i.e., the fat tails of the probability distribution function can influence the scaling exponents of lower-order moments [117, 118]. According to these results, the anomalous scaling of the two-time Lagrangian velocity correlation function is likely to be influenced by rare events.

4.4 Future work

4.4.1 Stochastic modeling

Lévy walk models seem to own some of the same properties of the turbulent relative dispersion. First, particles exhibit piecewise ballistic motions. In Lévy walk models, duration of the ballistic motion and the velocity during the duration are randomly determined according to given probabilities. In the turbulent relative dispersion, particle pairs ballistically expand on average for a small time, that is the Batchelor regime. Thalabard *et al.* [113] and Bourgoin [29] modeled the turbulent relative dispersion using this properties by means of the continuous random walk model. Second, both have a self-similar probability distribution function at the central part and rare events at the right fat tail. Recently, properties of the right fat tail were revealed by means of the big-jump principle [117, 118] in terms of the generalized Lévy walk.

On the other hand, there are also different properties. The breaking of the self-similarity at the left tail, which is observed in the turbulent relative dispersion, does not occur in Lévy walk models, to our knowledge. Hence, we should develop the Lévy walk to possess particle pairs slowly or hardly expanding. Furthermore, the turbulent relative dispersion is an aging phenomenon, but the standard Lévy walk is not. Recently, several studies [82, 106] extended the Lévy walk to be aging and investigated its properties.

Although there are these problems, it may be easier to model the turbulent relative dispersion with Lévy walk in such a way that the probability distribution function of the model can be consistent with experimental data of the relative separation of particle pairs. This is because recent Lévy walk models are very flexible enough to fit the data. However, it is rather more difficult to justify from experimental data that the turbulent relative dispersion actually possesses consistent probabilities with Lévy walk such as a power-law distribution of the waiting time.

Even if we overcome all of the problems described above, we are not convinced that the Lévy walk is the final word for the turbulent relative dispersion. As described in the next subsection, the goal is to derive the model from the Navier-Stokes equations. The Lévy walk model, where one supposes a random walker, may not be easy to be deduced from the deterministic Navier-Stokes equations. We need a (generalized) Langevin approach [40, 81, 121].

4.4.2 Deductive theories from the Navier-Stokes equations

Finally, we must derive the above model from the Navier-Stokes equations. In this task, closure problems confront us. In terms of the closure problems of Eulerian turbulence, Kraichnan [71] conjectured that any Fourier modes of the Eulerian velocity $\tilde{u}_j(\boldsymbol{k}, t)$ are infinitesimally weak coupling with (but not completely independent of) the other modes $\tilde{u}_m(\boldsymbol{k}')$ and its linear response function $\zeta_{jm}(\boldsymbol{k}')$ for $\boldsymbol{k}' \neq \pm\boldsymbol{k}$. Kraichnan [71] called this conjecture the weak dependence principle. This conjecture enables to derive the closed equations for appropriate representatives for the second-order moment and the response function by perturbation methods [58, 73]. On the other hand, the weak dependence principle does not explicitly deal with a noise induced by the nonlinearity of turbulence.

Then, let us consider the closure problems of turbulent relative dispersion. From the Langevin model envisaged in the previous subsection, we may model the noise explicitly. Therefore, it is probably possible to make a conjecture appropriately for the closure problem. Namely, we can obtain the (generalized) Langevin equations for the turbulent relative dispersion through the conjecture.

Bibliography

[1] Abramowitz, Milton & Stegun, Irene A. 1964 *Handbook of Mathematical Functions with Formulas, Graphs, and Mathematical Tables*, ninth dover printing, tenth gpo printing edn. New York: Dover.

[2] Albers, Tony & Radons, Günter 2018 Exact results for the nonergodicity of d-dimensional generalized Lévy walks. *Physical Review Letters* **120** (10).

[3] Artale, Vincenzo, Boffetta, Guido, Celani, Antonio, Cencini, Massimo & Vulpiani, Angelo 1997 Dispersion of passive tracers in closed basins: Beyond the diffusion coefficient. *Physics of Fluids* **9** (11), 3162–3171.

[4] Balkovsky, Eugene & Lebedev, V 1998 Instanton for the Kraichnan passive scalar problem. *Physical Review E* **58** (5), 5776–5795.

[5] Barenblatt, Grigory Isaakovich 1996 *Scaling, Self-similarity, and Intermediate Asymptotics: Dimensional Analysis and Intermediate Asymptotics*. *Cambridge Texts in Applied Mathematics* . Cambridge University Press.

[6] Barenblatt, Grigory Isaakovich 2003 *Scaling*. *Cambridge Texts in Applied Mathematics* . Cambridge University Press.

[7] Barenblatt, Grigory Isaakovich 2014 *Flow, Deformation and Fracture: Lectures on Fluid Mechanics and the Mechanics of Deformable Solids for Mathematicians and Physicists*. *Cambridge Texts in Applied Mathematics* . Cambridge University Press.

[8] Batchelor, George Keith 1950 The application of the similarity theory of turbulence to atmospheric diffusion. *Quarterly Journal of the Royal Meteorological Society* **76** (328), 133–146.

[9] Batchelor, George Keith 1952 Diffusion in a field of homogeneous turbulence: II. The relative motion of particles. *Mathematical Proceedings of the Cambridge Philosophical Society* **48** (2), 345–362.

[10] Batchelor, George Keith 1953 *The theory of homogeneous turbulence*. Cambridge University Press.

[11] Batchelor, George Keith 1969 Computation of the energy spectrum in homogeneous two-dimensional turbulence. *Physics of Fluids* **12** (12), II–233.

[12] Bennett, Andrew 2006 *Lagrangian Fluid Dynamics*. Cambridge University Press.

[13] Berg, Jacob, Lüthi, Beat, Mann, Jakob & Ott, Søren 2006 Backwards and forwards relative dispersion in turbulent flow: An experimental investigation. *Physical Review E* **74** (1), 016304.

[14] Bernard, Denis 1999 Three-point velocity correlation functions in two-dimensional forced turbulence. *Physical review. E, Statistical physics, plasmas, fluids, and related interdisciplinary topics* **60** (5 Pt B), 6184–7.

[15] Biferale, Luca, Boffetta, Guido, Celani, Antonio, Devenish, Benjamin, Lanotte, Alessandra S. & Toschi, Federico 2005 Lagrangian statistics of particle pairs in homogeneous isotropic turbulence. *Physics of Fluids* **17** (11), 1–9.

[16] Biferale, Luca, Lanotte, Alessandra S., Scatamacchia, R & Toschi, Federico 2014 Intermittency in the relative separations of tracers and of heavy particles in turbulent flows. *Journal of Fluid Mechanics* **757** (6), 550–572.

[17] Birkhoff, Garrett 1960 *Hydrodynamics*. Princeton University Press.

[18] Bitane, Rehab, Homann, Holger & Bec, Jérémie 2012 Time scales of turbulent relative dispersion. *Physical Review E* **86** (4), 045302.

[19] Bitane, Rehab, Homann, Holger & Bec, Jérémie 2013 Geometry and violent events in turbulent pair dispersion. *Journal of Turbulence* **14** (2), 23–45.

[20] Boffetta, Guido 2007 Energy and enstrophy fluxes in the double cascade of two-dimensional turbulence. *Journal of Fluid Mechanics* **589**, 253–260.

[21] Boffetta, Guido, Celani, Antonio, Crisanti, Andrea & Vulpiani, Angelo 1999 Pair dispersion in synthetic fully developed turbulence. *Europhysics Letters* **60** (6), 6734–6741.

[22] Boffetta, Guido., Celani, Antonio & Vergassola, Massimo 2000 Inverse energy cascade in two-dimensional turbulence: Deviations from Gaussian behavior. *Physical Review E* **61** (1), R29–R32.

[23] Boffetta, Guido & Ecke, Robert E. 2012 Two-dimensional turbulence. *Annual Review of Fluid Mechanics* **44** (1), 427–451.

[24] Boffetta, Guido. & Musacchio, Stefano 2010 Evidence for the double cascade scenario in two-dimensional turbulence. *Physical Review E* **82** (1), 016307.

[25] Boffetta, Guido & Sokolov, Igor M. 2002 Relative dispersion in fully developed turbulence: the Richardson's law and intermittency corrections. *Physical Review Letters* **88** (9), 094501.

[26] Boffetta, Guido & Sokolov, Igor M. 2002 Statistics of two-particle dispersion in two-dimensional turbulence. *Physics of Fluids* **14** (9), 3224–3232.

[27] Bothe, Marius, Sagues, Francesc & Sokolov, Igor M. 2019 Mean squared displacement in a generalized Lévy walk model. *Physical Review E* **100** (1), 012117.

[28] Bourgoin, Mickaël 2006 The role of pair dispersion in turbulent flow. *Science* **311** (5762), 835–838.

[29] Bourgoin, Mickaël 2015 Turbulent pair dispersion as a ballistic cascade phenomenology. *Journal of Fluid Mechanics* **772**, 678–704.

[30] Bragg, Andrew D., Ireland, Peter J. & Collins, Lance R. 2016 Forward and backward in time dispersion of fluid and inertial particles in isotropic turbulence. *Physics of Fluids* **28** (1).

[31] Bruneau, Charles-Henri & Kellay, Hamid 2005 Experiments and direct numerical simulations of two-dimensional turbulence. *Physical Review E* **71** (4), 046305.

[32] Buaria, Dhawal, Sawford, Brian L. & Yeung, Pui-Kuen 2015 Characteristics of backward and forward two-particle relative dispersion in turbulence at different Reynolds numbers. *Physics of Fluids* **27** (10), 105101.

[33] Buaria, Dhawal, Yeung, Pui-Kuen & Sawford, Brian L. 2016 A Lagrangian study of turbulent mixing: forward and backward dispersion of molecular trajectories in isotropic turbulence. *Journal of Fluid Mechanics* **799**, 352–382.

[34] Cardy, John, Falkovich, Gregory & Gawedzki, Krzysztof 2008 *Nonequilibrium Statistical Mechanics and Turbulence. London Mathematical Society Lecture Note Series* . Cambridge University Press.

[35] Castiglione, P, Mazzino, Andrea, Muratore-Ginanneschi, P & Vulpiani, Angelo 1999 On strong anomalous diffusion. *Physica D* **134**, 75–93.

[36] Chaves, Marta, Gawdzki, Krzysztof, Horvai, Peter, Kupiainen, Antti & Vergassola, Massimo 2003 Lagrangian dispersion in Gaussian self-similar velocity ensembles. *Journal of Statistical Physics* **1136** (5).

[37] Chen, Lin-Yuan, Goldenfeld, Nigel & Oono, Yoshi 1991 Renormalization-group theory for the modified porous-medium equation. *Physical Review A* **44** (10), 6544–6550.

[38] Chen, Shiyi, Ecke, Robert E., Eyink, Gregory L., Rivera, Michael K., Wan, Minping & Xiao, Zuoli 2006 Physical mechanism of the two-dimensional inverse energy cascade. *Physical Review Letters* **96** (8), 084502.

[39] Danilov, Sergei D & Gurarie, David 2001 Nonuniversal features of forced two-dimensional turbulence in the energy range. *Physical Review E* **63** (2), 020203.

[40] Eule, Sven, Zaburdaev, Vasily, Friedrich, R & Geisel, Theo 2012 Langevin description of superdiffusive Lévy processes. *Physical Review E - Statistical, Nonlinear, and Soft Matter Physics* **86** (4), 41134.

[41] Eyink, Gregory L. & Benveniste, Damien 2013 Diffusion approximation in turbulent two-particle dispersion. *Physical Review E* **88** (4), 041001.

[42] Falkovich, Gregory, Gawedzki, Krzysztof & Vergassola, Massimo 2001 Particles and fields in fluid turbulence. *Reviews of Modern Physics* **73** (4), 913–975.

[43] Fjørtoft, Ragnar 1953 On the changes in the spectral distribution of kinetic energy for twodimensional, nondivergent flow. *Tellus* **5** (3), 225–230.

[44] Francois, Nicolas, Xia, Hua, Punzmann, Horst & Shats, Michael 2013 Inverse energy cascade and emergence of large coherent vortices in turbulence driven by faraday waves. *Physical Review Letters* **110** (19), 194501.

[45] Frisch, Uriel 1995 *Turbulence: The Legacy of AN Kolmogorov*. Cambridge University Press.

[46] Frisch, Uriel & Sulem, Pierre-Louis 1984 Numerical simulation of the inverse cascade in two-dimensional turbulence. *Physics of Fluids* **27** (8), 1921.

[47] Gardiner, Crispin 2009 *Stochastic Methods A Handbook for the Natural and Social Sciences*, 4th edn. Springer.

[48] Goldenfeld, Nigel 1992 *Lectures on Phase Transitions and the Renormalization Group*. Westview Press.

[49] Gotoh, Toshiyuki & Kaneda, Yukio 1991 Lagrangian velocity autocorrelation and eddy viscosity in two-dimensional anisotropic turbulence. *Physics of Fluids A: Fluid Dynamics* **3** (10), 2426.

[50] Gotoh, Toshiyuki, Rogallo, Robert S., Herring, Jackson R. & Kraichnan, Robert H. 1993 Lagrangian velocity correlations in homogeneous isotropic turbulence. *Physics of Fluids A: Fluid Dynamics* **5** (11), 2846–2864.

[51] He, Guowei, Jin, Guodong & Yang, Yue 2017 Space-time correlations and dynamic coupling in turbulent flows. *Annual Review of Fluid Mechanics* **49** (1), 51–70.

[52] He, Guowei, Jin, Guodong & Zhao, Xin 2009 Scale-similarity model for Lagrangian velocity correlations in isotropic and stationary turbulence. *Physical Review E* **80** (6), 066313.

[53] Herring, Jackson R., Orszag, Steven A., Kraichnan, Robert H. & Fox, Douglas G. 1974 Decay of two-dimensional homogeneous turbulence. *Journal of Fluid Mechanics* **66** (3), 417–444.

[54] Ishihara, Takashi, Gotoh, Toshiyuki & Kaneda, Yukio 2009 Study of high–Reynolds number isotropic turbulence by direct numerical simulation. *Annual Review of Fluid Mechanics* **41** (1), 165–180.

[55] Ishihara, Takashi & Kaneda, Yukio 2002 Relative diffusion of a pair of fluid particles in the inertial subrange of turbulence. *Physics of Fluids* **14** (11), L69–L72.

[56] Jullien, Marie-Caroline, Paret, Jérôme & Tabeling, Patrick 1999 Richardson pair dispersion in two-dimensional turbulence. *Physical Review Letters* **82**, 2872.

[57] Kanatani, Kentaro, Ogasawara, Takeshi & Toh, Sadayoshi 2009 Telegraph-type versus diffusion-type models of turbulent relative dispersion. *Journal of the Physical Society of Japan* **78** (2), 024401.

[58] Kaneda, Yukio 1981 Renormalized expansions in the theory of turbulence with the use of the Lagrangian position function. *Journal of Fluid Mechanics* **107** (-1), 131.

[59] Kaneda, Yukio, Gotoh, Koji & Ishihara, Takashi 1998 Taylor Expansions and Padé Approximations of Lagrangian and Eulerian Two-Time Velocity Correlations in Turbulence. *Journal of the Physical Society of Japan* **67** (4), 1075–1078.

[60] Kaneda, Yukio & Gotoh, Toshiyuki 1991 Lagrangian velocity autocorrelation in isotropic turbulence. *Physics of Fluids A: Fluid Dynamics* **3** (8), 1924–1933.

[61] Kaneda, Yukio, Ishihara, Takashi & Gotoh, Koji 1999 Taylor expansions in powers of time of Lagrangian and Eulerian two-point two-time velocity correlations in turbulence. *Physics of Fluids* **11** (8), 2154–2166.

[62] de Kármán, Theodore & Howarth, Leslie 1938 On the statistical theory of isotropic turbulence. *Proceedings of the Royal Society of London. Series A - Mathematical and Physical Sciences* **164** (917), 192–215.

[63] Kellay, Hamid & Goldburg, Walter I 2002 Two-dimensional turbulence: A review of some recent experiments. *Rep. Prog. Phys.* **65**, 845–894.

[64] Kida, Shigeo & Goto, Susumu 1997 A Lagrangian direct-interaction approximation for homogeneous isotropic turbulence. *Journal of Fluid Mechanics* **345** (September 2000), 307–345.

[65] Kishi, Tatsuro, Matsumoto, Takeshi & Toh, Sadayoshi 2020 Non-Kolmogorov scaling for two-particle relative velocity in two-dimensional inverse energy-cascade turbulence. *Physical Review Fluids* **5** (5), 054601.

[66] Kistler, A. L. & Vrebalovich, T. 1966 Grid turbulence at large Reynolds numbers. *Journal of Fluid Mechanics* **26** (01), 37.

[67] Klafter, Joseph, Shlesinger, Michael F. & Zumofen, Gert 1996 Beyond Brownian motion. *Physics Today* **49** (2), 33–39.

[68] Klafter, Joseph. & Sokolov, Igor M. 2011 *First Steps in Random Walks*. Oxford University Press.

[69] Kolmogorov, Andrey N. 1941 Dissipation of energy in the locally isotropic turbulence. *Dokl. Akad. Nauk SSSR A* **32**, 16–18.

[70] Kolmogorov, Andrey N. 1941 The local structure of turbulence in incompressible viscous fluid for very large reynolds numbers. *Dokl. Akad. Nauk SSSR* **30**, 301–305.

[71] Kraichnan, Robert H 1959 The structure of isotropic turbulence at very high Reynolds numbers. *Journal of Fluid Mechanics* **5** (04), 497.

[72] Kraichnan, Robert H 1964 Kolmogorov's hypotheses and eulerian turbulence theory. *Physics of Fluids* **7** (11), 1723.

[73] Kraichnan, Robert H 1965 Lagrangian-history closure approximation for turbulence. *Physics of Fluids* **8** (4), 575.

[74] Kraichnan, Robert H 1966 Dispersion of particle pairs in homogeneous turbulence. *Physics of Fluids* **9** (10), 1937.

[75] Kraichnan, Robert H 1967 Inertial ranges in two-dimensional turbulence. *Physics of Fluids* **10** (7), 1417.

[76] Kraichnan, Robert H 1968 Small-scale structure of a scalar field convected by turbulence. *Physics of Fluids* **11** (5), 945–953.

[77] Landau, Lev D. & Lifshitz, Evgeny M. 1987 *Fluid Mechanics, Second Edition: Volume 6 (Course of Theoretical Physics)*, 2nd edn. *Course of theoretical physics / by L. D. Landau and E. M. Lifshitz, Vol. 6* . Butterworth-Heinemann.

[78] Leith, C E 1968 Diffusion approximation for two-dimensional turbulence. *Physics of Fluids* **11** (3), 671.

[79] Lesieur, Marcel. 1987 *Turbulence in Fluids*, *Mechanics of Fluids and Transport Processes*, vol. 6. Dordrecht: Springer Netherlands.

[80] Lindborg, Erik 1999 Can the atmospheric kinetic energy spectrum be explained by two-dimensional turbulence? *Journal of Fluid Mechanics* **388**, 259–288.

[81] Magdziarz, Marcin, Szczotka, Władysław & Zebrowski, Piotr 2012 Langevin Picture of Lévy Walks and Their Extensions. *Journal of Statistical Physics* **147** (1), 74–96.

[82] Magdziarz, Marcin & Zorawik, Tomasz 2017 Aging ballistic Lévy walks. *Physical Review E* **95** (2), 022126.

[83] Mandelbrot, Benoit B. & Van Ness, John W. 1968 Fractional Brownian motions, fractional noises and applications. *SIAM Review* **10** (4), 422–437.

[84] Metzler, Ralf & Klafter, Joseph 2000 The random walk's guide to anomalous diffusion. *Physics Reports* **339** (339), 1–77.

[85] Mizuta, Atsushi, Matsumoto, Takeshi & Toh, Sadayoshi 2013 Transition of the scaling law in inverse energy cascade range caused by a nonlocal excitation of coherent structures observed in two-dimensional turbulent fields. *Physical Review E* **88** (5), 53009.

[86] Monin, Andrei S. & Yaglom, Akiva M. 1971 *Statistical Fluid Mechanics*, , vol. 1. MIT Press.

[87] Obukhov, Alexander M. 1941 On the distribution of energy in the spectrum of turbulent flow. *Izv. Akad. Nauk SSSR, Ser. Geogr. Geofi* **5**, 453–466.

[88] Ogasawara, Takeshi & Toh, Sadayoshi 2006 Model of turbulent relative dispersion: a self-similar telegraph equation. *Journal of the Physical Society of Japan* **75** (8), 083401.

[89] Ogasawara, Takeshi & Toh, Sadayoshi 2006 Turbulent relative dispersion in two-dimensional free convection turbulence. *Journal of the Physical Society of Japan* **75** (10), 104402.

[90] Ott, Søren & Mann, Jakob 2000 An experimental investigation of the relative diffusion of particle pairs in three-dimensional turbulent flow. *J. Fluid Mech* **422**, 207–223.

[91] Ouellette, Nicholas T., Xu, Haitao, Bourgoin, Mickaël & Bodenschatz, Eberhard 2006 An experimental study of turbulent relative dispersion models. *New Journal of Physics* **8** (6), 109–109.

[92] Paret & Tabeling 1998 Intermittency in the two-dimensional inverse cascade of energy: Experimental observations. *Physics of Fluids* **10** (12), 3126.

[93] Paret, Jérôme, Jullien, Marie-Caroline & Tabeling, Patrick 1999 Vorticity Statistics in the two-dimensional enstrophy cascade. *Physical Review Letters* **83** (17), 3418–3421.

[94] Paret, Jérôme & Tabeling, Patrick 1997 Experimental observation of the two-dimensional inverse energy cascade. *Physical Review Letters* **79** (21), 4162–4165.

[95] Porrà, Josep M, Wang, Ke Gang & Masoliver, Jaume 1996 Generalized Langevin equations: Anomalous diffusion and probability distributions. *Physical Review E - Statistical Physics, Plasmas, Fluids, and Related Interdisciplinary Topics* **53** (6), 5872–5881.

[96] Rebenshtok, Adi, Denisov, Sergey, Hänggi, Peter & Barkai, Eli 2014 Infinite densities for Lévy walks. *Physical Review E - Statistical, Nonlinear, and Soft Matter Physics* **90** (6), 062135.

[97] Rebenshtok, Adi, Denisov, Sergey, Hänggi, Peter & Barkai, Eli 2014 Non-normalizable densities in strong anomalous diffusion: Beyond the central limit theorem. *Physical Review Letters* **112** (11), 110601.

[98] Richardson, Lewis F 1926 Atmospheric diffusion shown on a distance-neighbour graph. *Proceedings of the Royal Society A: Mathematical, Physical and Engineering Sciences* **110** (756), 709–737.

[99] Rivera, Michael K. & Ecke, Robert E 2005 Pair dispersion and doubling time statistics in two-dimensional turbulence. *Physical Review Letters* **95** (19), 194503.

[100] Rivera, Michael K. & Ecke, Robert E. 2016 Lagrangian statistics in weakly forced two-dimensional turbulence. *Chaos: An Interdisciplinary Journal of Nonlinear Science* **26** (1), 013103.

[101] Rivera, Michael K., Vorobieff, Peter & Ecke, Robert E 1998 Turbulence in flowing soap films: velocity, vorticity, and thickness fields. *Physical Review Letters* **81** (7), 1417–1420.

[102] Rutgers, Maarten A. 1998 Forced 2D turbulence: experimental evidence of simultaneous inverse energy and forward enstrophy cascades. *Physical Review Letters* **81** (11), 2244–2247.

[103] Salazar, Juan P.L.C. & Collins, Lance R 2009 Two-particle dispersion in isotropic turbulent flows. *Annual Review of Fluid Mechanics* **41** (1), 405–432.

[104] Sawford, Brian L., Yeung, Pui-Kuen & Hackl, Jason F. 2008 Reynolds number dependence of relative dispersion statistics in isotropic turbulence. *Physics of Fluids* **20** (6), 065111.

[105] Scatamacchia, R., Biferale, Luca & Toschi, Federico 2012 Extreme events in the dispersions of two neighboring particles under the influence of fluid turbulence. *Physical Review Letters* **109** (14), 144501.

[106] Schulz, Johannes H.P., Barkai, Eli & Metzler, Ralf 2014 Aging renewal theory and application to random walks. *Physical Review X* **4** (1), 011028.

[107] Shlesinger, Michael F., Zaslavsky, George M. & Klafter, Joseph 1993 Strange kinetics. *Nature* **363** (6424), 31–37.

[108] Sreenivasan, Katepalli R & Antonia, Robert A 1997 The phenomenology of small-scale turbulence. *Annual Review of Fluid Mechanics* **29** (1), 435–472.

[109] Tabeling, Patrick 2002 Two-dimensional turbulence: A physicist approach. *Physics Report* **362** (1), 1–62.

[110] Taylor, Geoffrey Ingram 1922 Diffusion by continuous movements. *Proceedings of the London Mathematical Society* **s2-20** (1), 196–212.

[111] Tennekes, Henk 1975 Eulerian and Lagrangian time microscales in isotropic turbulence. *Journal of Fluid Mechanics* **67** (3), 561–567.

[112] Tennekes, Henk & Lumley, John L. 1972 *A first course in turbulence*. MIT Press.

[113] Thalabard, Simon, Krstulovic, Giorgio & Bec, Jérémie 2014 Turbulent pair dispersion as a continuous-time random walk. *Journal of Fluid Mechanics* **755**, R4.

[114] Tran, Chuong V. & Bowman, John C. 2004 Robustness of the inverse cascade in two-dimensional turbulence. *Physical Review E* **69** (3), 036303.

[115] Tran, Chuong V. & Shepherd, Theodore G. 2002 Constraints on the spectral distribution of energy and enstrophy dissipation in forced two-dimensional turbulence. *Physica D: Nonlinear Phenomena* **165** (3-4), 199–212.

[116] Vallgren, Andreas 2011 Infrared reynolds number dependency of the two-dimensional inverse energy cascade. *Journal of Fluid Mechanics* **667**, 463–473.

[117] Vezzani, Alessandro, Barkai, Eli & Burioni, Raffaella 2019 Single-big-jump principle in physical modeling. *Physical Review E* **100** (1), 012108.

[118] Vezzani, Alessandro, Barkai, Eli & Burioni, Raffaella 2020 Rare events in generalized Lévy Walks and the Big Jump principle. SUPPLEMENTARY MATERIALS. *Scientific Reports* **10** (1), 2732.

[119] Von Kameke, Alexandra, Huhn, Florian, Fernández-García, G, Muñuzuri, Alberto P. & Pérez-Muñuzuri, Vicente 2011 Double cascade turbulence and richardson dispersion in a horizontal fluid flow induced by Faraday waves. *Physical Review Letters* **107** (7), 074502.

[120] Wallace, James M. 2014 Space-time correlations in turbulent flow: A review. *Theoretical and Applied Mechanics Letters* **4** (2), 022003.

[121] Wang, Xudong, Chen, Yao & Deng, Weihua 2019 Lévy-walk-like Langevin dynamics. *New Journal of Physics* **21** (1), 013024.

[122] Xiao, Z., Wan, Minping, Chen, Shiyi & Eyink, Gregory L. 2009 Physical mechanism of the inverse energy cascade of two-dimensional turbulence: a numerical investigation. *Journal of Fluid Mechanics* **619**, 1–44.

[123] Yaglom, Akiva M. 1990 Alexander Mikhailovich Obukhov, 1918-1989. *Boundary-Layer Meteorology* **53** (1-2), v–xi.

[124] Yakhot, Victor 1999 Two-dimensional turbulence in the inverse cascade range. *Physical Review E* **60** (5), 5544–5551.

[125] Yeung, Pui-Kuen 1994 Direct numerical simulation of two-particle relative diffusion in isotropic turbulence. *Physics of Fluids* **6** (10), 3416–3428.

[126] YEUNG, Pui-Kuen & BORGAS, MICHAEL S. 2004 Relative dispersion in isotropic turbulence. Part 1. Direct numerical simulations and Reynolds-number dependence. *Journal of Fluid Mechanics* **503**, 93–124.

[127] Zaburdaev, Vasily, Denisov, Sergiy & Klafter, Joseph 2015 Lévy walks. *Reviews of Modern Physics* **87** (2), 483–530.

[128] 木田, 重雄 & 柳瀬, 眞一郎 1999 乱流力学. 朝倉書店, japanese script.